SOOT FORMATION IN LAMINAR JET DIFFUSION FLAMES

by

Peter Bradford Sunderland

A dissertation submitted in partial fulfillment
of the requirements for the degree of
Doctor of Philosophy
(Aerospace Engineering)
in The University of Michigan
1995

Doctoral Committee:

Professor Gerard M. Faeth, Chairman
Professor Vedat S. Arpaci
Professor James F. Driscoll
Professor Martin Sichel

ACKNOWLEDGMENTS

I express deep gratitude to my advisor, Professor Gerard M. Faeth, for his conception and direction of this research, for his active technical involvement, and for his invaluable instruction. I thank also, for assistance with the gas-chromatography measurements, Saeed Mortazavi, S. F. Aldrin Wong and James C. Kim; for apparatus and facilities assistance, the technician staff of the Aerospace Engineering Department; and for assistance with the airborne experiments, Dr. David L. Urban, Daniel G. Gotti and Dennis P. Stocker.

This research was funded in part by NASA (grant number NAG3-1245) under the technical management of Dr. David L. Urban. This research also was funded in part by the Office of Naval Research (grant number N00014-93-0321) under the technical management of G. D. Roy.

TABLE OF CONTENTS

LIST OF TABLES

LIST OF FIGURES

LIST OF APPENDICES

NOMENCLATURE

C_i	mass of carbon per mole of species i
d	fuel port diameter
d_p	mean primary soot particle diameter
f	fuel element mass fraction (mixture fraction)
f_s	soot volume fraction
Fr	burner exit Froude number, $u_o^2/(gd)$
g	acceleration of gravity
[i]	molar concentration of species i
k	Boltzmann constant
k_g	soot growth rate constant
k_n	soot nucleation rate constant
L	flame length
L_0	reference flame length
M_i	molecular weight of species i
n	reaction order
n_p	number of primary particles per unit volume
$\bar{N}$	mean number of primary particles per aggregate
p	pressure
r	radial distance
Re	burner exit Reynolds number, $u_o d/\nu_o$
S	soot surface area per unit volume
t	time

t_r	residence time
t_{r0}	reference residence time
T	temperature
u	streamwise velocity
v	radial velocity
v_g	soot growth velocity
$\bar{v}_i$	mean molecular velocity of species i
w_g	soot growth rate
w_n	soot nucleation rate
X_i	mole fraction of species i
z	streamwise distance

Greek

ϕ	fuel-equivalence ratio
η_i	collision efficiency of species i
ν	kinematic viscosity
ρ	gas density
ρ_s	soot density

Subscripts

o	burner exit condition

CHAPTER I

INTRODUCTION

1.1 General Statement of the Problem

The present investigation considers the formation of soot in buoyant and nonbuoyant laminar jet diffusion flames. Soot is of great concern during practical combustion processes because it affects the performance of propulsion systems, the hazards of unwanted fires, and the pollutant emissions from combustors (Viskanta and Mengüc 1987). Similarly, continuum radiation from soot is the dominant mechanism for the growth and spread of unwanted fires, while soot-containing clouds emitted from these flames obscure fire fighting efforts (Faeth et al. 1989; Law and Faeth 1994; Tien and Lee 1982). Finally, black soot-containing exhaust plumes, and carbon monoxide emissions intrinsically associated with soot emissions, represent objectionable pollutants and also are the main source of fatalities in unwanted fires (Köylü and Faeth 1991; Köylü et al. 1991).

Motivated by these observations, three issues concerning soot formation were addressed during the present study. First, measurements were carried out at low gravity in order to evaluate how the laminar smoke point properties of nonbuoyant and buoyant flames compared. Second, measurements were completed in weakly-buoyant (which was achieved by considering low-pressure conditions) acetylene-fueled flames in order to investigate soot formation (nucleation and growth) in diffusion flames. Finally, similar work in both buoyant and weakly-buoyant diffusion flames burning hydrocarbons other than acetylene allowed investigation of the effects of various light hydrocarbons on soot formation (nucleation and growth) processes.

The present investigation was limited to laminar jet diffusion flames burning in still or slowly coflowing air, at pressures of 13-202 kPa. A variety of gaseous hydrocarbon fuels were used during this study, including acetylene, ethane, propane, n-butane, ethylene, propylene and 1,3-butadiene. The measurements generally involved pure fuels, however, some fuel streams were diluted with nitrogen to limit soot concentrations and make the measurements more tractable.

1.2 Previous Related Studies

The present discussion of previous research is only a brief overview; greater detail is given at the beginning of Chapters 2, 3 and 4, which consider laminar smoke point properties, soot processes in acetylene/air diffusion flames and soot processes for fuels other than acetylene in diffusion flames, respectively.

The laminar smoke point properties of jet diffusion flames have proven to be useful global measures of the soot properties of diffusion flames. Measurements of laminar smoke point properties generally are based on round buoyant jet diffusion flames because these properties are largely independent of burner diameter and coflow velocity, which has helped to promote their acceptance as global measures of soot properties (Glassman 1988). However, recent studies suggest potential for fundamental differences between the laminar smoke point properties of buoyant and nonbuoyant flames (Glassman 1988; Faeth 1991; Law and Faeth 1994). Thus, due to their relevance to many practical combustion processes where effects of buoyancy are small, as well as for issues of spacecraft fire safety, evaluation of nonbuoyant laminar smoke point properties was undertaken during the present investigation.

Studies of soot formation (nucleation and growth) in flames have been reviewed by Haynes and Wagner (1981), Glassman (1988) and Howard (1990). A popular configuration for experimental studies of soot processes in diffusion flames has been the

buoyant laminar jet diffusion flame that typically is used for measurements of laminar smoke point properties (Glassman 1988). However, past studies of soot processes within diffusion flames have not included measurements of gas-phase chemical compositions which are imperative in order to resolve the mechanisms of soot growth and nucleation. Similar studies in premixed flames, on the other hand, have involved more complete measurements, yielding a better understanding of soot formation; see the work of Bockhorn et al. (1982, 1984), Harris and Weiner (1983a, 1983b, 1984) and Ramer et al. (1986). These studies found that soot mainly is produced by particle growth rather than nucleation, that reaction between acetylene and soot particles mainly is responsible for soot growth, and that the rate of soot growth decreases with increasing residence time. The relevance of these results for premixed flames to soot processes in diffusion flames, however, has not been established. Additionally, past work in premixed flames has involved optical determinations of soot structure, an uncertain technique which is inferior to measurements using transmission electron microscopy (Köylü and Faeth 1994).

1.3 Specific Objectives

The preceding brief review reveals several gaps in current understanding of soot processes in laminar jet diffusion flames, in spite of the importance of such processes in practical combustion systems. Thus the present investigation seeks to contribute to an improved understanding of soot processes in laminar flames according to the following objectives:

1. To measure the laminar smoke point flame properties of nonbuoyant diffusion flames, and to compare these properties to the corresponding properties of buoyant diffusion flames.

2. To complete detailed measurements of both soot and flame properties in weakly-buoyant acetylene-air and hydrocarbon-air laminar jet diffusion flames.

3. To exploit these measurements in order to gain a better understanding of soot growth and nucleation rates in laminar jet diffusion flames.

This dissertation presents the three phases of this work as follows: laminar smoke points of nonbuoyant jet diffusion flames (Chapter 2); soot formation in acetylene/air diffusion flames (Chapter 3); and soot formation in hydrocarbon/air diffusion flames (Chapter 4). Following the conclusions (Chapter 5) are appendices presenting considerations of experimental uncertainties, data tabulations, and a listing of the rate analysis computer program.

CHAPTER II

LAMINAR SMOKE POINTS OF NONBUOYANT JET DIFFUSION FLAMES

2.1 Introduction

The laminar smoke point properties of jet diffusion flames — the luminous flame length, the residence time, and the fuel flow rate, at the onset of soot emission from the flames — have proven to be useful global measures of the soot properties of nonpremixed flames. These measures provide a means to predict several aspects of the sooting properties of flames: the relative tendency of various fuels to emit soot from flames (Clarke et al. 1946; Schalla et al. 1954; Schalla and McDonald 1954; Schalla and Hubbard 1959); the relative effects of fuel structure, flame temperature and pressure on the soot properties of flames (Schug et al. 1980; Glassman and Yaccarino 1980a, 1980b; Gomez et al. 1984; Glassman 1988; Flower and Bowman 1986); and the relative levels of continuum radiation from soot in flames (Markstein 1988; Sivathanu and Faeth 1990a; Köylü and Faeth 1991). Measurements of laminar smoke point properties generally are based on round buoyant jet diffusion flames, surrounded by a coflowing air (or oxidant) stream to prevent the flame pulsations characteristic of buoyant diffusion flames in still environments. Laminar smoke point properties found from this configuration are relatively independent of burner diameter and coflow velocities, which has helped to promote their acceptance as global measures of soot properties (Glassman 1988). However, recent studies suggest the potential for fundamental differences between the laminar smoke point properties of buoyant and nonbuoyant flames (Glassman 1988; Faeth 1991; Law and Faeth 1994). Thus, the overall objective of this phase of the present investigation was to measure the laminar smoke point properties of nonbuoyant flames, due to their relevance to many industrial processes where effects of buoyancy are small.

The potential differences between the laminar smoke point properties of buoyant and nonbuoyant flames can be attributed mainly to the different hydrodynamic properties of these flames (Faeth 1991; Law and Faeth 1994). This is illustrated in Fig. 2.1 where some features of axisymmetric buoyant and nonbuoyant laminar jet diffusion flames are plotted as a function of streamwise and radial distance, z and r, normalized by the flame length and jet exit diameter, L and d. The results for the buoyant flame are based on measurements (Santoro et al. 1983; Santoro and Semerjian 1984; Santoro et al. 1987) while the results for the nonbuoyant flame are based on predictions (Mortazavi et al. 1993; Spalding 1979). The region bounded by fuel-equivalence ratios, $\phi = 1$ and 2, is marked on the figures because this range of conditions is associated with processes of soot nucleation and growth (Glassman 1988). The dividing streamline, or locus of conditions where the radial velocity $v = 0$, also is shown on the plots. Soot particles are too large to diffuse like gas molecules so that they are convected by gas velocities, aside from minor effects of thermophoresis; therefore, soot particles tend to convect toward the dividing streamline, i.e., radial velocities inside and outside the dividing streamline are positive and negative, respectively. Due to flow acceleration and entrainment within buoyant diffusion flames, the dividing streamline moves toward the flame axis with increasing streamwise distance and generally lies inside the soot nucleation and growth region. In contrast, due to flow deceleration in nonbuoyant diffusion flames, the dividing streamline moves away from the flame axis with increasing streamwise distance and generally lies outside the soot nucleation and growth region. As discussed next, these differences in the location of the dividing streamline, and associated velocity properties along streamlines, have a significant impact on soot processes in these flames.

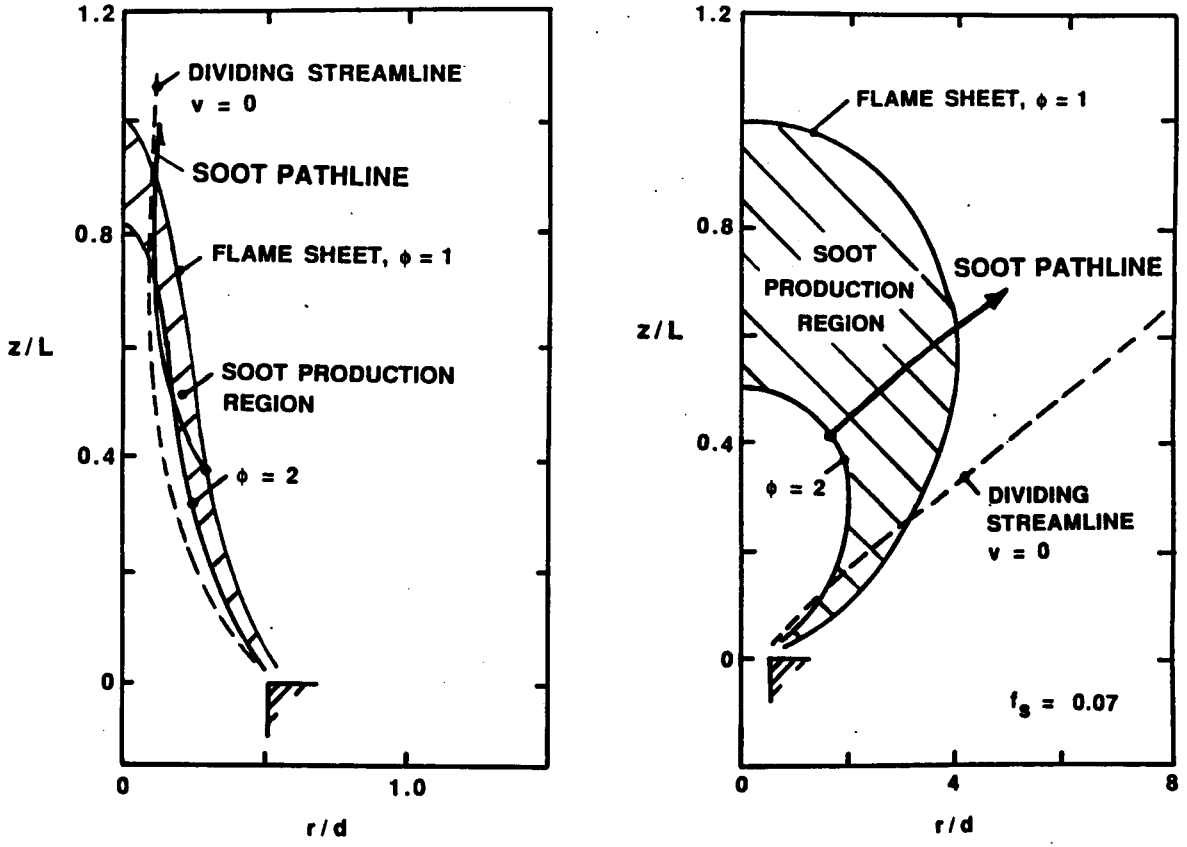

Figure 2.1 Sketch of Soot Paths in Buoyant and Nonbuoyant Jet Diffusion Flames

Recalling that initial emission of soot from a flame (which generally defines laminar smoke point properties) is associated with the region near the flame tip (Santoro et al. 1983; Santoro and Semerjian 1984; Santoro et al. 1987), the paths of soot in the tip region are illustrated in Fig. 2.1 for both buoyant and nonbuoyant diffusion flames. For buoyant flames, soot nucleates near the outer boundary of the soot nucleation and growth region (i.e. near the flame sheet where $\phi = 1$) and then moves radially inward toward cooler and less reactive conditions at higher fuel equivalence ratios for a time before finally crossing the flame sheet near its tip within an annular soot layer in the vicinity of the dividing streamline. In contrast, the soot particles responsible for the initial emission of soot in nonbuoyant flames nucleate at relatively high equivalence ratios near the inner boundary of the soot nucleation and growth region (at conditions where roughly $\phi = 2$), and then are drawn directly toward and through the flame sheet so that they experience a monotonic reduction of fuel equivalence ratio throughout their lifetime. Additionally, velocities along these two different soot paths progressively increase for buoyant flames but progressively decrease for nonbuoyant flames. This implies that the ratios of residence times for soot nucleation and growth to residence times for soot oxidation generally are smaller for nonbuoyant than for buoyant flames (Faeth 1991; Law and Faeth 1994; Santoro et al. 1983; Santoro and Semerjian 1984; Santoro et al. 1987). Finally, even the existence of global laminar smoke point properties has been questioned for nonbuoyant diffusion flames, because nonbuoyant jet diffusion flames have residence times that are independent of flame length under the boundary layer approximations (and assuming constant physical properties), unlike buoyant flames where residence times increase with increasing flame length (Glassman 1988). Clearly, the soot nucleation, growth and oxidation environment of buoyant and nonbuoyant diffusion flames is quite different, providing ample reasons for different laminar smoke point properties as well. Thus, study of effects of buoyancy on laminar smoke point properties should help to provide a better understanding of soot processes in diffusion flames.

Prior to the present study, no experiments had reported nonbuoyant laminar smoke point properties. Thus, the present objective was to measure the laminar smoke point flame lengths and residence times of nonbuoyant flames. The scope of the study was limited to round ethylene and propane jet diffusion flames burning in slightly vitiated air at pressures of 0.5-2.0 atm. A low-gravity test environment was used to obtain nonbuoyant flames at the small flow velocities characteristic of laminar smoke point conditions.

2.2 Experimental Methods

2.2.1 Apparatus

The experiments were conducted using the NASA KC-135 low-gravity facility. This aircraft flies parabolic trajectories to provide roughly 20s at low gravity (~ 10^{-2} g) conditions (see Fig. 2.2). The flames were observed within a cylindrical chamber having an internal volume of roughly 87 liters. The chamber could be evacuated in flight to roughly 0.36 atm by venting overboard, and was refilled using air stored under pressure in cylinders so that levels of vitiation were limited to less than 10% oxygen consumption by volume. The chamber had two windows and an interior light so that soot emission could be observed. The chamber pressure was recorded using an absolute pressure transducer.

Three round burners, having burner exit diameters of 1.6, 2.7 and 5.9 mm, were studied. The outside surfaces of the burner tubes had a 30 deg. chamfer at the exit, in order to minimize disturbances of the air entrained into the flames. The fuel flow passage had a constant diameter section with a length-to-diameter ratio of 20:1, to yield fully-developed laminar pipe flow at the burner exit. Fuel was delivered from storage bottles through solenoid valves and a needle metering valve to the plenum of the fuel port. The flames were ignited using a retractable hot wire coil near the burner exit.

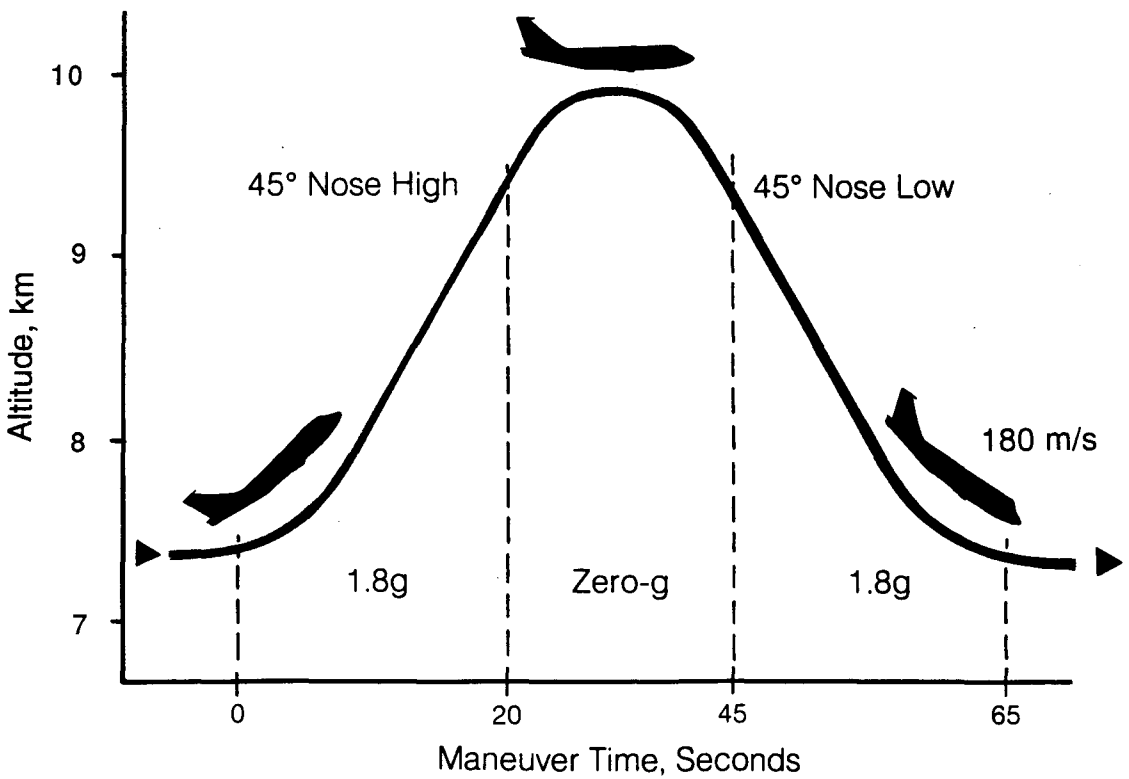

Figure 2.2 Sketch of the KC-135 Parabolic Trajectory

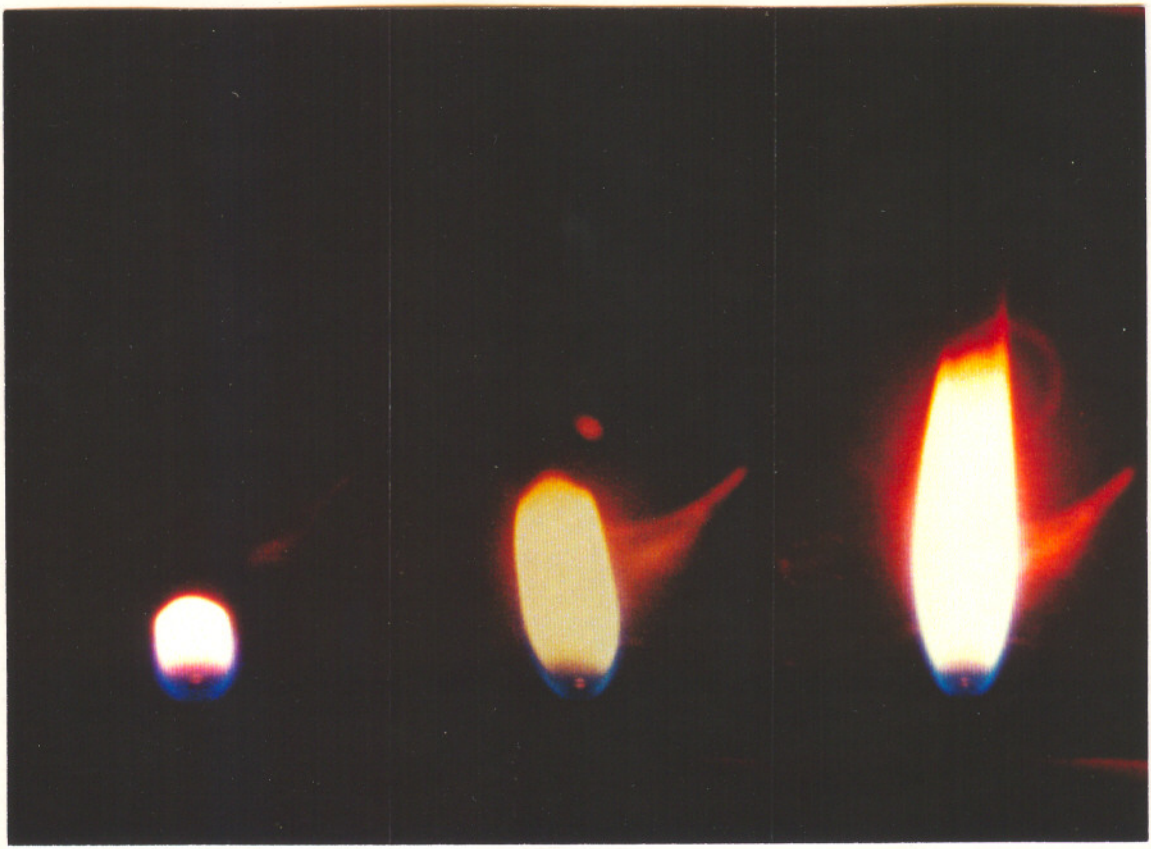

Figure 2.3 Nonbuoyant Ethylene Flame Photographs

Fuels considered were propane and ethylene. Photographs of three of the present nonbuoyant ethylene flames are shown in Fig. 2.3. These flames are burning on the 2.7 mm burner at a pressure of 1 atm. Direct visual observation revealed that of the three flames shown in Fig. 2.3 only the longest one emitted soot.

2.2.2 Instrumentation

The appearance of the flames was recorded by a color video camera. This allowed post-flight determination of when the flames were disturbed by departures from the parabolic flight path, so that observations at these conditions could be eliminated. The video records also were used to measure flame lengths, which were taken to be the length of the visible luminous portion of the flames. Flame lengths were found by averaging the video records when fully-developed flame shapes were reached, which typically required roughly 2s. Sooting conditions were found by visual observation of the flames, based on the appearance of a dark soot streak projecting from the flame tip. The chamber pressure and the observations of soot emission from the flames were recorded orally by two observers at different view ports using the audio channel of the video recorder.

The flame lengths measured at the onset of sooting actually were flame luminosity lengths, which is similar to the definition used for the laminar smoke point flame lengths of buoyant laminar jet diffusion flames (Clarke et al. 1946; Schalla et al. 1954; Schalla and McDonald 1954; Schalla and Hubbard 1959; Schug et al. 1980; Glassman and Yaccarino 1980a, 1980b; Gomez et al. 1984; Glassman 1988; Flower and Bowman 1986; Markstein 1988; Sivathanu and Faeth 1990a). Due to the presence of the soot oxidation region at fuel-lean conditions, however, the luminosity length is longer than the conventional flame length where stoichiometric conditions are reached at the flame axis. Fortunately, the ratios of the conventional to luminous flame lengths at the laminar smoke point are similar for nonbuoyant and buoyant flames, ca. 0.6 (Santoro et

al. 1983; Santoro and Semerjian 1984; Santoro et al. 1987; Mortazavi et al. 1993; Spengler and Kern 1969; Boedeker and Dobbs 1986). Thus, the luminous laminar smoke point flame length provides a reasonable basis to compare the sooting properties of both nonbuoyant and buoyant flames.

Experiments for roughly ten flight parabolas were used to find the laminar smoke point luminosity length for a given fuel, burner diameter and pressure. Based on the accuracy of flame luminosity length determinations, potential errors due to acceleration-induced flame tilt along the camera axis, and the range of conditions between nonsooting and sooting flames, the experimental uncertainties (95% confidence) of the laminar smoke point flame luminosity lengths are estimated to be less than 15%. The measurements were repeatable within this range.

2.3 Theoretical Methods

Laminar smoke point residence times are a useful measure of the sooting properties of a fuel. This is particularly true for nonbuoyant flames where residence times vary considerably with varying burner diameter for a given flame length, in contrast to buoyant flames where flame lengths and residence times are closely correlated (Glassman 1988; Sivathanu and Faeth 1990a; Köylü and Faeth 1991). Laminar smoke point residence times (defined as the time between termination of fuel flow into the base of the flame and the disappearance of all flame luminosity) have been measured directly for buoyant flames (Sivathanu and Faeth 1990a; Köylü and Faeth 1991). Similar results were not available, however, for the present nonbuoyant flames. Thus, the residence times for the nonbuoyant flames were found using a computational simulation. For these computations, the flame residence time was defined as the time required for a fluid parcel to convect along the flame axis from the burner exit to the flame sheet.

Details concerning the flame structure predictions are provided in Mortazavi et al. (1993). The major assumptions of the simulations are as follows: steady laminar axisymmetric flow, constant radiative heat loss fraction of the chemical energy release

for all parts of the flame, the laminar flamelet approximation for all scalar properties (which requires the previous radiation approximation and implies equal binary diffusivities of all species, negligible thermal diffusion and unity Lewis number), small flame standoff distance at points of flame attachment, constant property ambient environment, ideal gas mixture with negligible soot volumes and a constant Prandtl/Schmidt number, and multicomponent mixing laws for the mixture viscosity. The state relationships for gas species concentrations as a function of mixture fraction were found from correlations of measurements within buoyant laminar diffusion flames (Gore and Faeth 1986; Sivathanu and Faeth 1990c). The corresponding state relationships for temperature were computed given the state relationships for major gas species and the radiative heat loss fraction, as described by Sivathanu and Faeth (1990c). Following the recommendation of Edelman and Bahadori (1986), the full elliptic governing equations were solved for the present low Reynolds number flames, rather than adopting the boundary layer approximations.

The flame structure predictions were evaluated using measured flame shapes and lengths. The predictions were in reasonably good agreement (within 15%) with measured flame lengths reported by Haggard and Cochran (1972) for nonbuoyant ethylene/air flames at atmospheric pressure and having various Reynolds numbers. Flame shape predictions for weakly-buoyant ethylene and acetylene/air flames at various pressures and burner exit Reynolds numbers also were satisfactory (within 10%) (Mortazavi et al. 1993). Thus, while additional evaluation of the structure predictions would be desirable, the approach should provide adequate estimates of residence times for present purposes.

Predictions of flame residence times, t_r, for nonbuoyant laminar jet flames are illustrated in Figs. 2.4 and 2.5, in order to assist the interpretation of the laminar smoke point measurements. These results are for ethylene/air flames, at a pressure, p = 1 atm; findings for propane/air flames are essentially the same. Additionally, residence times are roughly proportional to pressure for a given flame length, L (Mortazavi et al. 1993).

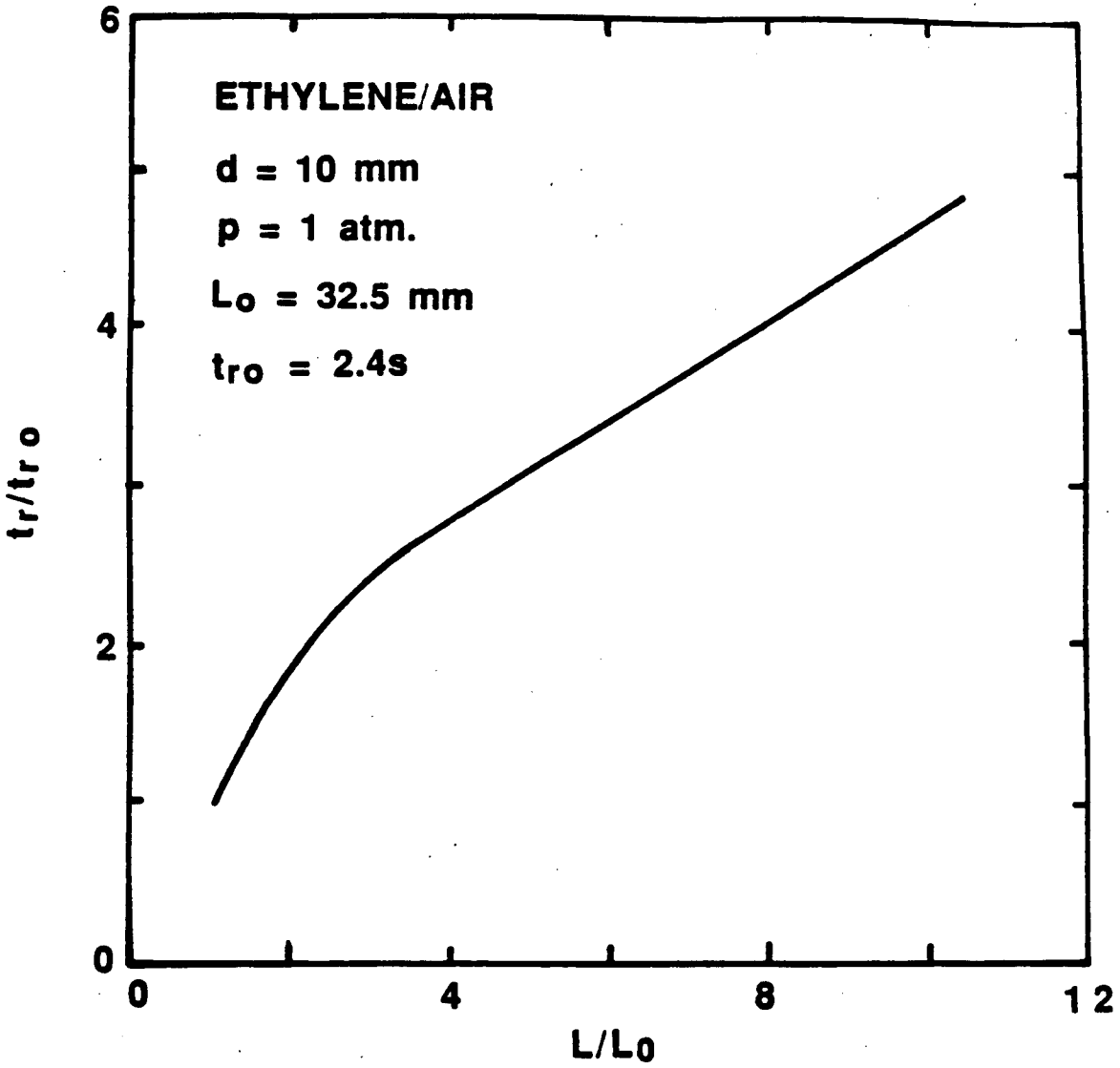

Figure 2.4 Predicted Flame Residence Times as a Function of Flame Length for Nonbuoyant Ethylene/Air Laminar Jet Diffusion Flames

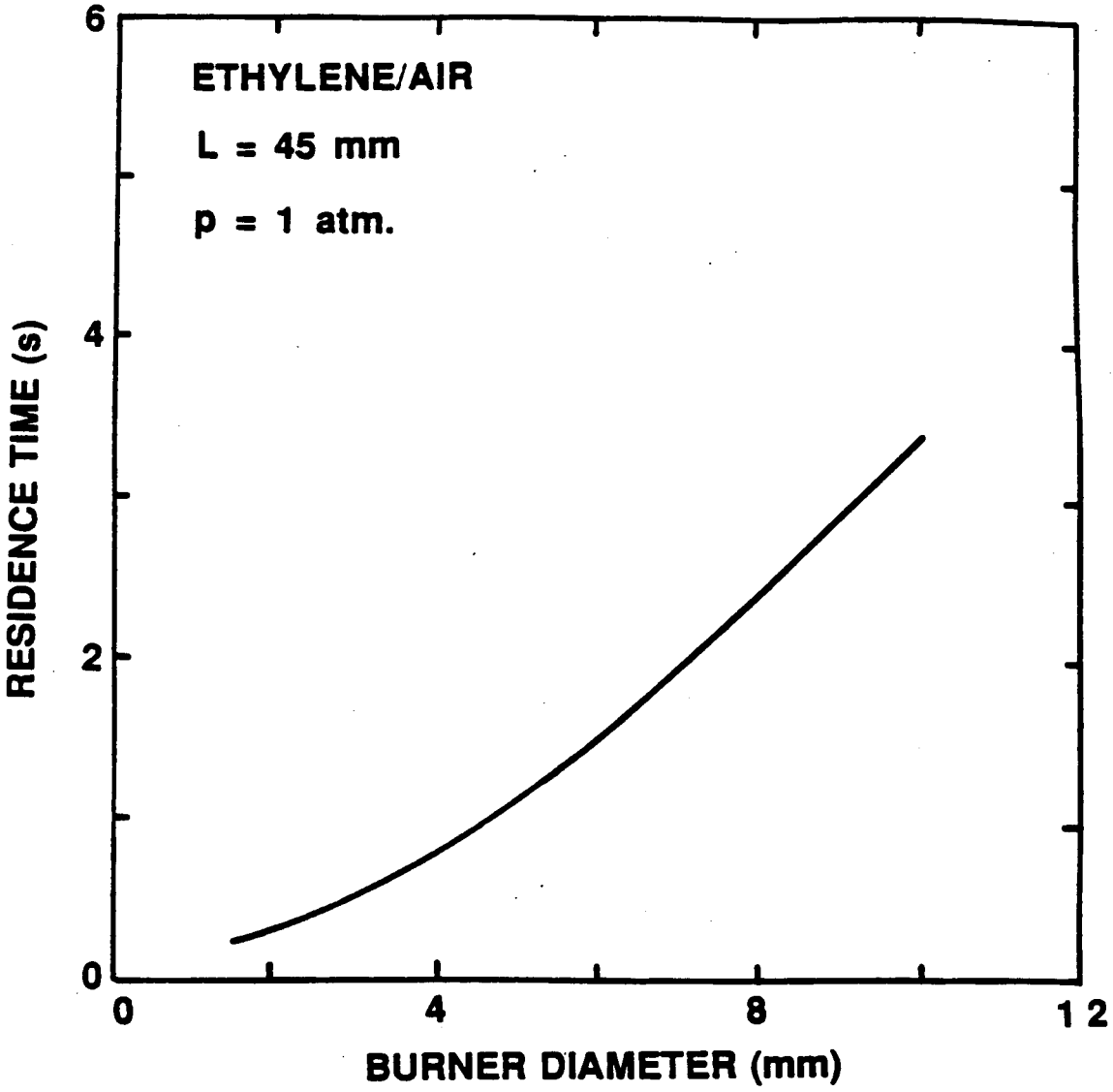

Figure 2.5 Predicted Flame Residence Times as a Function of Burner Diameter for Nonbuoyant Ethylene/Air Laminar Jet Diffusion Flames

The results illustrated in Fig. 2.4 show that increasing flame lengths for a fixed burner exit diameter, d, yield progressively increasing residence times. This behavior is similar to buoyant flames, where residence times are proportional to the square root of the flame length (Glassman 1988; Sivathanu and Faeth 1990a; Köylü and Faeth 1991). However, this behavior differs from constant-property estimates of residence times for nonbuoyant flames based on the boundary layer approximations, where residence times are independent of the flame length and only vary with the burner diameter (Glassman 1988; Spalding 1979). This difference primarily is caused by effects of diffusion in the streamwise direction.

The results illustrated in Fig. 2.5 show that residence times increase with increasing burner diameter for a fixed flame length. This behavior also is observed for boundary layer treatments of nonbuoyant laminar jet diffusion flames and is caused by reduced flow velocities at the burner exit as the burner diameter is increased for a fixed flame length (Spalding 1979). This behavior, however, differs from buoyant laminar jet diffusion flames where residence times largely are a function of flame length, and are relatively independent of burner diameter and exit velocity because buoyancy largely controls flow velocities within these flames (Glassman 1988; Spalding 1979).

2.4 Experimental Results and Discussion

Laminar smoke point luminosity lengths for ethylene and propane diffusion flames are summarized in Table 2.1. Results for nonbuoyant flames come from the present measurements at pressures of 0.5, 1.0 and 2.0 atm and burner exit diameters of 1.6, 2.7 and 5.9 mm. Results for buoyant flames come from the measurements of Schug et al. (1980) and Sivathanu and Faeth (1990a) at atmospheric pressure for a burner exit diameter of roughly 10 mm, although effects of burner diameter on the laminar smoke point properties of buoyant flames are small, as noted earlier.

Table 2.1 Laminar Smoke Point Luminosity Lengths (mm)

Burner Diameter (mm)	Pressure (atm)		
	0.5	1.0	2.0
	Ethylene/Air Flames		
Nonbuoyant[a]			
1.6	85	36	--
2.7	80	25	13
5.9	110	28	13
Buoyant[b]			
10.0	---	106-135	--
	Propane/Air Flames		
Nonbuoyant[a]			
1.6	130	42	16
2.7	140	38	18
5.9	130	42	20
Buoyant[b]			
10.0	---	162-169	--

[a]Determined from present measurements for round laminar jet diffusion flames in still air at low-gravity.

[b]Determined from Schug et al. (1980) and Sivathanu and Faeth (1990a) for round laminar jet diffusion flames in coflowing air at normal gravity.

There are several interesting features about the measurements summarized in Table 2.1. First, the nonbuoyant flames do exhibit laminar smoke point luminosity lengths, in contrast to the conjecture that these lengths would not exist because nonbuoyant flames have residence times that are independent of flame length under the boundary layer approximations (Glassman 1988). The latter behavior does not occur because streamwise diffusion causes residence times to increase as flame lengths are increased, leading to conditions where the flames emit soot as discussed in connection with Fig. 2.4. Next, the laminar smoke point luminosity lengths of nonbuoyant flames exhibit little variation with burner diameter, which is similar to findings for buoyant flames (Köylü and Faeth 1991). This behavior is expected for buoyant flames because their residence times largely are functions of flame lengths. Similar behavior was not expected for nonbuoyant flames, however, because their residence times increase with increasing burner diameter for a given flame length, see Fig. 2.5. Additionally, laminar smoke point luminosity lengths are roughly four times smaller for nonbuoyant flames than for buoyant flames at otherwise comparable conditions. On the other hand, laminar smoke point residence times are much longer for nonbuoyant than for buoyant flames, e.g., 200-1500 ms for nonbuoyant flames at atmospheric pressure, based on the predictions discussed in connection with Figs. 2.4 and 2.5, in comparison to 40-50 ms for the same fuels in buoyant flames (Sivathanu and Faeth 1990a).

Other properties of the laminar smoke point luminosity lengths summarized in Table 2.1 are qualitatively similar for nonbuoyant and buoyant flames. For example, laminar smoke point luminosity lengths are slightly longer for propane than for ethylene in both cases. Additionally, the pressure variation of laminar smoke point luminosity lengths for buoyant flames found by Flower and Bowman (1986), $\sim p^{-1.3}$, agrees with trends of present measurements for nonbuoyant flames with an average error of 25%. This quantitative agreement probably is somewhat fortuitous, however, due to the different soot paths in buoyant and nonbuoyant flames discussed earlier. Nevertheless, the reduction of laminar smoke point luminosity lengths with increasing pressure is

consistent with increased residence times at higher pressures for nonbuoyant flames, with effects of pressure on reaction rates being a contributing factor.

2.5 Conclusions

The reasons for the differences between the laminar smoke point properties of nonbuoyant and buoyant laminar jet diffusion flames are not quantitatively understood at present. However, the two general phenomena discussed earlier — differences in the soot paths and differences in the velocity distribution along the soot paths for nonbuoyant and buoyant flames — clearly play a role in this behavior. Different sites for initial soot nucleation and different conditions for subsequent soot nucleation and growth, should lead to different maximum primary soot particle sizes for nonbuoyant and buoyant flames of comparable length. The longer soot oxidation period relative to the soot nucleation and growth period for nonbuoyant flames in comparison to buoyant flames, due to the different velocity distributions along soot paths, also provides a mechanism for increased residence times prior to soot emission for the nonbuoyant flames, as observed during the present investigation. Finally, the longer residence times of nonbuoyant flames should enhance radiation heat losses, with corresponding temperature variations altering the reactive environment of soot as well.

In view of these differences in soot paths and flow structure it is not surprising that the soot emission properties of nonbuoyant and buoyant jet diffusion flames are different. It also is clear that nonbuoyant jet diffusion flames provide an interesting new perspective to gain a better understanding of soot mechanisms in diffusion flame environments. Subsequent work during the present investigation will exploit the advantages of reduced effects of buoyancy for observations of soot processes in jet diffusion flames, in order to gain both a better understanding of soot formation (nucleation and growth) processes, and insight into the present observations of effects of buoyancy on laminar smoke point properties.

CHAPTER III

SOOT FORMATION IN ACETYLENE/AIR DIFFUSION FLAMES

3.1 Introduction

Soot processes within nonpremixed hydrocarbon-fueled flames are important because they affect the durability and performance of propulsion systems, the hazards of unwanted fires, the pollutant and particulate emissions from combustion processes, and the potential for developing capabilities for computational combustion. Motivated by these observations, this phase of the present investigation involved an experimental study of the structure and soot properties of round laminar jet diffusion flames, seeking an improved understanding of soot formation (growth and nucleation) within diffusion flames. This work emphasized weakly-buoyant diffusion flame behavior that is typical of many practical applications (see Chapter 2).

Past studies of soot processes in flames have been reviewed by Haynes and Wagner (1981), Glassman (1988) and Howard (1990). A popular configuration for experimental studies of soot processes in diffusion flames has been the buoyant laminar jet diffusion flame that typically is used for measurements of laminar smoke point properties (Glassman 1988). Representative recent studies of these flames include the work of Kent and Wagner and coworkers (Kent et al. 1980; Kent and Wagner 1982, 1984; Kent and Honnery 1990, 1991; Honnery and Kent 1990; Honnery et al. 1992), Dobbins and Santoro and coworkers (Santoro et al. 1983, 1987; Santoro and Semerjian 1984; Megaridis and Dobbins 1988, 1989; Dobbins et al. 1994; Puri et al. 1993, 1994), and others (Flower and Bowman 1984, 1986, 1987; Axelbaum et al. 1988a, 1988b; Garo et al. 1986, 1990; Saito et al. 1991; Bockhorn et al. 1982). It is well known, however, that buoyancy affects soot processes within laminar jet diffusion flames because soot

particles are too large to diffuse so that they convect at flow velocities aside from small effects of thermophoresis. This behavior causes soot particles to mainly nucleate near the flame sheet and initially move toward fuel-rich conditions within buoyant laminar diffusion flames, while they mainly nucleate near the cool core of the flame and move directly toward fuel-lean conditions within nonbuoyant laminar diffusion flames (Chapter 2; Haynes and Wagner 1981; Glassman 1988). As a result, the soot nucleation and growth processes of buoyant and nonbuoyant laminar jet diffusion flames are quite different, providing incentive for studying soot processes for nonbuoyant flame conditions of significant practical interest. Additionally, a limitation of past studies of soot processes in diffusion flames (Haynes and Wagner 1981; Glassman 1988; Kent et al. 1980; Kent and Wagner 1982, 1984; Kent and Honnery 1990, 1991; Honnery and Kent 1990; Honnery et al. 1992; Santoro et al. 1983, 1987; Santoro and Semerjian 1984; Megaridis and Dobbins 1988, 1989; Puri et al. 1993, 1994; Flower and Bowman 1984, 1986; Garo et al. 1986, 1990; Saito et al. 1991) is that both soot properties and the local reactive environment were not sufficiently defined for detailed consideration of soot formation processes.

In contrast to studies of soot processes within laminar diffusion flames, significant progress concerning soot formation has been made from studies of fuel-rich premixed laminar flames. Representative investigations along these lines include Bockhorn et al. (1982, 1984), Harris and Weiner (1983a, 1983b, 1984), and Ramer et al. (1986). The findings of these studies indicated that soot mainly is produced by particle growth rather than nucleation, that the reaction between acetylene and soot particles mainly is responsible for soot growth, and that the rate of soot growth decreases (i.e. ages) with increasing residence time (Bockhorn et al. 1982, 1984; Harris and Weiner 1983a, 1983b, 1984; Ramer et al. 1986; Tesner 1991). Nevertheless, the relevance of

these results for premixed flames to soot processes within diffusion flames has not been established.

In view of this status, this phase of the present investigation had two main objectives, as follows: (1) to complete measurements of both soot and flame properties within weakly-buoyant, acetylene/air, laminar jet diffusion flames, and (2) to exploit these results to gain a better understanding of processes of soot growth and nucleation within laminar diffusion flames.

3.2 Experimental Methods

3.2.1 Apparatus

Present measurements involved weakly-buoyant, acetylene/air, laminar jet diffusion flames at low pressures, exploiting the fact that the effective buoyant acceleration scales as p^2g for laminar jet diffusion flames (Law and Faeth 1994); therefore, present tests involved pressures on the order of 0.1 atm to yield effective gravitational levels on the order of 0.01 g.

The test arrangement, shown in Fig. 3.1, consisted of a round fuel jet injecting vertically upward, surrounded by a slow concentric flow of air. The flames burned along the axis of a vertical, windowed, cylindrical chamber having a diameter and length of 300 mm. The top and bottom of the chamber consisted of porous metal plates that separated the flame chamber from plenum chambers for air inflow and exhaust outflow and provided a uniform distribution of air flow over the flame chamber cross section. The fuel and air flows were measured with rotameters, calibrated in turn by wet-test meters, while the exhaust flow was removed using a vacuum pump. The flames were ignited by a hot-wire coil that could be retracted from the burner exit once ignition was complete. The entire test chamber could be traversed in the vertical and horizontal directions in order to accommodate rigidly-mounted optical instruments.

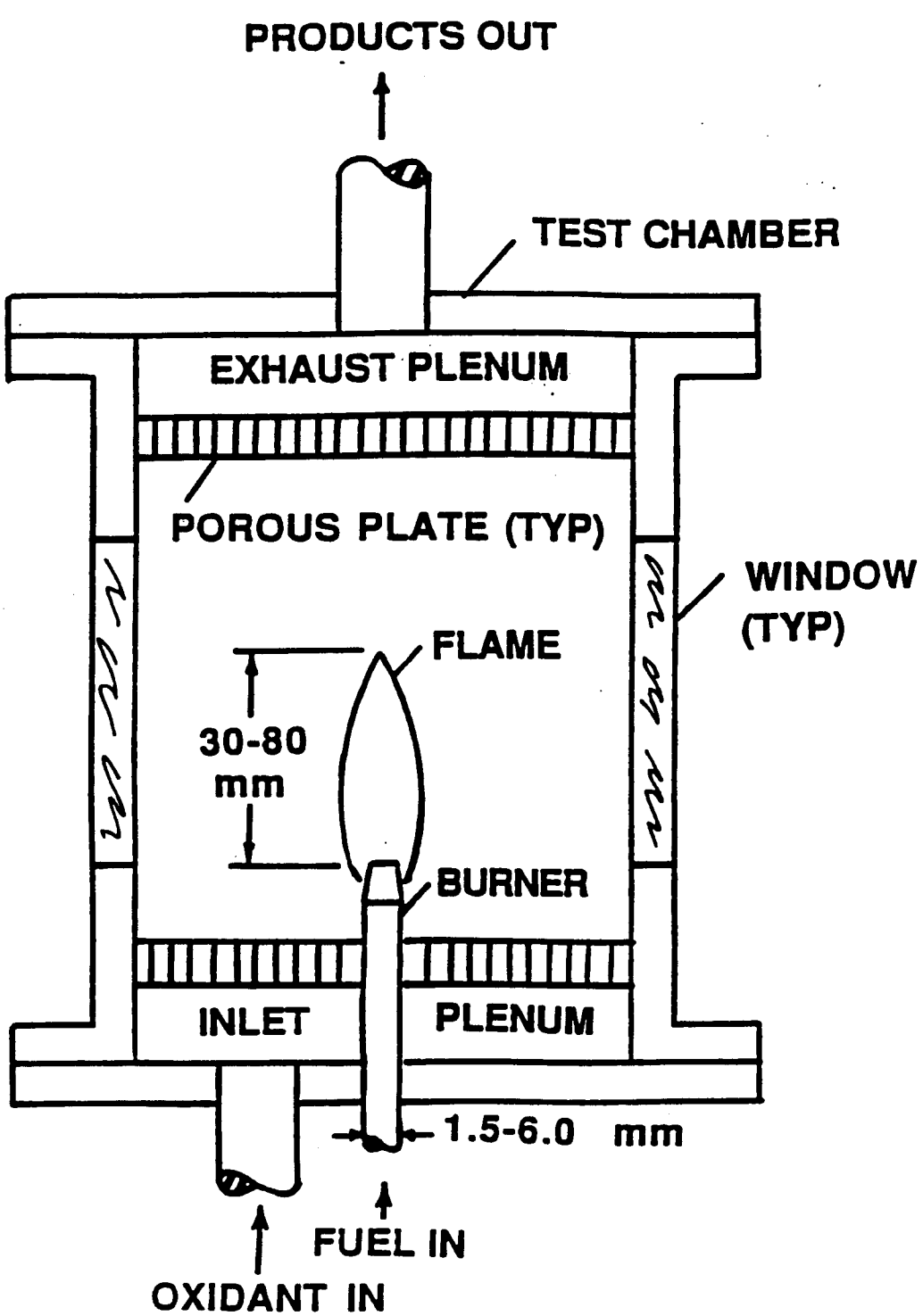

Figure 3.1 Apparatus Schematic

3.2.2 Instrumentation

Soot volume fractions were measured by deconvoluting laser extinction measurements for chord-like paths through the flames, similar to Santoro et al. (1983), Gore and Faeth (1988) and Köylü and Faeth (1994). The data were reduced assuming that soot optical properties satisfy the small-particle (Rayleigh) scattering limit, which was justified because scattering was small. Refractive indices were taken from Dalzell and Sarofim (1969) similar to past work (Gore and Faeth 1988; Köylü and Faeth 1994). Experimental uncertainties of these measurements (95% confidence) are estimated to be less than 10% for $f_s > 0.1$ ppm.

In regions where soot was absent, gas temperatures were measured with bare wire Pt/Pt - 10% Rh thermocouples having 270 μm diameter junctions. These measurements were corrected for radiation errors based on emissivities from Bradley and Entwhistle (1961). Experimental uncertainties of these measurements (95% confidence) were less than 50 K. Temperatures within soot-containing regions were found using multiline emission measurements similar to Cashdollar (1979), Klingenberg (1985) and Sivathanu and Faeth (1990b). This involved deconvoluting spectral radiation intensities for chord-like paths through the flames and finding temperatures from measurements at three line pairs: 600/750, 700/830 and 600/830 nm. Temperature differences between the average and any of the line pairs were less than 30 K while experimental uncertainties (95% confidence) of these measurements are estimated to be less than 50 K.

Soot structure was measured using thermophoretic sampling and analysis by transmission electron microscopy (TEM), similar to Megaridis and Dobbins (1988, 1989) and Dalzell and Sarofim (1969). Effects of soot aggregate size cause a negligible sampling bias for $\bar{N}$ for present test conditions (Köylü and Faeth 1994; Rosner et al. 1991). Primary particle diameters also were very nearly monodisperse, with a standard deviation less than 10%. Experimental uncertainties (95% confidence) of these

properties were dominated by finite sampling limitations, and were as follows: mean primary particle diameter, d_p < 10% and mean number of primary particles per aggregate, $\bar{N}$ < 20%. The number of primary soot particles per unit volume, n_p, was computed from the other measurements, as follows:

$$n_p = 6 f_s / (\pi d_p^3) \tag{3.1}$$

The resulting experimental uncertainties (95% confidence) for n_p are less than 32% for f_s > 0.1 ppm.

Gas compositions were measured by sampling and analysis using gas chromatography, similar to Gore and Faeth (1988). A stainless steel radiatively cooled sampling probe was used, having a port diameter of 2.1 mm. Acetylene was the only hydrocarbon present in significant quantities in the test flames; therefore, major gas species considered during gas analysis were as follows: N_2, O_2, C_2H_2, CO_2, CO, H_2O and H_2. Experimental uncertainties of these measurements generally were less than 15% for mole fractions greater than 0.5%, dominated by uncertainties in measuring chromatogram-peak areas.

In order to find soot processes as a function of time, streamwise velocities were measured using laser velocimetry (LV), similar to Gore and Faeth (1988). A dual-beam forward scattering arrangement was used with the flow seeded with aluminum oxide particles. Experimental uncertainties (95% confidence) of the velocity measurements were less than 5%, dominated by calibration uncertainties.

3.2.3 Test Conditions

The four test flames are summarized in Table 3.1 and shown in Fig. 3.2. The burner flows involved C_2H_2/N_2 mixtures with combustion in coflowing air at 0.125-0.250 atm. Visible flame lengths were 50 mm (z/d = 15.2), while the position of the

Table 3.1 Acetylene Flame Summary[a]

Test Flame	1	2	3	4
Pressure (atm)	0.250	0.188	0.125	0.250
Burner flow (% C_2H_2 by vol.)	100	100	100	59
C_2H_2 flow rate (cc/s)	8.12	13.6	25.0	8.96
N_2 flow rate (cc/s)	---	---	---	6.24
Air flow rate (cc/s)	395	755	1450	395
Burner exit velocity (mm/s)[b]	939	1570	2880	1760
Air coflow velocity (mm/s)[b]	5.27	10.1	19.4	5.27
Stoich. flame length (z/d)	9.5	13.9	15.2	12.2
Char. res. time (ms)	19.7	22.6	16.9	19.4
Re (-)[b]	80	100	122	149
Fr (-)[b]	27	76	256	96
Rad. heat loss (% LHV)	34.2	32.3	29.4	31.7

[a]Laminar round jet diffusion flames with 3.3 mm inside diameter burner, a visible flame length of roughly z/d = 15.2, and C_2H_2/N_2 mixtures flowing from the burner in an air coflow. Purified grade acetylene (99.6% purity), prepurified grade nitrogen (99.98% purity).

[b]Nominal average value based on an injection temperature of 298 ± 2K.

Flame 1 Flame 2 ne 3 Flame 4

Figure 3.2 Acetylene Flame Photographs

flame tips (where the stoichiometric flame sheet reaches the axis) were in the range z/d = 9.5-15.2. Characteristic residence times for convection from the burner exit to the flame tip were 16.9-22.6 ms. Reynolds and Froude numbers were 80-149 and 27-256, respectively. Radiative heat loss fractions were 29-34%.

Contamination of acetylene with acetone can be a problem for studies of acetylene reaction phenomena (Hamins et al. 1986; Colket et al. 1989, 1991). Present tests generally involved acetone mole fractions less than 2%. Thus, the effect of acetone contamination at this level was evaluated using the purifying train of Hamins et al. (1986) to reduce the acetone concentration to 0.1%, finding negligible differences from the soot and flame properties measured at the higher acetone concentrations.

3.3 Results and Discussion

3.3.1 Flame Structure

All the results considered in the following are for conditions along the axis of the flames, where mixture fractions decrease monotonically along a soot path similar to behavior in nonbuoyant diffusion flames. TEM photographs of soot within Flame 1 near the start, middle, and end of soot formation (heights above the burner of 9.4, 15.6 and 18.4 mm) are shown in Figs. 3.3, 3.4 and 3.5, respectively. These photographs are representative of Flames 1-4 and show soot which is similar to past observations of soot in flame environments (Megaridis and Dobbins 1988, 1989; Köylü and Faeth 1994). Thus, at a particular location in the flame, the soot consists of roughly spherical primary particles having nearly constant diameters, collected into aggregates having widely varying numbers of primary particles per aggregate. The degree of aggregation, quantified as $\bar{N}$, increases with increasing residence time (see Fig. 3.6).

An interesting feature of the results illustrated in Figs. 3.3-3.5 is that d_p is largest near the start (Fig. 3.3) of soot formation for the present soot path along the flame axis.

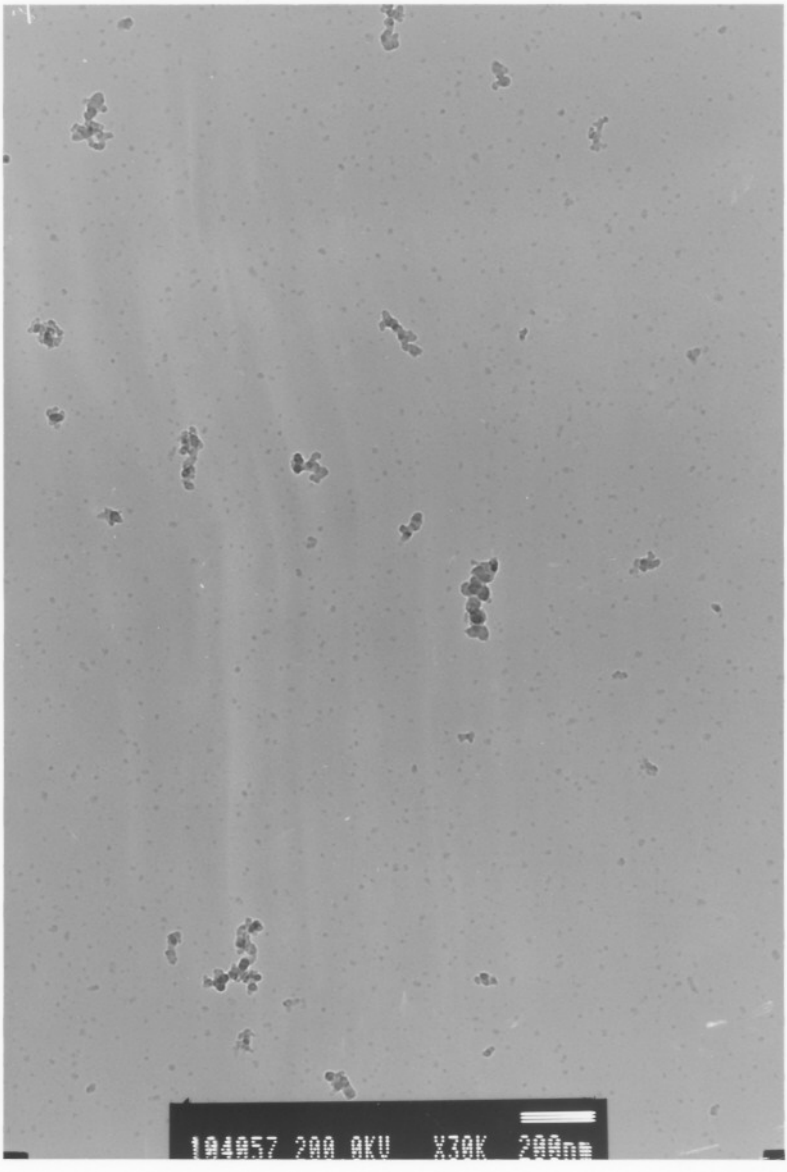

Figure 3.3 TEM Photograph of Soot from Flame 1 at z=9.4 mm

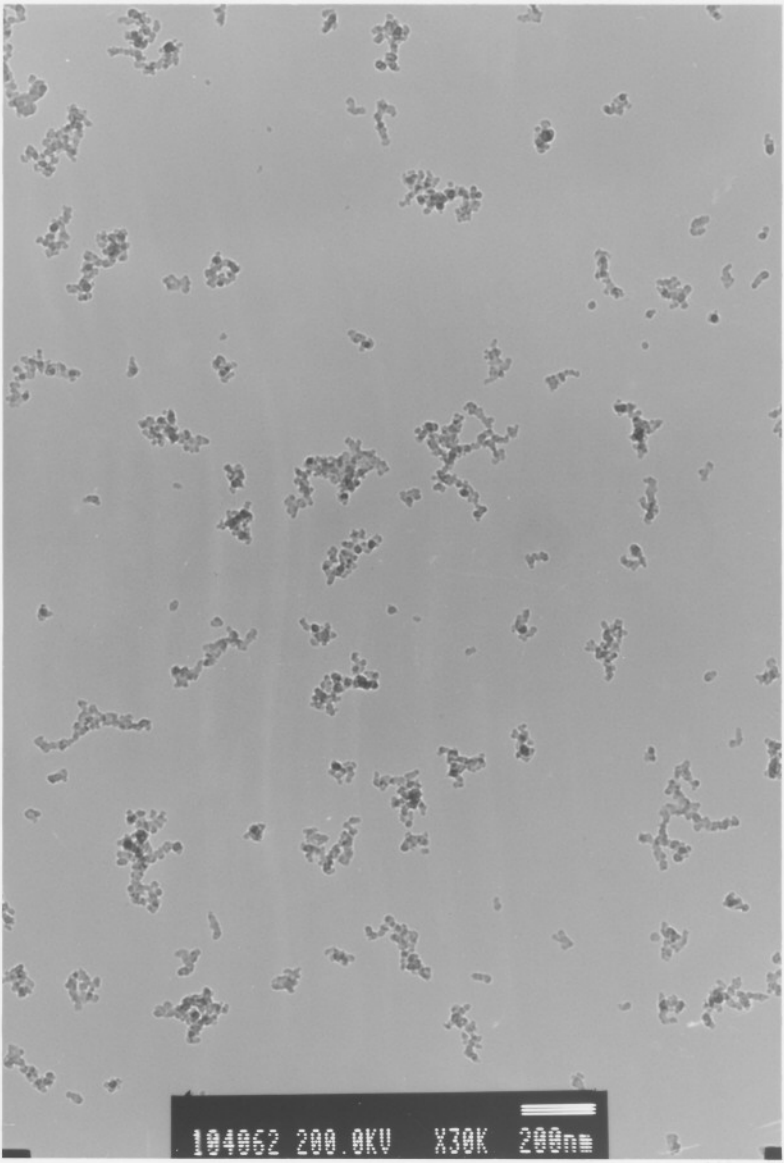

Figure 3.4 TEM Photograph of Soot from Flame 1 at z=15.6 mm

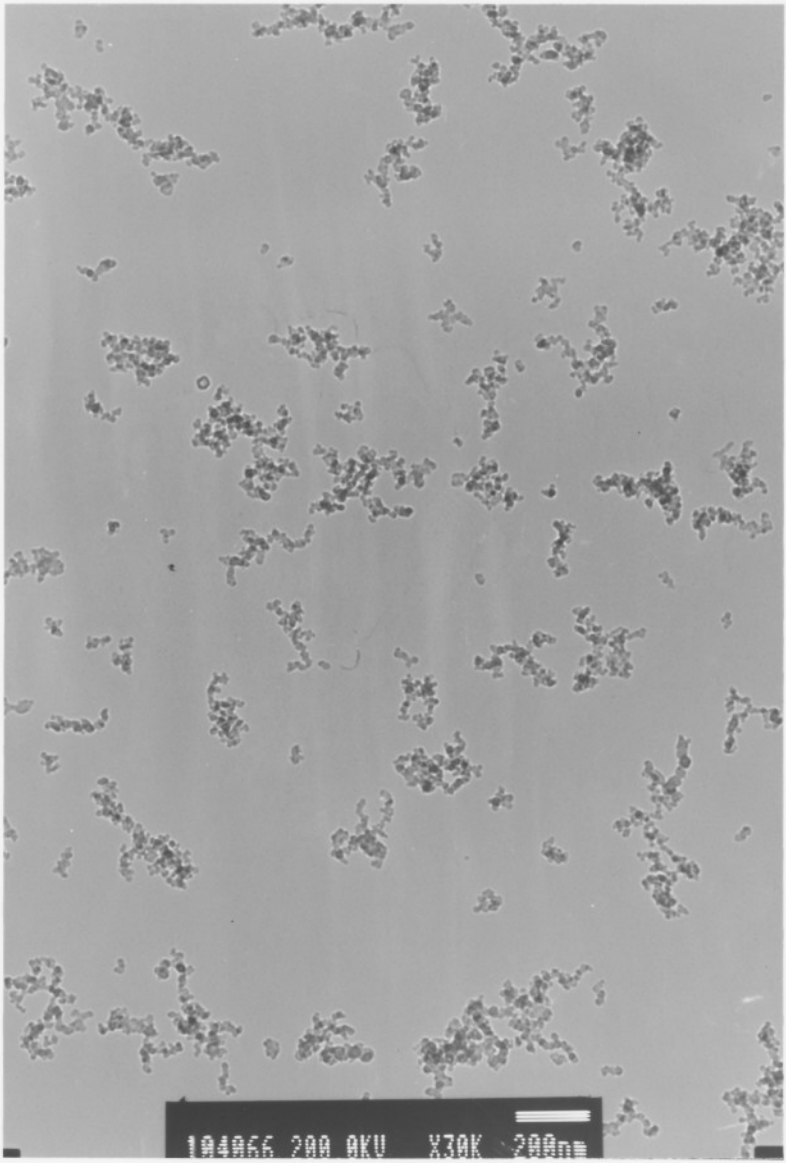

Figure 3.5 TEM Photograph of Soot from Flame 1 at z=18.4 mm

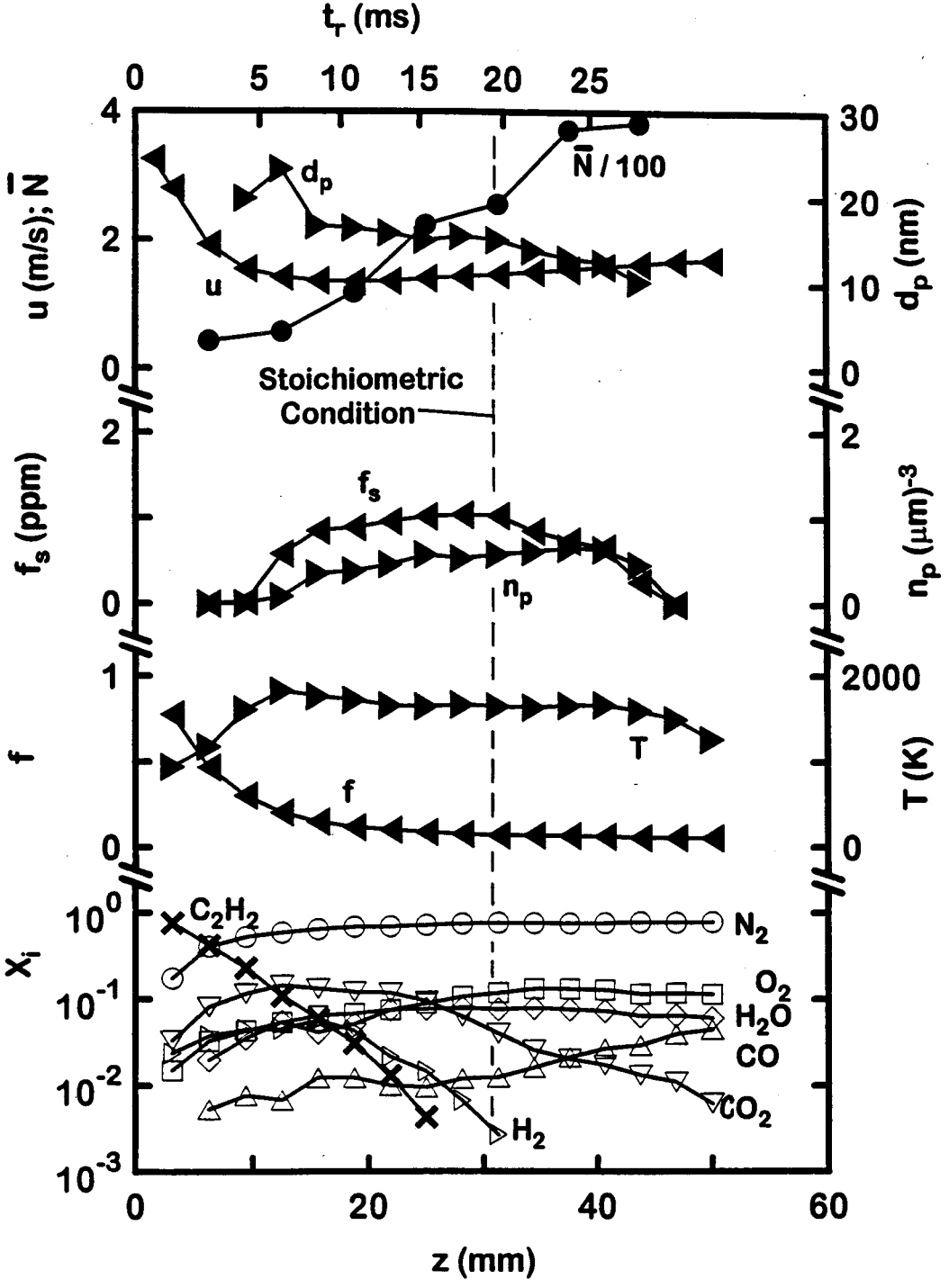

Figure 3.6 Soot and Flame Properties Along the Axis of Flame 1

This is quantified by measurements of d_p corresponding to Figs. 3.3-3.5: 19.9, 16.7 and 16.4 nm, respectively. This highlights an early observation of Tesner (1958; 1960), that the surface growth of soot persists to temperatures much lower than those required for significant soot particle nucleation (inception). This behavior causes rapid growth of the limited number of soot particles present near the start of the soot formation region, producing large primary particles, as observed in Fig. 3.3. Subsequently, accelerating nucleation rates create additional primary soot particles whose shorter growth period causes the average value of d_p to become smaller, as seen by comparing Fig. 3.3 with Figs. 3.4 and 3.5, even though overall soot concentration levels are increasing.

Another interesting feature of the TEM photographs is the presence of single (unaggregated) particles that are more translucent in appearance on the TEM photographs than the primary soot particles contained in the conventional soot aggregates. These more translucent objects were most evident near the start of soot formation (see Fig. 3.3) and essentially disappear in the region where most of the soot growth occurred (see Figs. 3.4 and 3.5). Notably, Megaridis and Dobbins (1989) observe similar objects near the start of soot formation along the axis of buoyant ethylene/air diffusion flames at atmospheric pressure, which they suggest may be a liquid phase associated with the early stages of soot formation. Unfortunately, it was not possible to resolve the role of these translucent particles in the soot formation process during the present investigation.

Both soot and flame properties along the axis of Flames 1-4 are illustrated in Figs. 3.6-3.9, respectively (see data summary in Tables B.1 and B.2 of Appendix B). These results are plotted in terms of axial distance, with residence time, i.e. the elapsed time for a fluid parcel to convect from the burner exit, shown at the top of each plot. The flame sheet locations (where the stoichiometric condition is reached along the flame axes) are noted on the figures as a reference. Species concentrations illustrated in the figures are in excellent agreement with past measurements of state relationships for major gas species

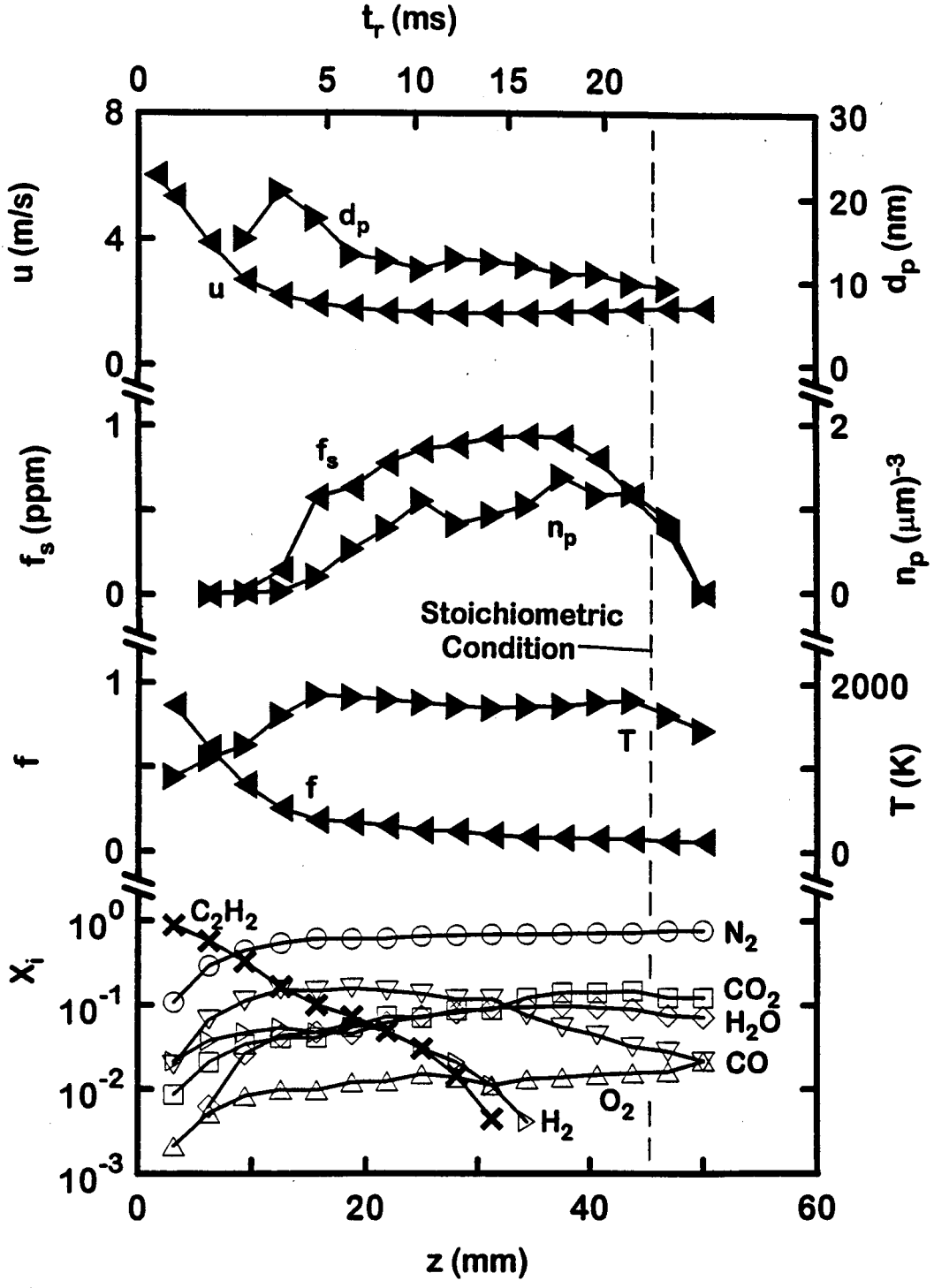

Figure 3.7 Soot and Flame Properties Along the Axis of Flame 2

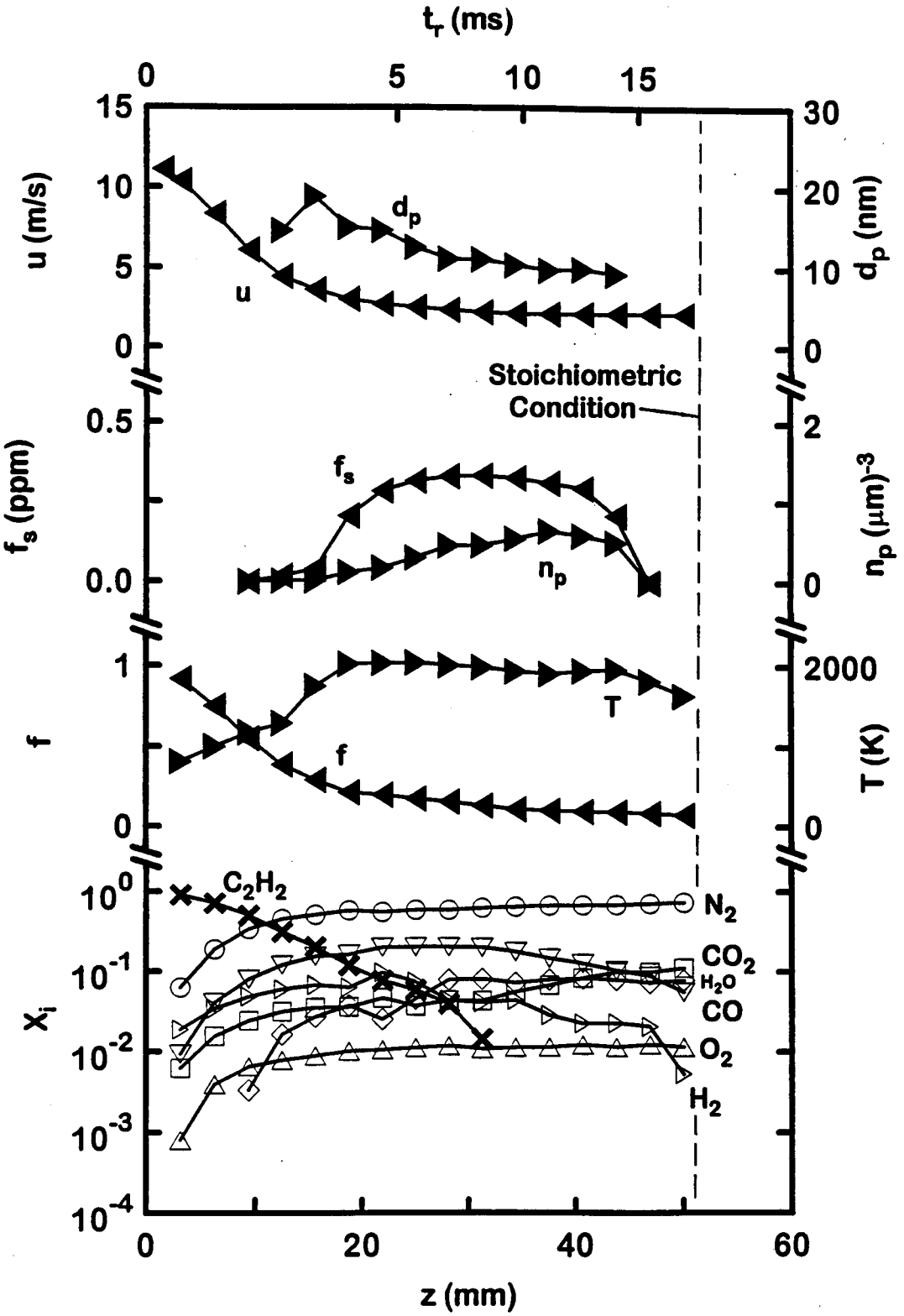

Figure 3.8 Soot and Flame Properties Along the Axis of Flame 3

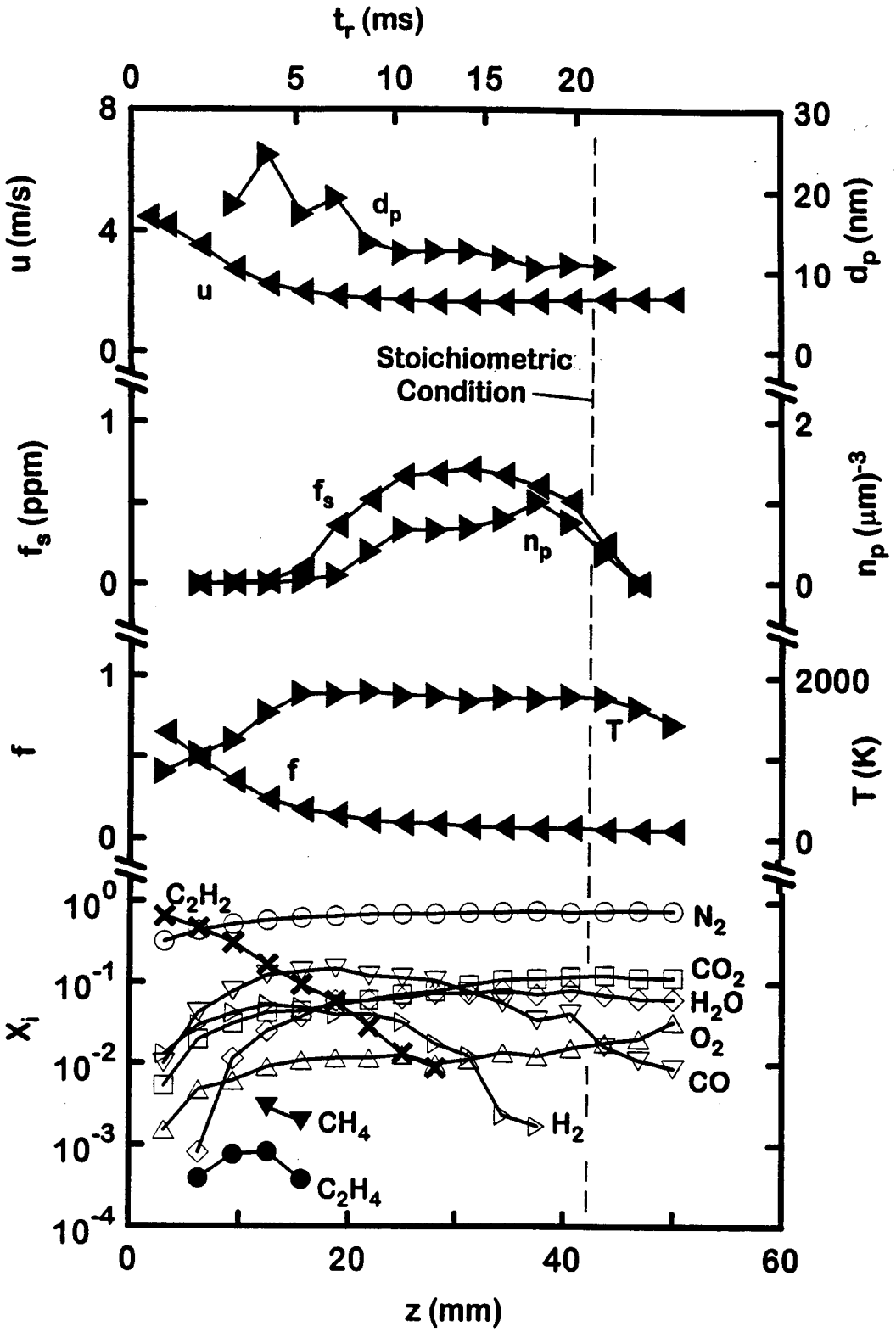

Figure 3.9 Soot and Flame Properties Along the Axis of Flame 4

as a function of mixture fraction at atmospheric pressure (Gore and Faeth 1988; Sivathanu and Faeth 1990c). Temperature reaches a maximum well before both the flame tip and the region of greatest soot production, which suggests significant effects of continuum radiation from soot, and possibly effects of incomplete combustion due to the presence of substantial concentrations of CO and soot on temperatures within the flame.

Significant levels of soot formation, based on increasing values of soot volume fractions, only are observed when temperatures exceed roughly 1250 K for Flames 1-4 in Figs. 3.6-3.9, respectively, which is typical of all the present flames as well as past observations (Haynes and Wagner 1981; Glassman 1988; Kent et al. 1980). The end of soot formation, which roughly corresponds to conditions where the maximum value of f_s is reached because gas densities are relatively uniform in this region, generally occurs when the concentration of acetylene becomes small. This condition is reached well before the flame sheet is reached, i.e., at a fuel-equivalence ratio of roughly 1.4. As mentioned in connection with Figs. 3.3-3.5, the relationship between soot concentrations and primary particle diameters is complex for these flames due to varying soot nucleation and growth rates. Thus, d_p reaches a maximum well before f_s does, with the intervening region involving a large increase of n_p due to rapid nucleation. Nucleation eventually ceases, however, near the maximum f_s condition, where acetylene disappears, as noted earlier. In contrast to the complex behavior of d_p, however, the aggregation of soot particles causes a progressive increase of $\bar{N}$ with time (see Fig. 3.6).

3.3.2 Soot Growth

Present measurements along the axis of the four test flames were used to study soot growth and nucleation in diffusion flames. As noted earlier, soot surface growth, rather than soot nucleation, dominates soot mass production. Additionally, effects of thermophoresis are small so that soot convects along streamlines because soot aggregates are too large to diffuse. Finally, the surface area available for soot growth was found by

assuming that soot aggregates approximate constant diameter spherical primary particles that meet at a point. Then defining the soot growth rate, w_g, as the rate of increase of soot mass per unit soot surface area and time, conservation of soot mass along a streamline under these assumptions yields:

$$w_g = \rho_s v_g = (\rho/S)d(\rho_s f_s/\rho)/dt \tag{3.2}$$

where v_g is the soot growth velocity. The soot surface area per unit volume, S, in Eq. 3.2 can be found from

$$S = \pi d_p^2 n_p = 6 f_s/d_p \tag{3.3}$$

where the last equality of Eq. 3.3 follows from Eq. 3.1. The local density in Eq. 3.2 was found from present concentration and temperature measurements, assuming an ideal gas mixture of the major gas species and neglecting the volume of soot (which was only present at ppm levels). The soot density in Eq. 3.2 was taken to be $\rho_s = 1850$ kg/m^3, as discussed by Puri et al. (1993). The temporal derivative in Eq. 3.2 was found from three-point least-squares fits of the argument of the derivative, $\rho_s f_s/\rho$ (see computer program listing in Appendix D). The typical uncertainty (95% confidence) of determining w_g from Eq. 3.2 is 41% (see Appendix A).

Based on existing observations, soot growth was associated with acetylene concentrations. In particular, observations of premixed flames generally correlate soot growth rates with acetylene concentrations (Bockhorn et al. 1982, 1984; Harris and Weiner 1983a, 1983b, 1984; Ramer et al. 1986; Tesner 1991). Additionally, soot formation ended when acetylene disappeared and acetylene was the only hydrocarbon present in significant quantities within the present acetylene diffusion flames, as noted earlier. Thus, the following expression for w_g was studied:

$$w_g = k_g(T)\,[C_2H_2]^n \tag{3.4}$$

where $k_g(T)$ normally is an Arrhenius expression. Evaluation of Eq. 3.4 using the present measurements for various values of n, however, suggested no temperature dependence for k_g. This behavior implies a small activation energy, which agrees with past suggestions of low activation energies for recombination-like soot growth processes (Haynes and Wagner, 1981; Bockhorn et al. 1982, 1984; Tesner 1958, 1960, 1991). Thus, a correlation of present measurements was sought by simply plotting w_g as a function of the molar concentration of acetylene as illustrated in Fig. 3.10 (see data summary in Table B.3 of Appendix B). Present test conditions yielded a range of acetylene concentrations of roughly $6x10^{-6}$-$1x10^{-3}$ kg-mol/m^3, a range of temperatures of 1250-2100 K, and a corresponding range of the observed soot growth velocities of roughly 0.01-10 μm/s. Over this range of conditions an empirical fit of the measurements was found which is illustrated in Fig. 3.10. Based on the units w_g (kg/m^2s) and $[C_2H_2]$ (kg-mol/m^3), this fit can be expressed as:

$$w_g = 4560\,[C_2H_2]^{1.65} \tag{3.5}$$

The standard deviation of the power in Eq. 3.5 is 0.18, and the correlation coefficient of the fit is 0.89. Thus, present gross measurements of soot growth exhibit an order with respect to the concentration of acetylene (95% confidence) within the range 1.29-2.01.

The order of soot growth with respect to acetylene concentrations observed in Fig. 3.10 is high compared to past suggestions based on measurements of soot growth in premixed flames (Bockhorn et al. 1982, 1984; Harris and Weiner 1983a, 1983b, 1984; Ramer et al. 1986). The premixed flame data from these references has been plotted in Fig. 3.10 to provide a direct comparison with present measurements (no prior study of soot growth in diffusion flames is sufficiently complete to allow inclusion in Fig. 3.10). The fuels used in the premixed flame experiments were propane, ethylene, toluene and

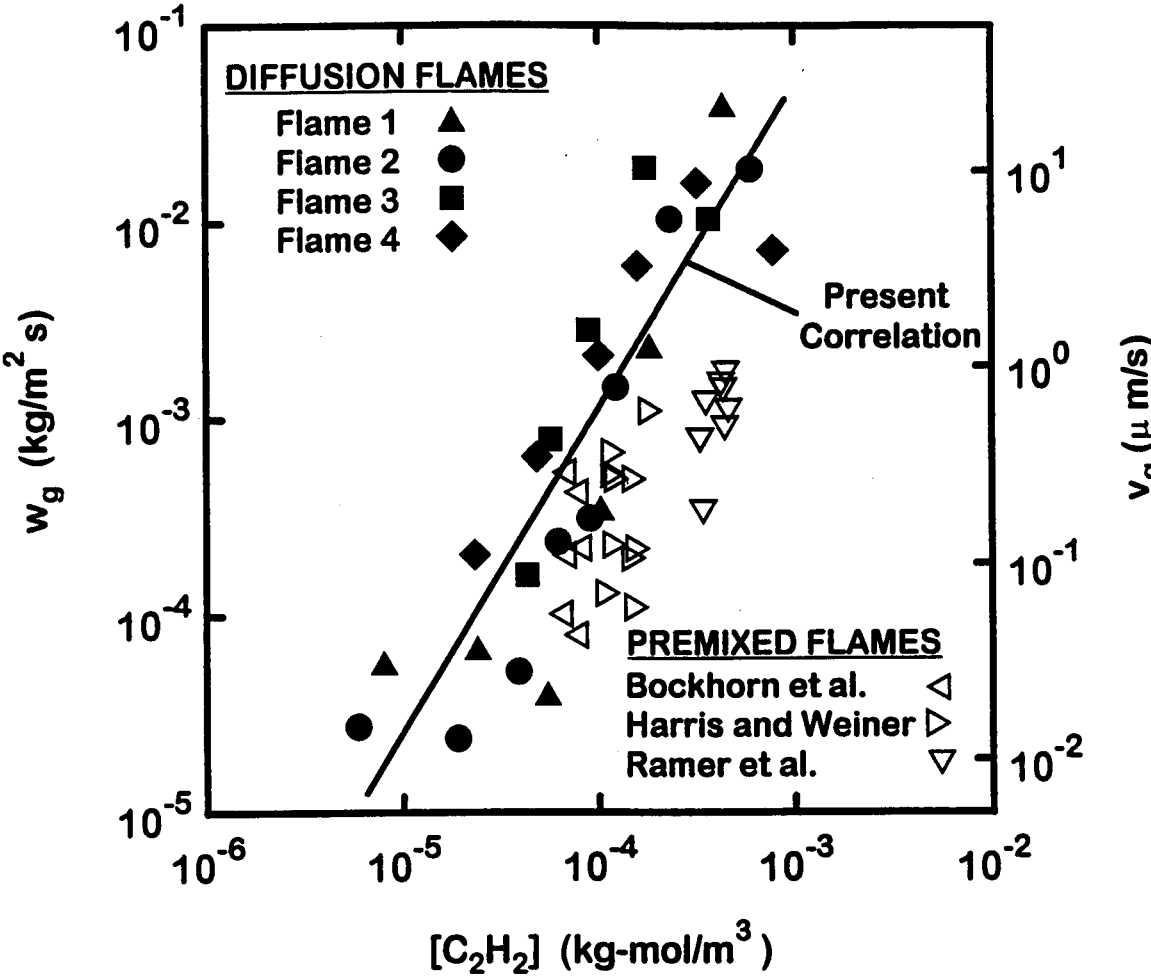

Figure 3.10 Gross Soot Growth Rates for Acetylene/Air Diffusion Flames

methane, although acetylene dominated hydrocarbon concentrations in the region where soot growth measurements were made. The experiments of Bockhorn et al. (1982, 1984) involved a pressure of 0.15 atm. while the remaining experiments were carried out at atmospheric pressure. Estimates of soot surface areas for the premixed flames were obtained from original sources, and were based on analysis of extinction and scattering measurements. Finally, rates of soot growth in premixed flames exhibit an effect of age, with the rate of growth decreasing as the residence time increases for a given ambient environment, as discussed earlier. This behavior is indicated by the vertical span of the premixed flame data in Fig. 3.10, with the largest w_g representing new soot at relatively small residence times (4-15 ms).

The premixed flame data illustrated in Fig. 3.10 is qualitatively similar to present measurements in diffusion flames. In particular, the growth rates of new soot in premixed flames approach the growth rates observed in the present diffusion flames (which have comparable residence times). However, the growth rates in the premixed flames consistently are lower than in the diffusion flames. While an effect of age could be responsible for this behavior, the apparent reduction of growth rates in premixed flames also could be caused by overestimation of the soot surface area due to use of simplified soot optical theories, with uncertainties about soot refractive indices being a contributing factor (Köylü and Faeth 1994). In particular, Harris and Weiner (1983a, 1983b) find that direct B.E.T. soot surface area measurements (see Brunauer et al. (1938) for a description of this technique) were roughly a factor of two lower than the optical measurements, which is sufficient to explain the discrepancy between their new soot growth data and the present measurements. Additionally, the acetylene concentration ranges of the individual premixed flame studies are rather narrow to provide an accurate determination of the reaction order with respect to acetylene concentration, while complications due to effects of aging prevent merging the various premixed flame results to find the reaction order with respect to acetylene.

A concern about present measurements of soot growth in diffusion flames is that effects of soot oxidation could mask the actual growth behavior found from the measurements illustrated in Fig. 3.10, particularly when acetylene concentrations become small near the end of the soot growth region. This possibility prompted consideration of soot oxidation by O_2, CO_2, H_2O, and OH using present measurements of species concentrations and temperatures along the axis. OH concentrations should remain small as long as fuel gases are present (Miller et al. 1992; Smyth et al. 1985), which implies that the OH soot oxidation mechanism of Neoh et al. (1980) can be ignored in the soot growth region. Conversely, soot oxidation by O_2, and to a lesser degree by CO_2 and H_2O, were determined to be significant in the soot growth region. In particular, the presence of oxygen mole fractions of roughly 0.01 in the soot growth region, see Figs. 3.6-3.9 and the generalized state relationships of Sivathanu and Faeth (1990c), imply significant potential for direct reaction between oxygen and soot. Based on the recent discussion of soot oxidation by Puri et al. (1994), the direct oxidation of soot in the soot growth region was estimated using the rate expression of Nagle and Strickland-Constable (1962), which was confirmed later by Park and Appleton (1973). Additionally, the presence of CO_2 and H_2O mole fractions of up to 0.07 in the soot growth region provides some potential for soot reaction with CO_2 and H_2O; these mechanisms were treated using the approach described in Libby and Blake (1979) and Johnstone et al. (1952), respectively, but the resulting corrections of w_g were relatively small. In order to check the combined O_2, CO_2 and H_2O soot oxidation mechanisms, the predictions were compared to present measurements of soot oxidation rates (i.e. negative growth using Eq. 3.2) in the fuel-lean portions of Flames 1-4; on average, predictions exceeded measurements by a factor of roughly 7:1. Based on this observation, present estimates of soot oxidation rates probably are somewhat overestimated; this effect will be dealt with subsequently.

The present soot growth rates, corrected for soot oxidation in the soot growth region, are plotted as a function of acetylene concentration in Fig. 3.11. The correction for soot oxidation only becomes significant near the end of the soot growth region when observed growth rates become small. The net effect of the correction is to yield the

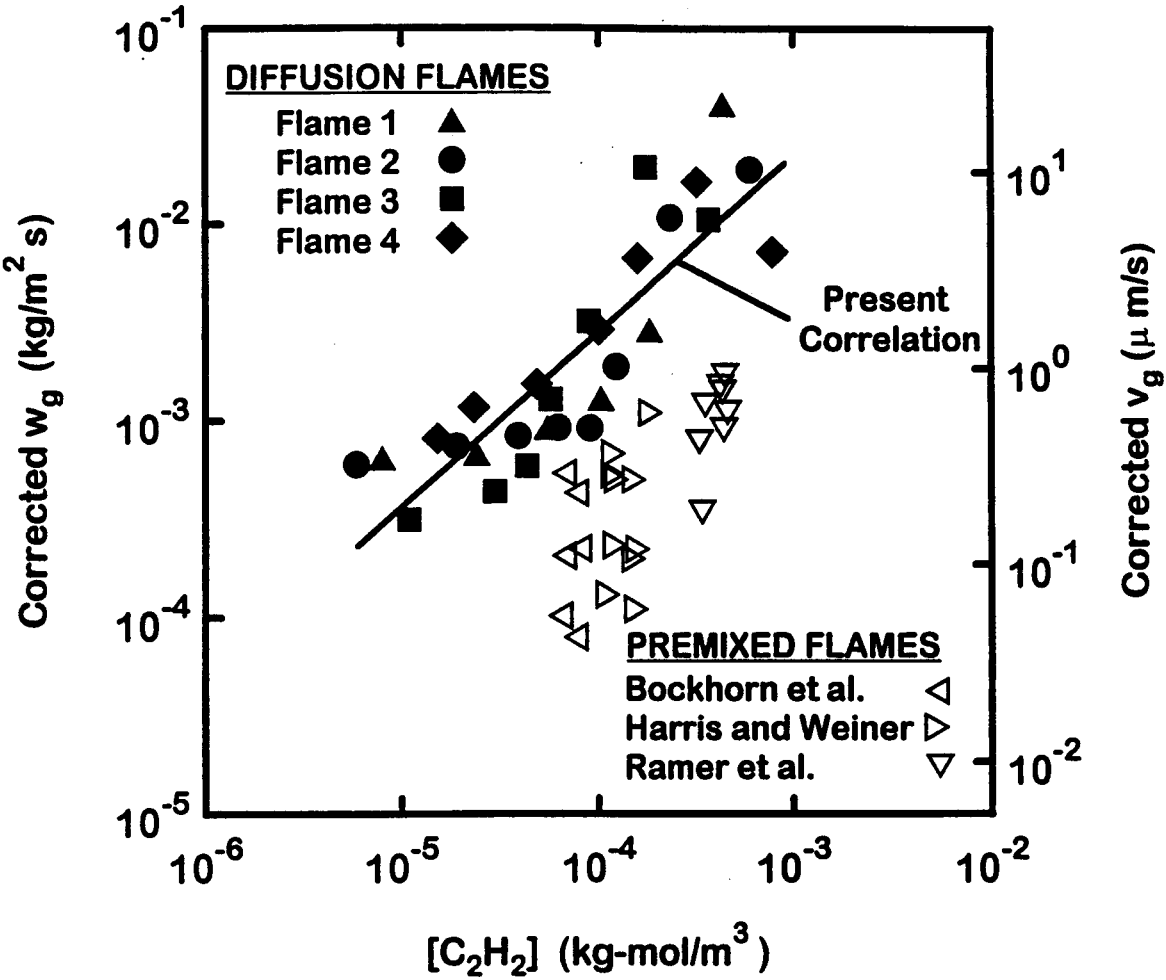

Figure 3.11 Net Soot Growth Rates for Acetylene/Air Diffusion Flames

following best fit correlation, based on the same units as Eq. 3.5, which is shown on the plot:

$$w_g = 11.0\,[C_2H_2]^{0.90} \tag{3.6}$$

The standard deviation of the power in Eq. 3.6 is 0.10, and the correlation coefficient of the fit is 0.87. Thus, the correlated data exhibit an order with respect to acetylene (95% confidence) within the range 0.70-1.10, which is not statistically different from unity. In addition, growth rate displayed no statistically significant variation with temperature, implying a negligible activation energy. Prompted by these observations, the corrected data were used to estimate a collision efficiency for acetylene, which is defined as the ratio of the corrected growth rate to the growth rate that would result if each C_2H_2/soot-surface collision added a soot mass of 24 kg/kgmol, finding a collision efficiency of 0.41% with an uncertainty (95% confidence) of 0.12% over the present test range. It also was determined that the corrections for oxidation had only a small impact on present estimates of soot growth collision efficiency; for example, eliminating measurements where the oxidation corrections exceeded 50% of the observed growth rate yielded a collision efficiency of 0.47%, which is not statistically different from the earlier estimate. Furthermore, this entire process was repeated using the results of Bradley et al. (1984) for carbon oxidation by CO_2 and H_2O, along with the results of Nagle and Strickland-Constable (1962) for carbon oxidation by O_2, yielding a soot growth collision efficiency of 0.47%, which also is not statistically different from the earlier result. Additionally, in contrast to existing premixed flame measurements, also plotted on Fig. 3.11, where age causes soot growth collision efficiencies to progressively decrease (Bockhorn et al. 1982, 1984; Harris and Weiner 1983a, 1983b, 1984; Ramer et al. 1986), no effect of age was observed for present measurements of collision efficiencies in diffusion flames (for a residence time range of 3-15 ms). Finally, the oxidation corrections cause an increase in the differences between the growth rates in the present diffusion flames and new soot in

premixed flames (cf., Fig. 3.10), however, these differences still are comparable to effects of uncertainties in optical estimates of soot surface areas for premixed flames, discussed earlier. Nevertheless, uncertainties about estimates of soot oxidation rates in diffusion flame environments (Puri et al. 1994), as well as potential effects of soot age on growth rates in both premixed (Bockhorn et al. 1982, 1984; Harris and Weiner 1983a, 1983b, 1984; Ramer et al. 1986) and diffusion flames environments, clearly merit further study in order to better define the soot growth process.

3.3.3 Soot Nucleation

Present measurements along the axis of the Flames 1-4 also were used to study the mechanism of soot nucleation. The soot nucleation rate, w_n, was defined as the rate of increase of the number of primary particles per unit volume and time. Based on the same assumptions used to determine soot growth rates from Eq. 3.2, the expression for soot nucleation rates for motion along a streamline becomes:

$$w_n = \rho d(n_p/\rho)/dt \tag{3.7}$$

The soot nucleation rates were correlated in terms of acetylene concentrations, similar to the earlier considerations of soot growth, i.e.

$$w_n = k_n(T)[C_2H_2]^n \tag{3.8}$$

where $k_n(T)$ is an Arrhenius expression. The typical uncertainty (95% confidence) of determining $k_n(T)$ from Eq. 3.8 is 62% (see Appendix A). Equation 3.7 was evaluated based on the present measurements by finding ρ and determining the argument of the derivative while locally smoothing the data using three-point least squares fits, in the same manner as for soot growth (see computer program listing in Appendix D). The measurements indicated that first-order behavior for nucleation was reasonable, in

agreement with earlier assessments of soot nucleation for various soot formation processes (Haynes and Wagner 1981; Tesner 1958, 1960; Leung et al. 1991).

Present soot nucleation measurements are plotted as a function of temperature, assuming first-order kinetics, in Fig. 3.12. The range of the present data is as follows: acetylene concentrations of $6x10^{-6}$-$1x10^{-3}$ kg-mol/m^3, temperatures of 1000-2100 K and k_n of 10^{-6}-10^{-2} s^{-1}. The scatter of the soot nucleation data is appreciable due to the strong sensitivity of n_p to d_p through Eq. 3.1. Based on the units w_n (kg-mol/m^{3}s), $[C_2H_2]$ (kg-mol/m^3) and T(K), the present measurements yield the following first-order nucleation rate correlation:

$$w_n = 10.6[C_2H_2]\exp(-16100/T) \tag{3.9}$$

with a standard deviation of the activation temperature of 1340 K, an activation temperature range (95% confidence) of 13300-18800 K and a correlation coefficient of the fit of 0.92. The activation energy corresponding to the activation temperature of Eq. 3.9 is modest, 32 kcal/gmol, which is not particularly surprising for recombination-like process such as soot nucleation (Haynes and Wagner 1981; Tesner 1958, 1960; Leung et al. 1991).

Leung et al. (1991) have evaluated soot nucleation data based on optical measurements from various sources and suggest, using the same units as Eq. 3.9:

$$w_n = 10000\,[C_2H_2]\exp(-21100/T) \tag{3.10}$$

which implies an activation energy of 42 kcal/gmol. Equation 3.10 also is plotted in Fig. 3.12 where it yields estimates of w_n that are roughly an order of magnitude larger than the present measurements. Discrepancies of this magnitude are not surprising, however, in view of the past uncertainties of interpreting optical measurements to find primary particle sizes needed to evaluate Eq. 3.9 (discussed in connection with the soot growth

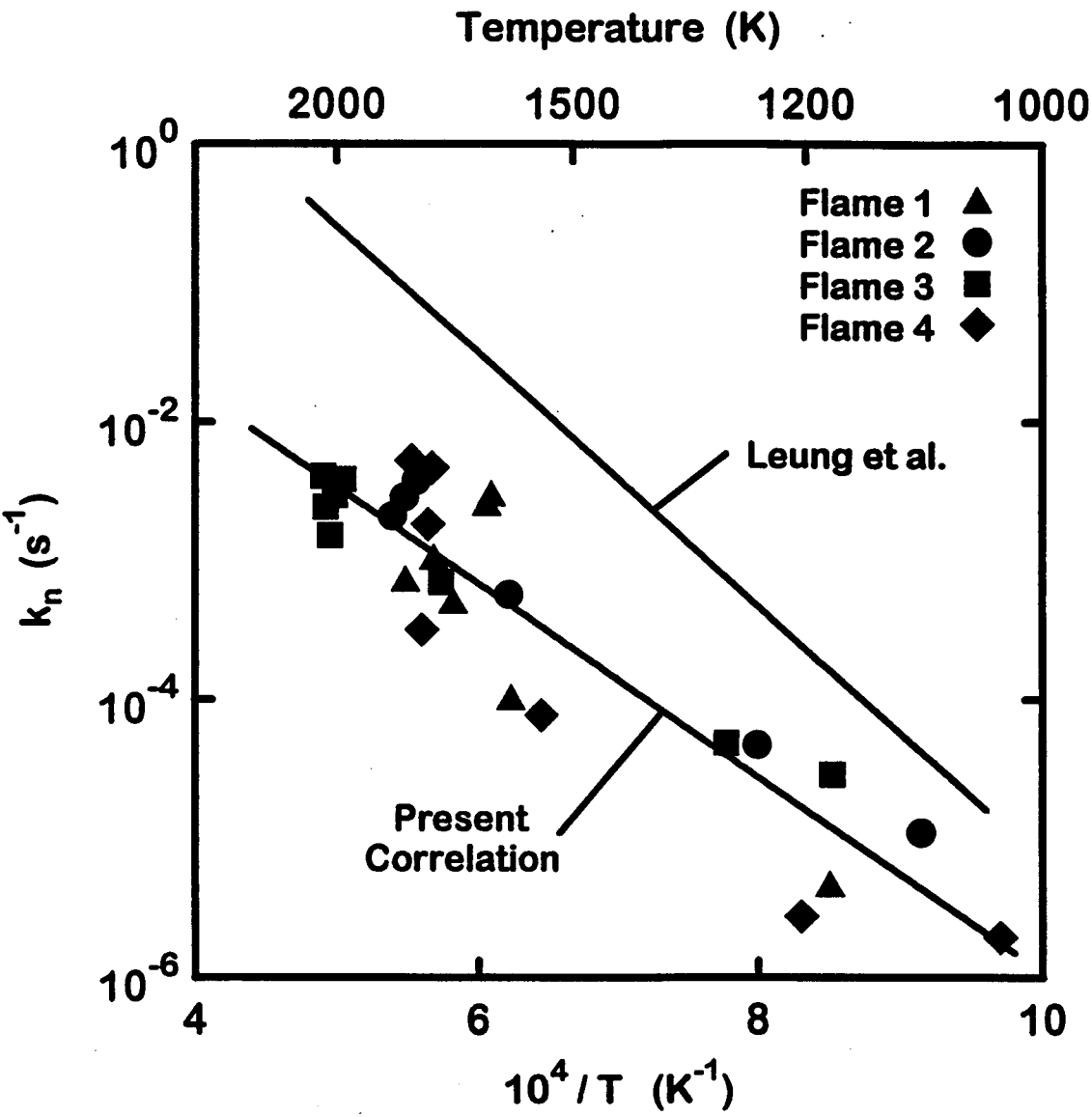

Figure 3.12 Soot Nucleation Rates for Acetylene/Air Diffusion Flames

measurements for premixed flames). Clearly, additional measurements are needed to better establish soot nucleation properties in diffusion flames, as well as the role of the translucent objects in the nucleation process.

3.4 Conclusions

Flame structure and soot processes were studied in weakly-buoyant, acetylene/air, laminar jet diffusion flames at 0.125-0.250 atm, emphasizing processes along the axis where soot first nucleates near the cool core of the flow and experiences a monotonic decrease of mixture fraction along a soot path line, similar to behavior in nonbuoyant flames (Chapter 2). The major conclusions of the study are as follows:

1. Significant soot nucleation and growth began when temperatures reached roughly 1250 K, and ended when acetylene disappeared at a fuel-equivalence ratio of roughly 1.4. Maximum primary soot particle diameters along the flame axes were observed near the beginning of soot formation due to the combined effects of soot nucleation and growth.

2. Present soot growth measurements, corrected for effects of soot oxidation, yielded first-order behavior with respect to acetylene with a collision efficiency of 0.41%. Present soot growth measurements in diffusion flames exhibited negligible effects of soot age with rates somewhat larger (roughly a factor of two) than past observations of new soot in premixed flames due to Bockhorn et al. (1982, 1984), Harris and Weiner (1983a, 1983b, 1984) and Ramer et al. (1986). However, uncertainties concerning soot oxidation rates in diffusion flames and effects of soot age, in both diffusion and premixed flames, must be resolved in order to better define soot growth processes.

3. Soot nucleation was roughly first-order with respect to acetylene concentration, with a modest activation energy of roughly 32 kcal/gmol; however, these

nucleation rates were roughly an order of magnitude smaller, with a smaller activation energy, than an expression proposed by Leung et al. (1991) based on earlier results in the literature. It is suspected that the approximations used by Leung et al. (1991) to estimate soot surface area from optical measurements are responsible for the discrepancies but the issue merits further study.

CHAPTER IV

SOOT FORMATION IN HYDROCARBON/AIR DIFFUSION FLAMES

4.1 Introduction

This phase of the present experimental study of the structure and soot properties of round laminar jet diffusion flames was undertaken to gain a better understanding of soot formation (nucleation and growth) in diffusion flames. The main objective was to extend the work concerning soot formation in laminar acetylene/air jet diffusion flames to consider hydrocarbon fuels other than acetylene.

Past studies of soot processes in flames were summarized in the introduction of Chapter 3. A major limitation of these studies, however, is that both soot properties and the local flame environment were not sufficiently defined for detailed consideration of soot formation (nucleation and growth) processes. Thus, work completed during an earlier phase of the present investigation and discussed in Chapter 3, as well as a later study by Lin et al. (1995) undertook extensive measurements in laminar acetylene/air jet diffusion flames in order to study soot nucleation and growth. These measurements included soot volume fractions, temperatures, soot structure, concentrations of major gas species and velocities. It was found that acetylene was the dominant hydrocarbon species in the soot formation region of the acetylene/air flames, with concentrations generally 2-4 orders-of-magnitude greater than the next most abundant hydrocarbon, which was methane (Lin et al. 1995). Soot formation began when temperatures exceeded 1250 K, and ended when fuel-equivalence ratios decreased to roughly 1.4, where the

concentrations of acetylene and other hydrocarbons became small. Soot growth rates were comparable to past observations of new soot in premixed flames. Soot growth was first-order with respect to acetylene concentration, with a negligible activation energy, yielding an acetylene/soot collision efficiency of 0.39% after correcting for effects of soot oxidation. Finally, soot nucleation rates were correlated as a first-order acetylene reaction, with a relatively modest activation energy of 39 kcal/gmol (Lin et al. 1995).

In view of this status, a major unresolved issue is the nature of soot formation processes in laminar diffusion flames involving hydrocarbon fuels other than acetylene. In particular, information is needed about the concentrations of various hydrocarbons in the soot formation region, and their impact on soot growth and nucleation. Thus, the objectives of the present study were to measure flame and soot properties in laminar diffusion flames of hydrocarbons other than acetylene burning in air, and to use these results to gain a better understanding of soot growth and nucleation. The experiments were limited to measurements along the axes of laminar jet diffusion flames at pressures of 25-99 kPa, considering ethane, propane, n-butane, ethylene, propylene and 1,3-butadiene burning in air.

4.2 Experimental Methods

4.2.1 Apparatus

Two test arrangements were used for the present experiments: (1) a buoyant laminar jet diffusion flame burner operating at atmospheric pressure, identical to the arrangement used by Gore and Faeth (1986), that was used for weakly-sooting fuels like ethane, propane, n-butane and ethylene; and (2) a weakly-buoyant laminar jet diffusion flame burner operating at low pressure, identical to the arrangement used for the acetylene/air study and discussed in Chapter 3, that was used for strongly-sooting fuels like propylene and 1,3-butadiene.

The atmospheric-pressure burner involved upward injection of fuel from a 14.3 mm diameter port surrounded by a concentric air flow from a 102 mm diameter port. The flow passages contained several layers of beads terminated by a honeycomb (1 mm cell size by 10 mm long) to provide a uniform flow. The flow-field was shielded by fine mesh screen and an outer plastic curtain in order to control effects of drafts. Fuel and air flow rates were measured with rotameters, calibrated in turn by a wet-test meter. The burner assembly was traversed with a positioning accuracy of 0.1 mm in order to accommodate rigidly-mounted optical instruments.

4.2.2 Instrumentation

The instrumentation was the same for both test arrangements, adopting methods already described in Chapter 3. Soot volume fractions were measured by deconvoluting laser extinction measurements for chord-like paths through the flames, similar to past work (Lin et al. 1995; Santoro et al. 1983; Gore and Faeth 1986). The data were reduced assuming that soot optical properties satisfied the small-particle (Rayleigh) scattering limit, which was justified because scattering levels were small (Köylü and Faeth 1994). These computations employed a soot refractive index of 1.57 - 0.56i, which was taken from Dalzell and Sarofim (1969) similar to past work (Lin et al. 1995; Santoro et al. 1983; Gore and Faeth 1986) as justified by recent *in situ* measurements in buoyant diffusion flames (Köylü and Faeth 1994). The experimental uncertainties of these measurements (95% confidence) are estimated to be less than 10% for $f_S > 0.1$ ppm.

Temperatures were measured using multiline emission in regions where soot was present and using thermocouples in regions where soot was absent. The multiline emission measurements were identical to Chapter 3 and Lin et al. (1995), i.e. they involved deconvoluting spectral radiation intensity measurements for chord-like paths through the flames. The temperatures were found from measurement at three line pairs: 600/750, 700/830 and 600/830 nm. Temperature differences between the average and

any of the line pairs were less than 30 K. The thermocouple measurements involved a bare wire Pt/Pt-10% Rh thermocouple junction having a diameter of 270 μm; these measurements were corrected for radiation errors. Both temperature measurements involved experimental uncertainties (95% confidence) less than 50 K (see Chapter 3 for a discussion of these error estimates).

Soot structure was measured using thermophoretic sampling and analysis by transmission electron microscopy (TEM), similar to earlier work (Lin et al. 1995; Megaridis and Dobbins 1988, 1989; Köylü and Faeth 1994). Effects of soot aggregate size cause a negligible sampling bias for present test conditions (Köylü and Faeth 1994; Rosner et al. 1991). As usual, soot consisted of nearly spherical and monodisperse primary particles (standard deviation of d_p less than 20%), collected into aggregates having widely varying numbers of primary particles per aggregate. Primary particle diameters were measured for more than 60 particles at each location to yield experimental uncertainties (95% confidence) for d_p less than 10%. The number of primary soot particles per unit volume was then found from the other measurements, as follows:

$$n_p = 6 f_s / (\pi d_p^3) \tag{4.1}$$

In view of the experimental uncertainties for f_s and d_p, Eq. 4.1 implies experimental uncertainties (95% confidence) for n_p less than 32% for $f_s > 0.1$ ppm.

Gas compositions were measured by sampling and analysis using gas chromatography similar to past work (Lin et al. 1995; Gore and Faeth 1986). A stainless-steel radiatively cooled sampling probe was used, having a port diameter of 2.1 mm. Gas species resolved by the analysis included N_2, O_2, CO_2, CO, H_2O, H_2, CH_4, C_2H_2, C_2H_4, C_2H_6, C_3H_8, C_3H_6, C_4H_{10} and C_4H_6. Experimental uncertainties (95%

confidence) of these measurements were less than 15% for mole fractions greater than 100 ppm.

Streamwise velocities along the flame axes were measured using laser velocimetry (LV). This involved a dual-beam forward-scatter arrangement with the flow seeded with aluminum oxide particles, similar to past work (Lin et al. 1995; Gore and Faeth 1986). Experimental uncertainties (95% confidence) of streamwise velocities are estimated to be less than 5%.

4.2.3 Test Conditions

The six test flames are summarized in Table 4.1 and four of them are shown in Fig. 4.1. All the flames were laminar over the measurement region. The atmospheric-pressure burner was used to test the lightly-sooting fuels (C_2H_6, C_3H_8, C_4H_{10} and C_2H_4) using visible flame lengths of roughly 70 mm. These flames had fuel-port Reynolds and Froude numbers of 34-43 and 0.00068-0.0033, respectively, and were strongly buoyant, i.e., velocities along the axes were relatively independent of burner exit velocity. Radiant heat loss fractions were in the range 16.1-25.9% of the lower heating value of the fuel (LHV), progressively increasing with the propensity of the fuel to form soot.

The low-pressure burner, operating at a pressure of 25.3 kPa, was used to test the heavily-sooting fuels (C_3H_6 and C_4H_6) using visible flame lengths of roughly 50 mm. In addition to the low pressure, it was necessary to dilute the 1,3-butadiene fuel with nitrogen in order to achieve manageable levels of soot concentrations in the flame. These flames had fuel-port Reynolds and Froude numbers of 87-107 and 13-21, respectively, and were weakly buoyant, i.e., velocities along the axis were closely correlated with burner exit velocities over the region of interest. Radiant heat loss fractions were in the range 26.0-29.2% of the LHV of the fuel.

Table 4.1 Hydrocarbon Flame Summary

Test Flame	1[a]	2[a]	3[a]	4[a]	5[b]	6[b]
Fuel[c]	C_2H_6	C_3H_8	C_4H_{10}	C_2H_4	C_3H_6	C_4H_6
Pressure (kPa)	98.8	98.8	98.8	98.8	25.3	25.3
Burner flow (% fuel by vol.)	100	100	100	100	100	48
Fuel flow rate (cc/s)	3.38	2.00	1.52	3.36	5.31	3.20
N_2 flow rate (cc/s)	---	---	---	---	---	3.43
Air flow rate (cc/s)	269	269	269	269	710	385
Burner exit velocity (mm/s)[d]	21.4	12.6	9.5	21.3	635	793
Air velocity (mm/s)[d]	32.8	32.8	32.8	32.8	9.7	5.3
Re(-)[d]	40	40	43	34	107	84
Fr(-)[d]	0.0033	0.0011	0.00064	0.0032	13	21
Rad. heat loss (% LHV)	16.1	21.0	21.3	25.9	26.0	29.2

[a]Laminar round jet diffusion flames in air coflow with a 14.3 mm diameter fuel port, a 102 mm diameter air port, a visible flame length of 70 mm and ambient conditions of 98.8 kPa and 294 K.

[b]Laminar round jet diffusion flame in air coflow with a 3.3 mm diameter fuel port, a visible flame length of 50 mm and a nominal ambient temperature of 294 K.

[c]Burner gas purities by volume as follows: C_2H_6 (99%), C_3H_8 (99.5%), C_4H_{10} (99%), C_2H_4 (99.5%), C_3H_6 (99%), C_4H_6 (99%), N_2 (99.98%).

[d]Nominal average value based on an injection temperature of 294 K and the test pressure.

C_2H_6 C_3H_8 C_4H_{10} C_2H_4

Figure 4.1 Hydrocarbon Flame Photographs

4.3 Results and Discussion

4.3.1 Flame Structure

The present study considered conditions along the axes of the flames, where mixture fractions decrease monotonically with increasing distance from the burner exit. In addition, present measurements were limited to fuel-rich conditions, where the mixture fraction was greater than the stoichiometric mixture fraction. Furthermore, none of the present flames emitted soot. Finally, as noted earlier, soot observed during the present experiments was similar to past observations in flame environments (Lin et al. 1995; Megaridis and Dobbins 1988; Köylü and Faeth 1994) and consisted of nearly monodisperse spherical primary soot particles collected into polydisperse aggregates, similar to the soot aggregates illustrated in Figs. 3.3-3.5.

Flame and soot structure measurements along the axes of the ethane, propane, n-butane and ethylene/air flames at atmospheric pressure are illustrated in Figs. 4.2-4.5; corresponding measurements for the propylene and 1,3-butadiene-nitrogen/air flames at 25.3 kPa are illustrated in Figs. 4.6 and 4.7 (see data summary in Tables C.1 and C.2 of Appendix C). Properties shown include u, d_p, f_s, n_p, f, T and the mole fractions of major gas species, all plotted as a function of distance from the burner exit. Elapsed time, found by integrating the streamwise velocity measurements, also is shown at the top of the plots; the time datum is arbitrarily set at the point where significant soot volume fractions are first observed along the axes.

The distinction between the buoyant (Figs. 4.2-4.5) and weakly-buoyant (Figs. 4.6 and 4.7) flames is most evident from the velocity distributions: the buoyant flames exhibit a progressive increase of velocities over the range of measurements; in contrast, the weakly-buoyant flames exhibit an initial rapid velocity decrease followed by a gradual velocity increase due to buoyancy.

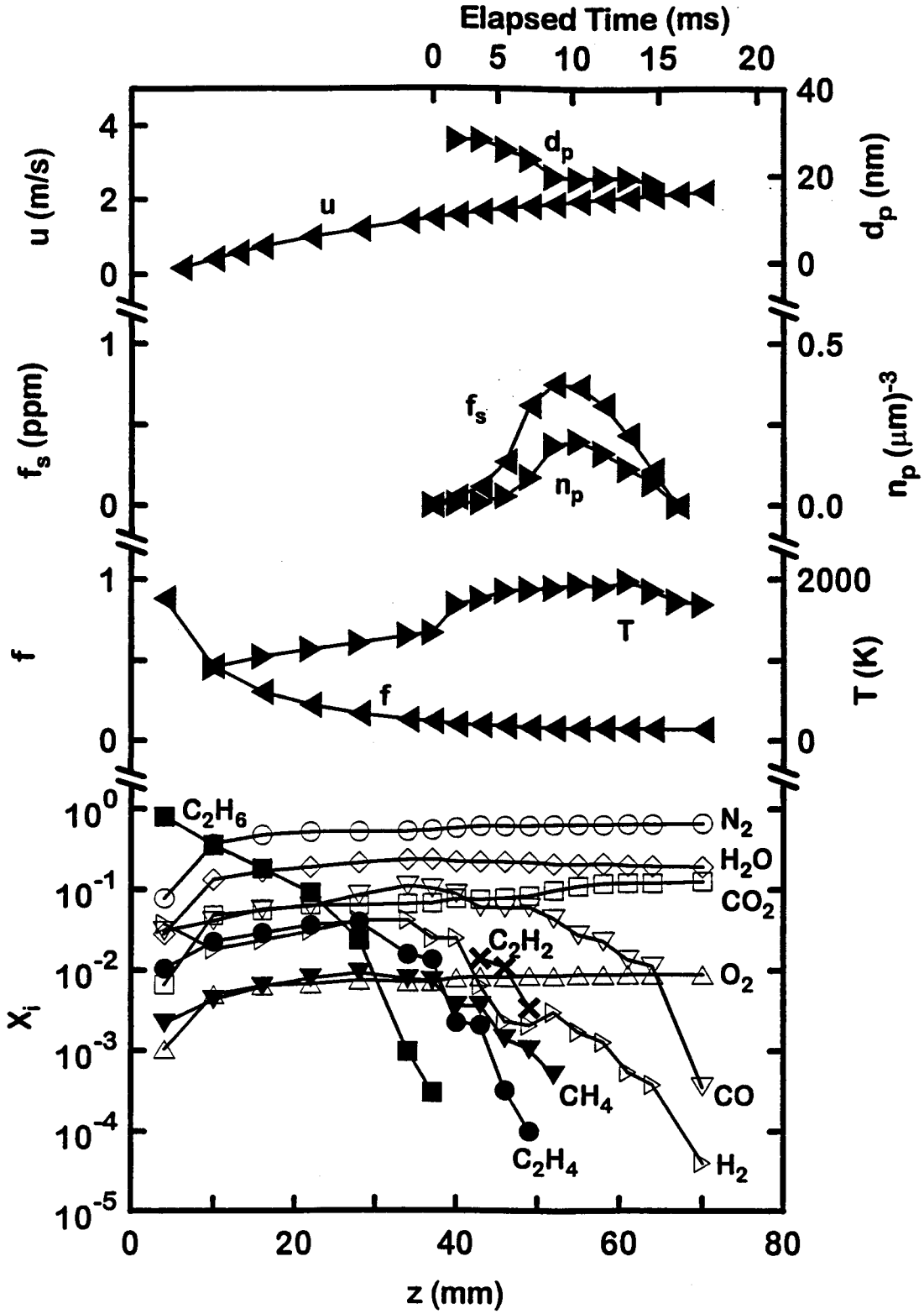

Figure 4.2 Soot and Flame Properties Along the Axis of the Ethane/Air Flame

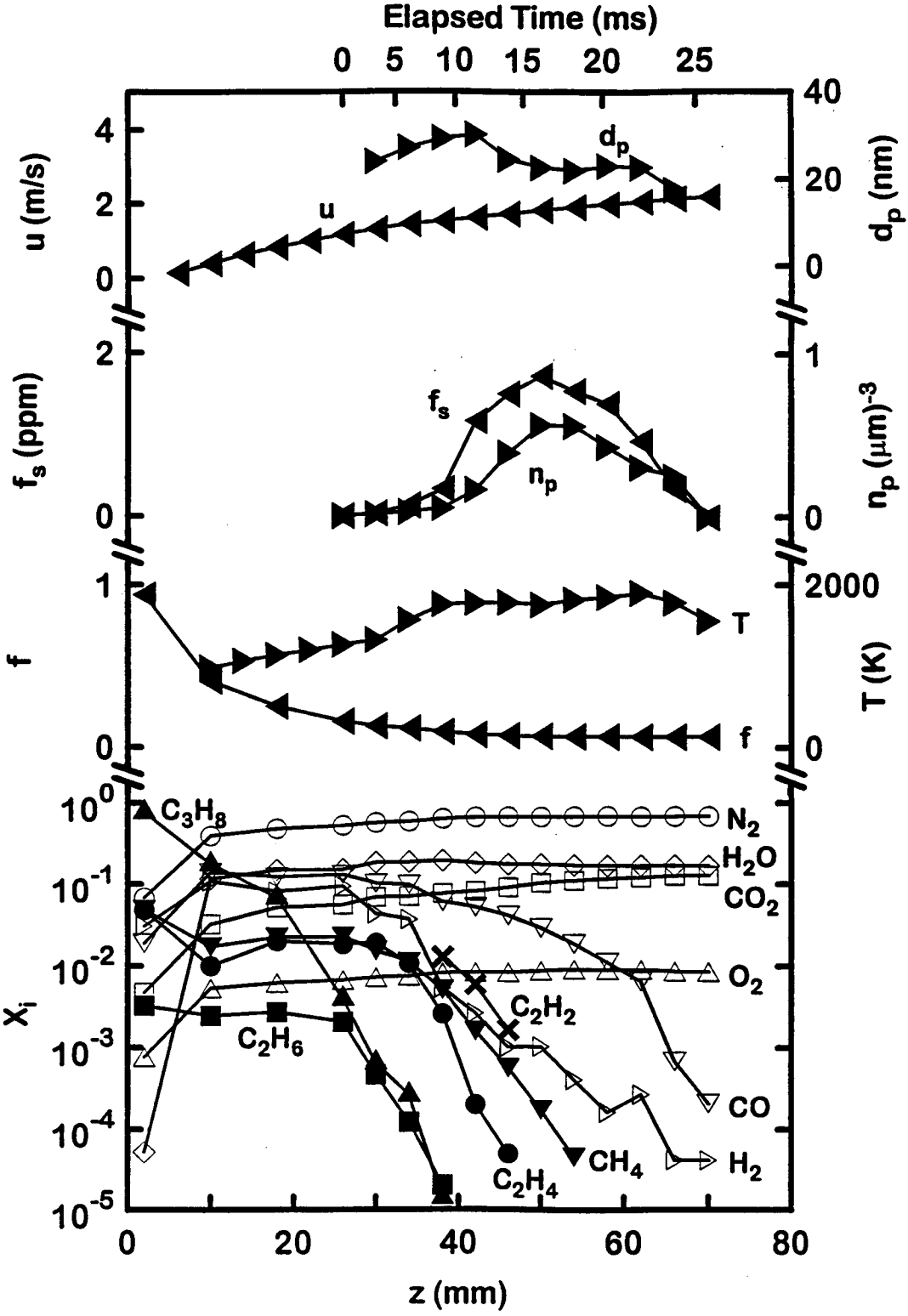

Figure 4.3 Soot and Flame Properties Along the Axis of the Propane/Air Flame

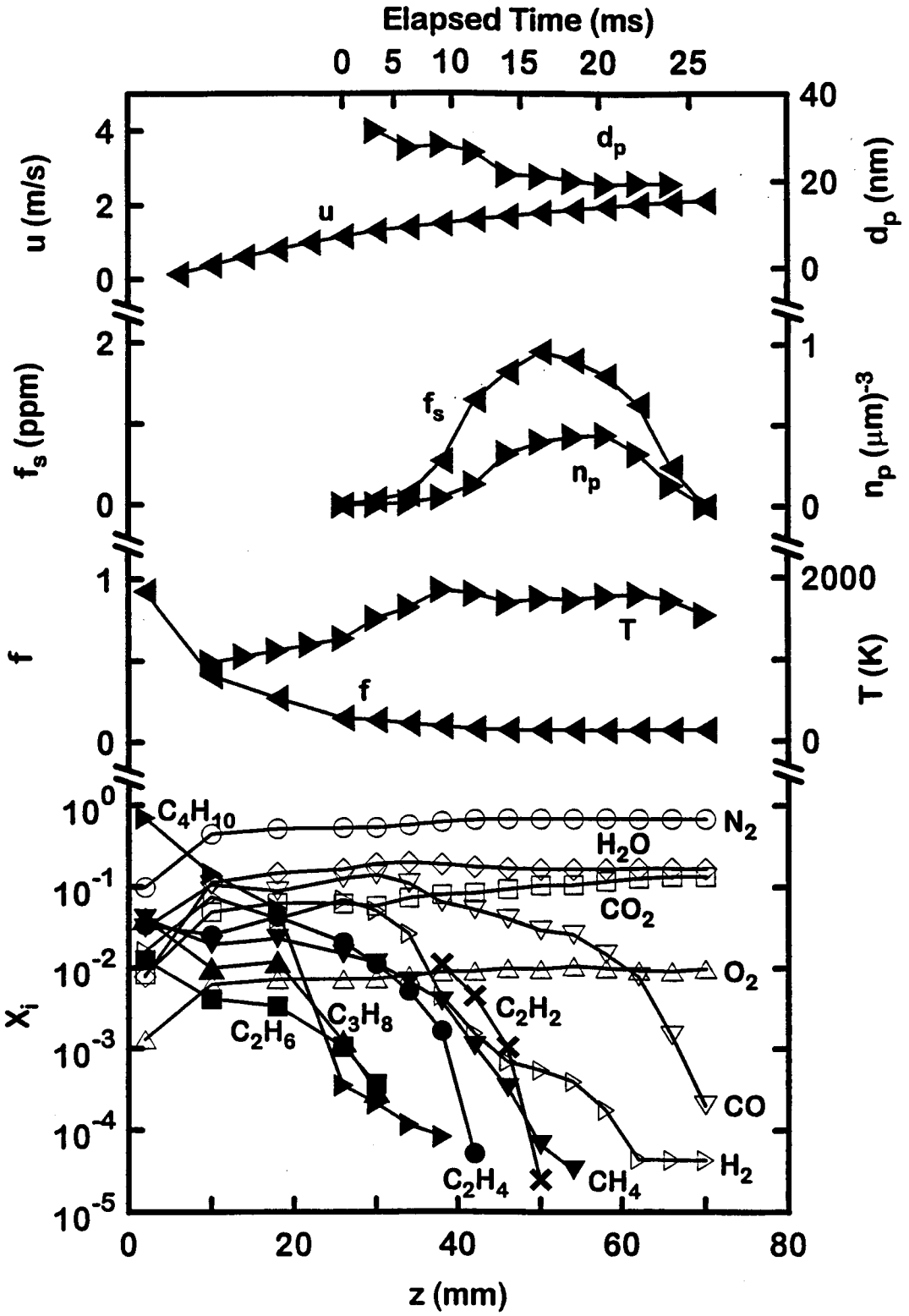

Figure 4.4 Soot and Flame Properties Along the Axis of the n-Butane/Air Flame

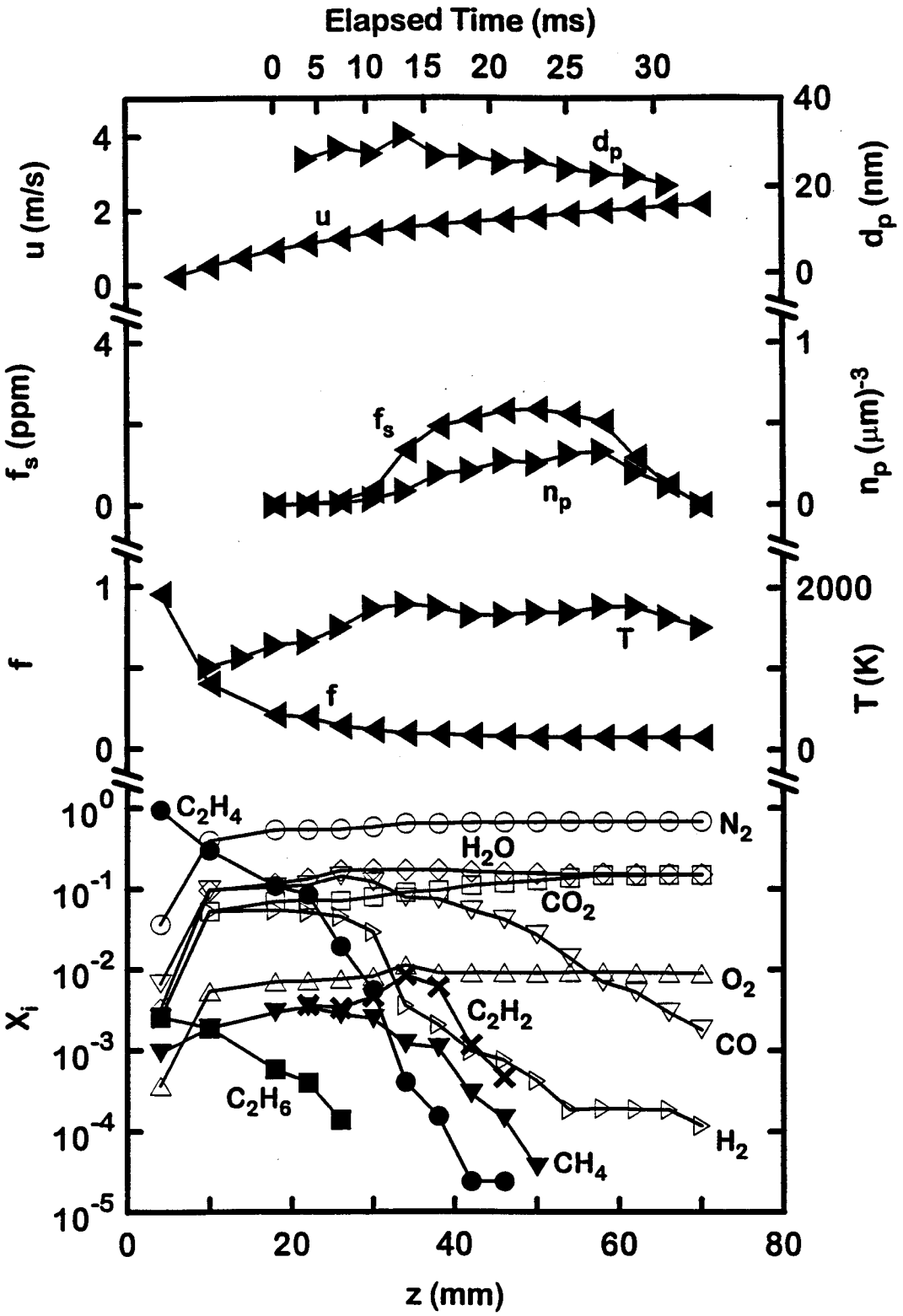

Figure 4.5 Soot and Flame Properties Along the Axis of the Ethylene/Air Flame

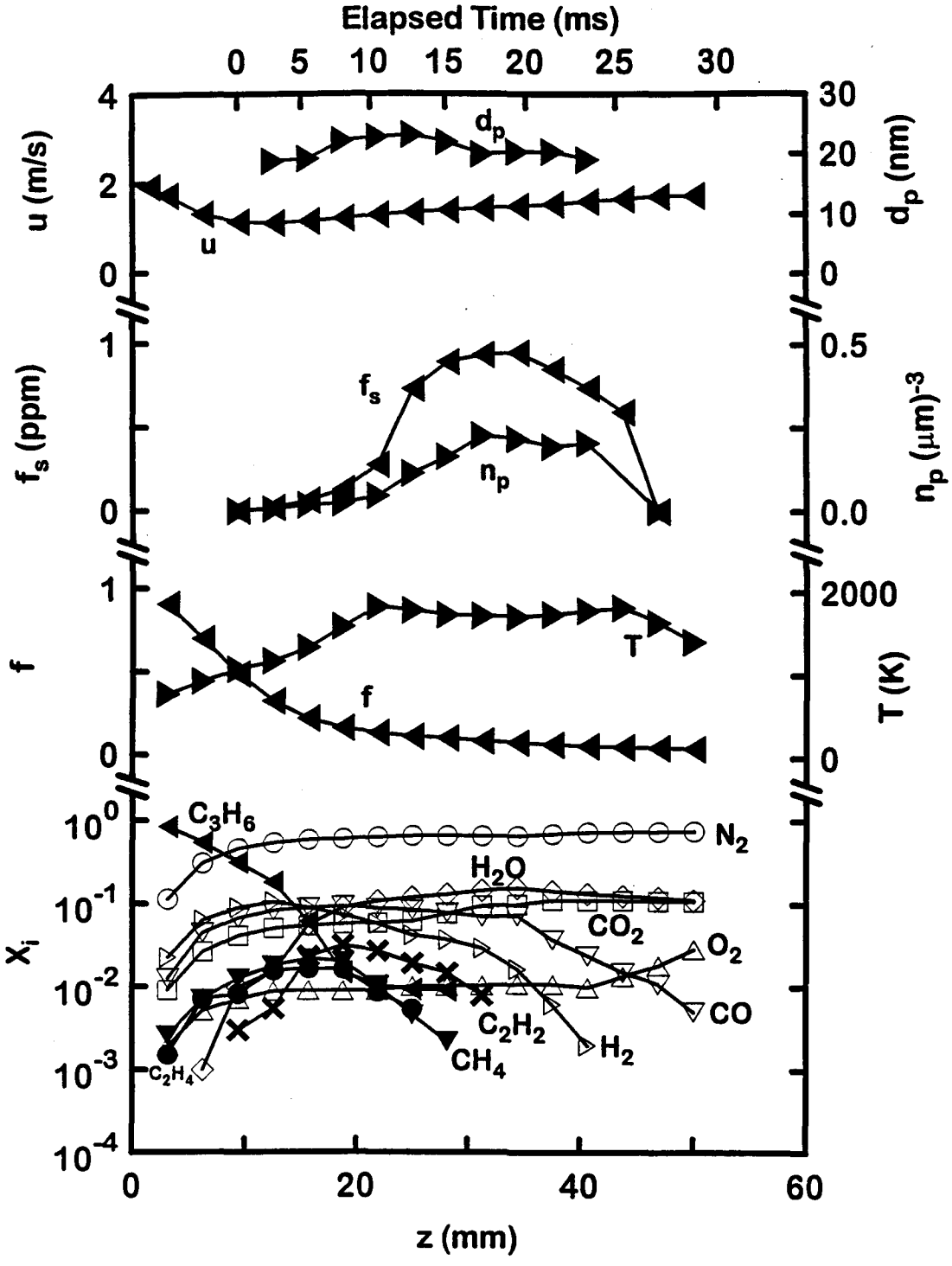

Figure 4.6 Soot and Flame Properties Along the Axis of the Propylene/Air Flame

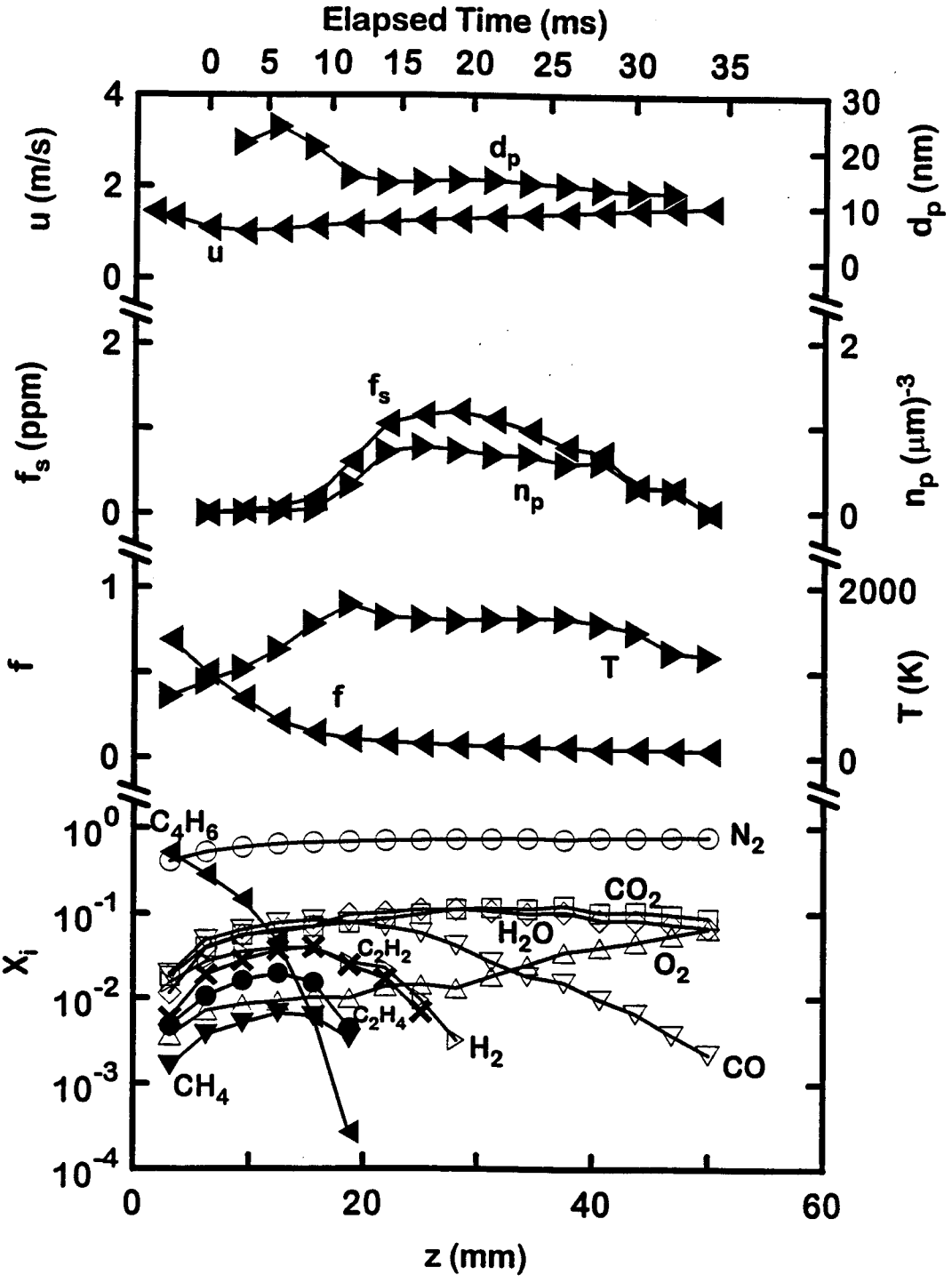

Figure 4.7 Soot and Flame Properties Along the Axis of the 1,3-Butadiene/Air Flame

Similar to other observations along the axes of diffusion flames (Lin et al. 1995), results in Figs. 4.2-4.7 show that d_p generally reaches a maximum well before the end of the soot formation region (which roughly corresponds to the point where f_s reaches a maximum). This behavior is consistent with Tesner's (1958, 1960) early observation that the surface growth of soot persists to temperatures much lower than required for significant soot nucleation. As a result, the limited number of primary soot particles present near the start of the soot formation region undergo rapid growth, becoming large. Subsequently, higher soot nucleation rates (evident from the rapid increase of n_p) create additional primary soot particles whose shorter period of growth implies smaller values of d_p even though overall soot concentration levels continue to increase. This behavior contrasts with behavior along the soot path through the maximum soot volume fraction condition in buoyant laminar jet diffusion flames, where relatively constant values of n_p along the path imply a closer correlation between f_s and d_p (Lin et al. 1995).

The variations of scalar properties along the axes of the present flames is qualitatively similar to earlier results for acetylene/air flames; see Chapter 3 and Lin et al. (1995). Temperature reaches a maximum before the flame tip (the point where the stoichiometric condition is reached at the axis, which generally occurs beyond the region of the data in Figs. 4.2-4.7). This behavior suggests significant effects of continuum radiation from soot, acting to reduce flow temperatures. There also may be contributing effects tending to reduce temperatures within the flames due to incomplete combustion, in view of the presence of significant concentrations of CO and soot. In addition, concentrations of major gas species — N_2, O_2, fuel, CO_2, H_2O, CO and H_2 — all are in reasonably good agreement with the generalized state relationships for hydrocarbon/air flames at atmospheric pressure, proposed in Sivathanu and Faeth (1990c).

The extent of the soot formation region in Figs. 4.2-4.7 also is similar to the earlier observations for acetylene/air flames; see Chapter 3 and Lin et al. (1995). In particular, significant rates of soot formation, evidenced by increasing f_S, are observed only when temperatures exceed 1250 K, in agreement with past observations in diffusion flames (Lin et al. 1995; Haynes and Wagner 1981; Glassman 1988; Howard 1990). The end of soot formation occurs when the concentrations of hydrocarbons become small, well before the flame sheet is reached, at a fuel-equivalence ratio of roughly 1.4, similar to earlier observations in acetylene/air flames; see Chapter 3 and Lin et al. (1995).

Another feature of soot formation in the present flames, is that it is concurrent with soot oxidation, similar to the earlier observations in acetylene/air flames discussed in Chapter 3. This is evident from the presence of soot-oxidizing species, e.g., O_2, CO_2 and H_2O, throughout the soot formation region, see Figs. 4.2-4.7. In fact, soot oxidation is sufficiently robust at fuel-rich conditions for the present flames that the soot disappears before fuel-lean conditions are reached along the axes. The measurements in acetylene/air flames suggest that O_2 concentrations on the order of 1%, invariably present throughout the soot formation region of hydrocarbon/air diffusion flames (Sivathanu and Faeth 1990c), contribute significantly to soot oxidation at fuel-rich conditions. It also is likely that oxidation by OH becomes important at the end of the fuel-rich region, once the hydrocarbons have disappeared and the concentrations of OH begin to increase (Miller et al. 1992; Smyth et al. 1985); unfortunately, measurements of OH were not obtained during the present investigation in order to establish the role of OH oxidation directly. Finally, the soot formation region involves the presence of a variety of light hydrocarbons; the role of these substances in soot growth and nucleation will be considered next.

4.3.2 Soot Growth

Soot growth along the axes of the test flames was studied similar to the acetylene/air flames discussed in Chapter 3. First of all, soot surface growth, rather than nucleation, was assumed to dominate soot mass production; this approximation is

plausible because primary particles become visible when they are relatively small, and exhibit significant increases of d_p and thus particle mass, over the observed period of growth. Next, effects of soot thermophoresis and mass diffusion are small for present conditions; therefore, soot was assumed to convect along streamlines at the local gas velocity. Finally, the surface area available for soot growth was found assuming that soot aggregates consist of mononsized spherical particles that meet at a point. Then the gross rate of soot mass growth along a streamline becomes (see Chapter 3):

$$w_g = \rho_s v_g = (\rho / S)\, d(\rho_s f_s / \rho) / dt\,. \tag{4.2}$$

The soot surface area per unit volume, S, in Eq. 4.2 is found as discussed in Chapter 3:

$$S = \pi d_p^2 n_p = 6 f_s / d_p\,. \tag{4.3}$$

The local gas density in Eq. 4.2 was found from present species concentration and temperature measurements, assuming an ideal gas mixture of the major gas species and neglecting the volume of soot (which is present only at ppm levels). The soot density in Eq. 4.2 was taken to be $\rho_s = 1850$ kg/m^3, as discussed by Puri et al. (1993) and used for the acetylene/air flames. Finally, the temporal derivative in Eq. 4.2 was found, using the same approach as Chapter 3, from three-point least-squares fits of $\rho_s f_s / \rho$ (see computer program listing in Appendix D).

The net soot growth rates found from Eqs. 4.2 and 4.3, and corrected for oxidation (as discussed subsequently), are plotted as a function of distance along the axis for the six test flames in Figs. 4.8-4.13 (see data summary in Table C.3 of Appendix C). In order to locate the soot growth region, nucleation rates for these conditions are shown on the plots as well (the method used to compute nucleation rates and the interpretation of these results will be taken up later). The onset of growth is controlled by the availability of primary soot particles and roughly corresponds with the first observations

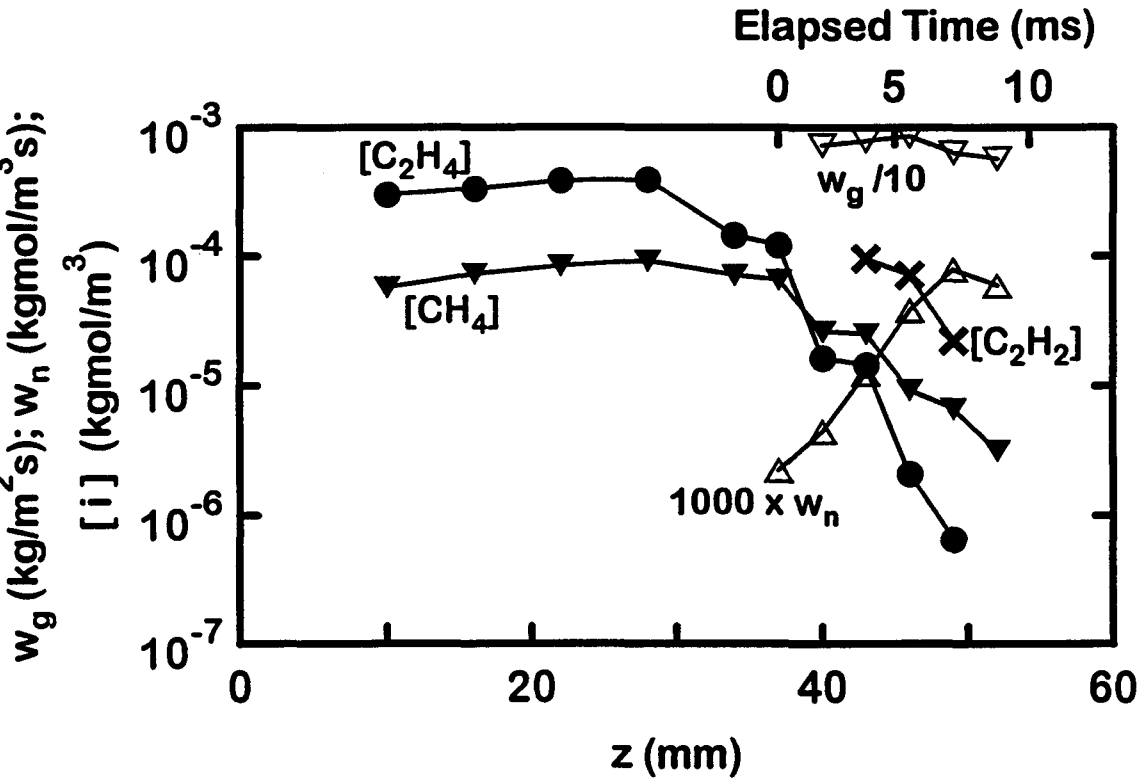

Figure 4.8 Net Soot Growth and Nucleation Rates for the Ethane/Air Flame

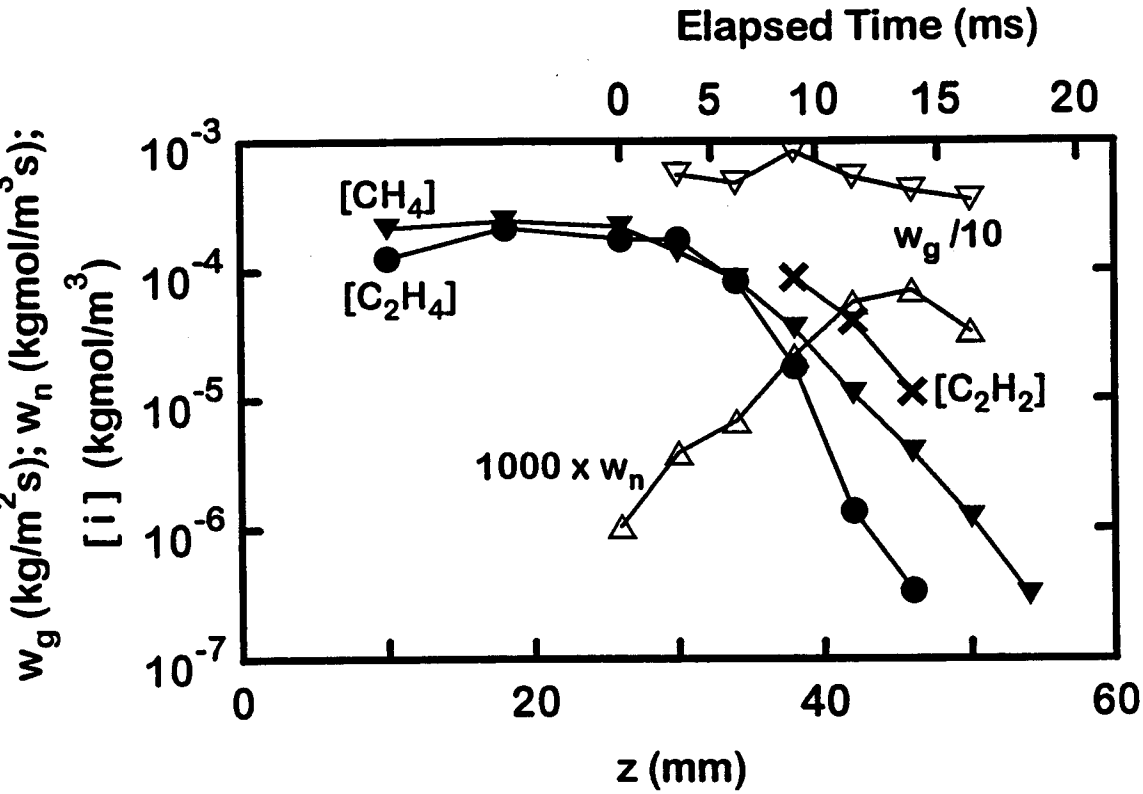

Figure 4.9 Net Soot Growth and Nucleation Rates for the Propane/Air Flame

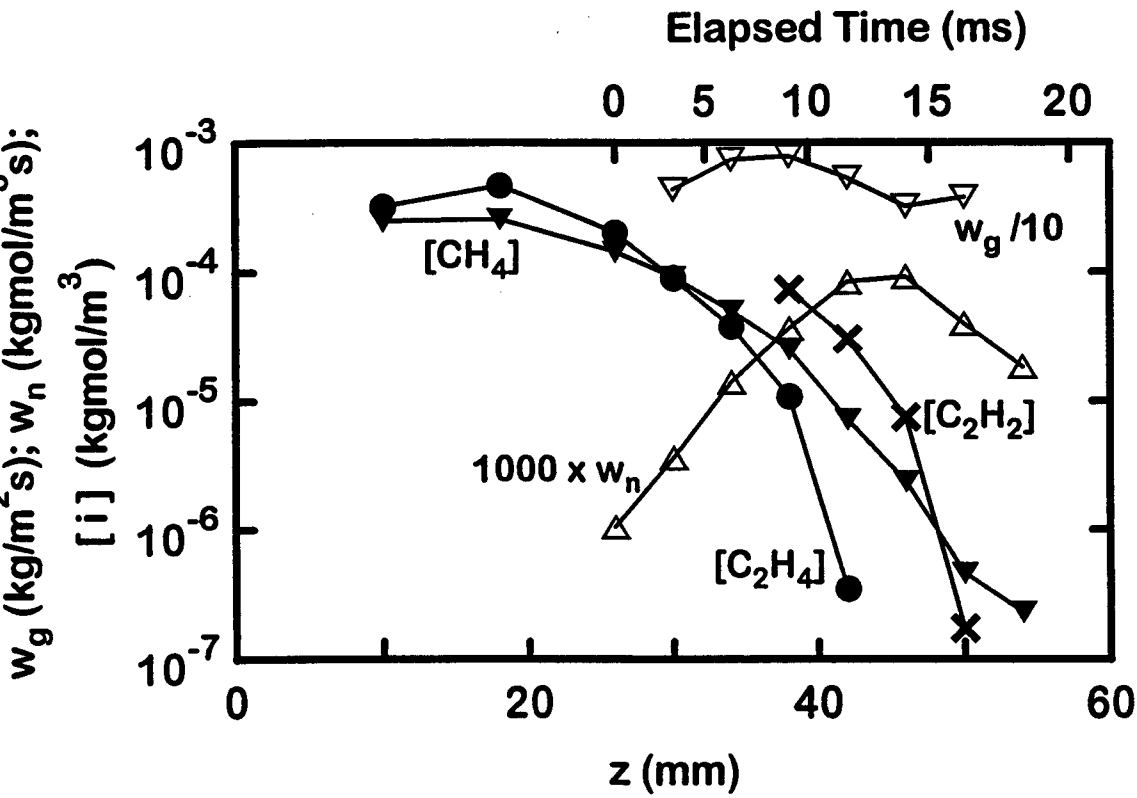

Figure 4.10 Net Soot Growth and Nucleation Rates for the n-Butane/Air Flame

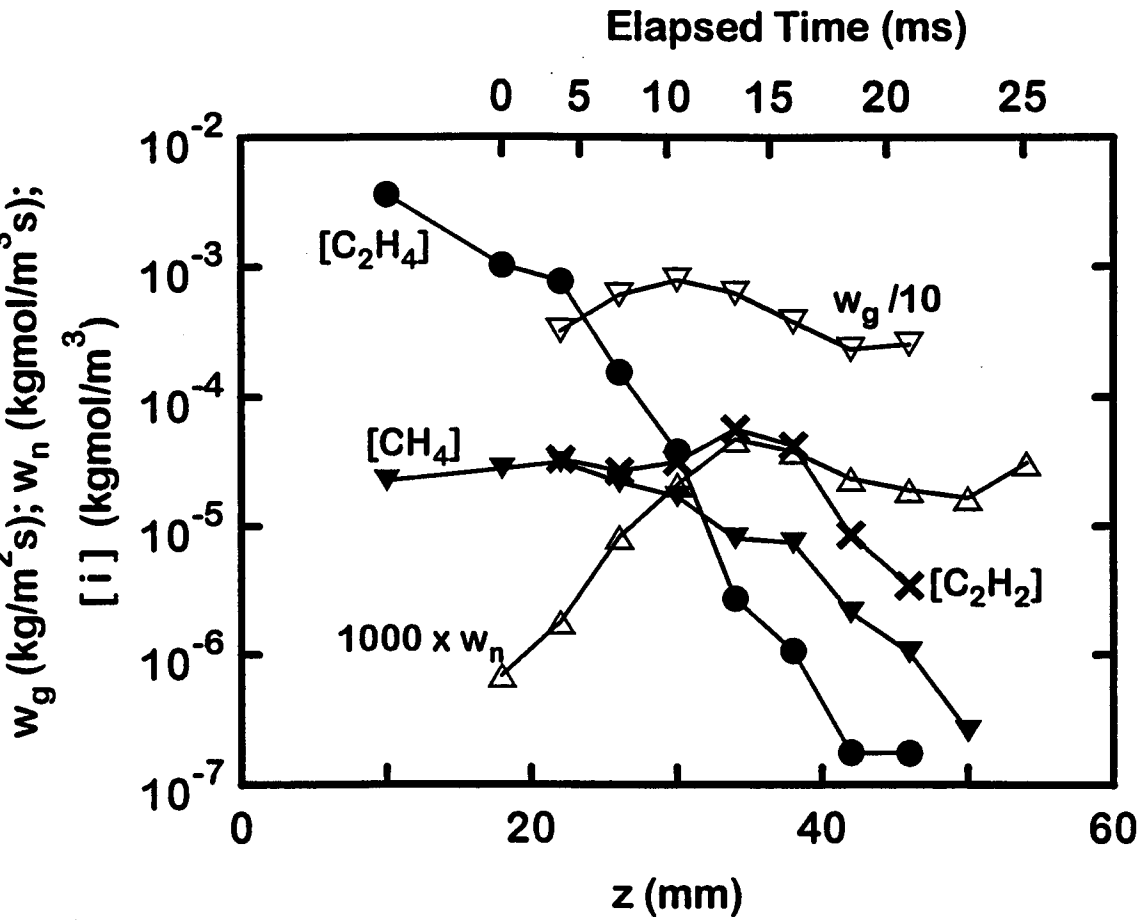

Figure 4.11 Net Soot Growth and Nucleation Rates for the Ethylene/Air Flame

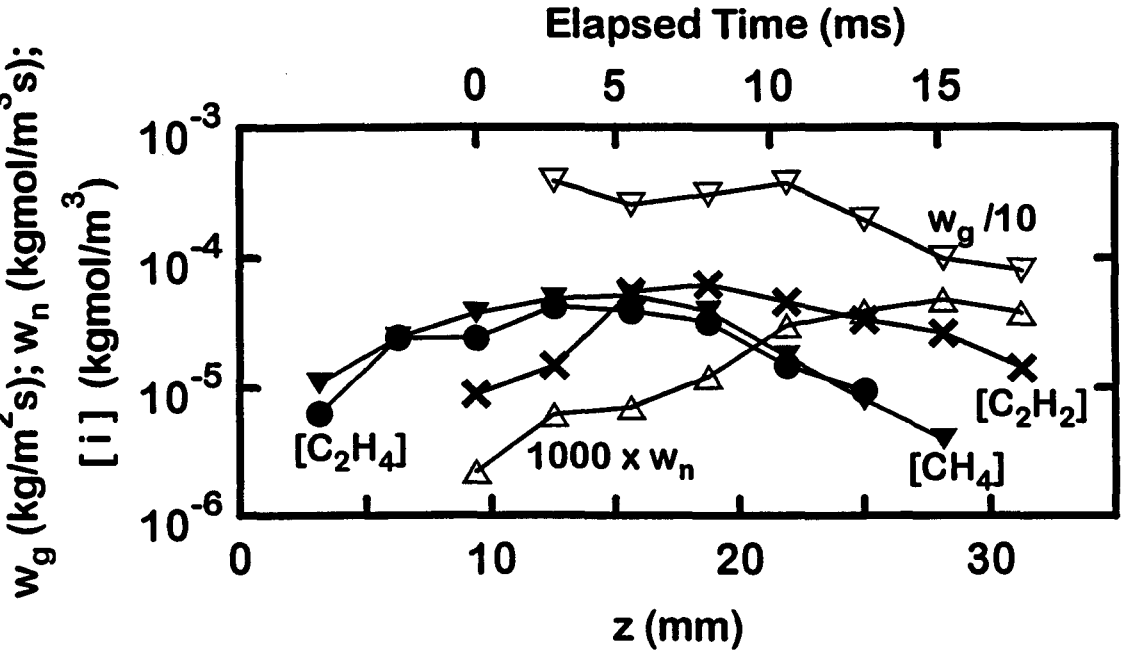

Figure 4.12 Net Soot Growth and Nucleation Rates for the Propylene/Air Flame

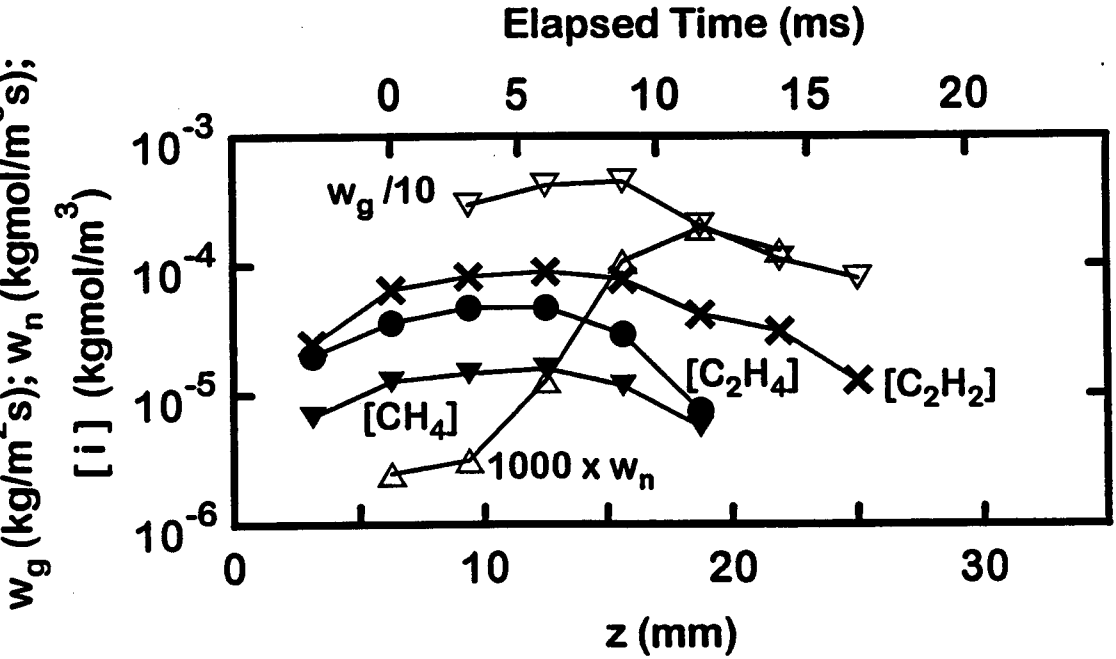

Figure 4.13 Net Soot Growth and Nucleation Rates for the 1,3-Butadiene/Air Flame

of soot nucleation. The end of the soot growth region is reached when f_s reaches a maximum along the axis, which is indicated by the last point where w_g is plotted in Figs. 4.8-4.13. Finally, the concentrations of the most prevalent hydrocarbons in the soot formation region — CH_4, C_2H_2 and C_2H_4 —are shown on the plots in order to assist the interpretation of the growth and nucleation rate measurements.

The net soot growth rates illustrated in Figs. 4.8-4.13 range from 10^{-3} to 10^{-2} kg/m^{2}s. Acetylene, which is correlated with soot growth in flow tubes (Tesner 1991; Tesner and Schurupov 1993, 1994), premixed flames (Bockhorn et al. 1982, 1984; Harris and Weiner 1983a, 1983b, 1984; Ramer et al. 1986), recent detailed models of premixed flames (Mauss et al. 1994; Kazakov et al. 1994) and in acetylene-fueled diffusion flames as discussed in Chapter 3, is the most abundant hydrocarbon near the end of the soot growth region and is observed to dominate soot production at these conditions. This behavior is supported by the observation that the end of the soot growth region coincides with the disappearance of acetylene. On the other hand, concentrations of ethylene are comparable to or greater than those of acetylene near the start of the soot growth region, suggesting potential for the participation of ethylene in soot growth as well. Additionally, methane concentrations are intermediate between acetylene and ethylene in the soot growth region, although there is little evidence for the direct participation of methane in soot growth (Tesner 1991; Tesner and Schurupov 1993, 1994; Mauss et al. 1994; Kazakov et al. 1994). Finally, hydrogen, which is thought to be involved in the activation of carbon surfaces (Mauss et al. 1994; Kazakov et al. 1994), has concentrations (see Figs. 4.2-4.7) that are comparable to acetylene concentrations in the soot growth region.

The first step in correlating soot growth was to associate gross soot growth with acetylene concentrations, similar to Chapter 3 and Lin et al. (1995), as follows:

$$w_g = k_g(T)[C_2H_2]^n, \tag{4.4}$$

where $k_g(T)$ normally is an Arrhenius expression. Similar to the acetylene/air diffusion flames, however, a significant temperature dependence for $k_g(T)$ was not found and a correlation of present measurements was sought by plotting w_g as a function of the molar concentration of acetylene as illustrated in Fig. 4.14. Other results illustrated on this figure include measurements and a correlation for acetylene/air diffusion flames from Chapter 3 and Lin et al. (1995) and measurements in premixed flames (Bockhorn et al. 1982, 1984; Harris and Weiner 1983a, 1983b, 1984; Ramer et al. 1986). These results represent gross soot growth rates, uncorrected for effects of simultaneous soot oxidation.

The results illustrated in Fig. 4.14 suggest comparable growth rates for acetylene/air diffusion flames and for new soot in premixed flames (the uppermost data points for the premixed flames), with differences between these rates attributed mainly to uncertainties concerning the soot surface area in the premixed flames, as discussed in Chapter 3. In contrast, growth rates for the present hydrocarbon/air flames are significantly higher than the acetylene/air flames of Chapter 3 and Lin et al. (1995) suggesting that the presence of significant concentrations of hydrocarbons other than acetylene either create soot growth channels other than the acetylene channel, or modify soot surface reactivity to reaction with acetylene. Although present rates of soot growth are significantly larger than the earlier results for acetylene/air flames, however, the apparent order of gross soot growth with respect to acetylene concentrations is similar, 1.11 with a standard deviation of 0.22.

Similar to results for acetylene/air flames discussed in Chapter 3, the apparent order of gross soot growth with respect to acetylene concentration for the present hydrocarbon/air diffusion flames is higher than past suggestions based on measurements in premixed flames (Bockhorn et al. 1982, 1984; Harris and Weiner 1983a, 1983b, 1984; Ramer et al. 1986). This difficulty is attributed to soot oxidation masking the actual (net)

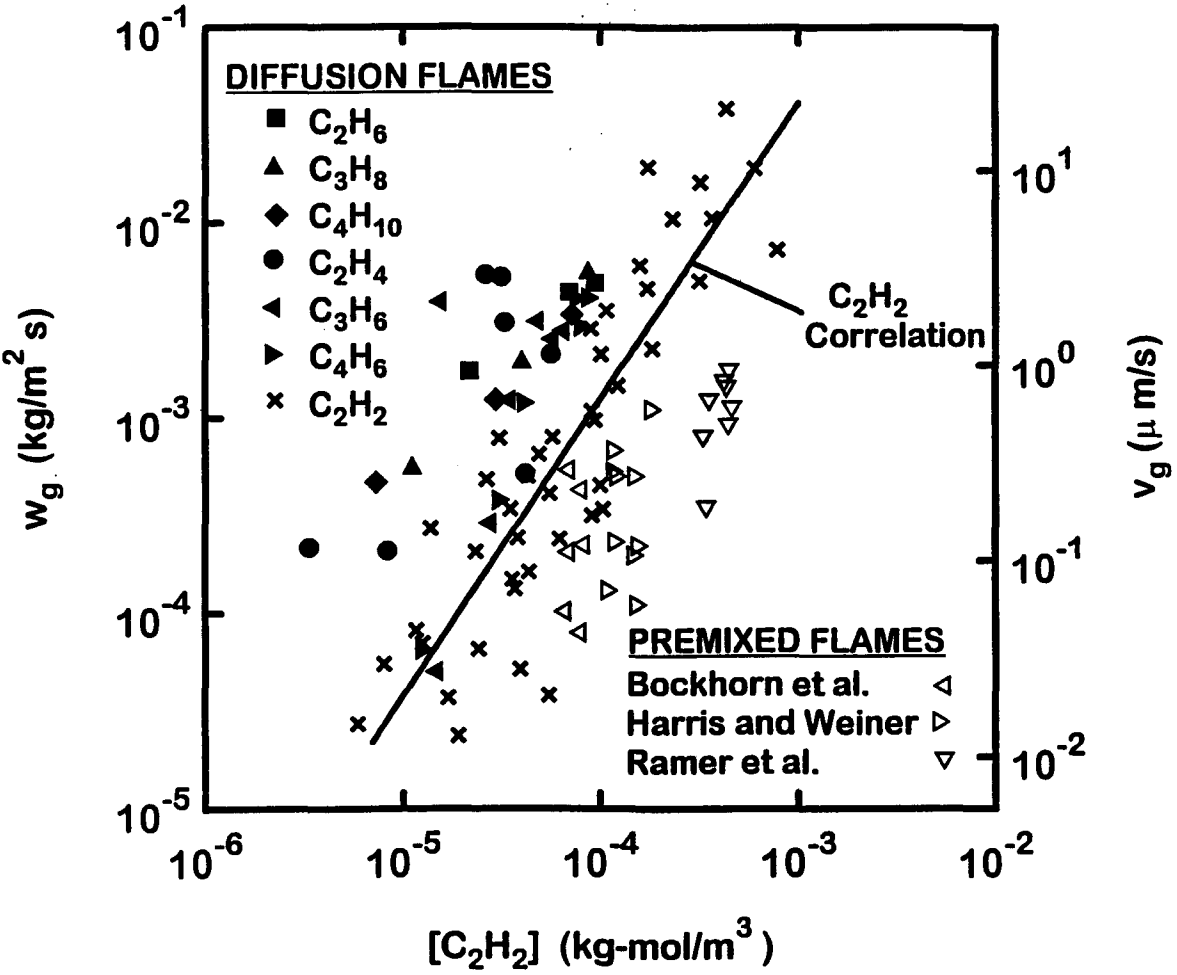

Figure 4.14 Gross Soot Growth Rates of Hydrocarbon/Air Diffusion Flames

soot growth rates, particularly when hydrocarbon concentrations become small near the end of the soot growth region. Corrections for soot oxidation were carried out in the same manner as for the acetylene/air flames discussed in Chapter 3: soot oxidation by O_2 was estimated using the rate expression of Nagle and Strickland-Constable (1962) which was subsequently confirmed by Park and Appleton (1973); and soot oxidation by CO_2 and H_2O was estimated following Johnstone et al. (1952) and Libby and Blake (1979, 1981), in agreement with Bradley et al. (1984). Soot oxidation by OH, as discussed by Neoh et al. (1980), was ignored because concentrations of OH are negligible in the soot formation region due to the presence of light hydrocarbon species (Miller et al. 1992; Smyth et al. 1985). Evaluation of these procedures in Chapter 3, based on observed soot oxidation rates in the fuel-lean region of acetylene/air flames, indicated that they significantly overestimated soot oxidation rates (by a factor of roughly 7:1); therefore, conditions where the oxidation corrections exceeded 60% of the observed (gross) growth rate were eliminated from the following results.

The present net soot growth rates, corrected for soot oxidation, are plotted as a function of acetylene concentration in Fig. 4.15. The net soot growth rate has been plotted in a manner that anticipates a simple collision efficiency expression, i.e.:

$$w_{g_i} = \eta_i C_i \bar{v}_i [i] / 4 \tag{4.5}$$

where

$$\bar{v}_i = (8kT / (\pi M_i))^{1/2} \tag{4.6}$$

is the (Boltzmann) equilibrium mean molecular velocity of species i. Also shown on the plot are results from acetylene/air diffusion flames found as discussed in Chapter 3 and by Lin et al. (1995), corrected for effects of soot oxidation in the same manner, and results for premixed flames (Bockhorn et al. 1982, 1984; Harris and Weiner 1983a,

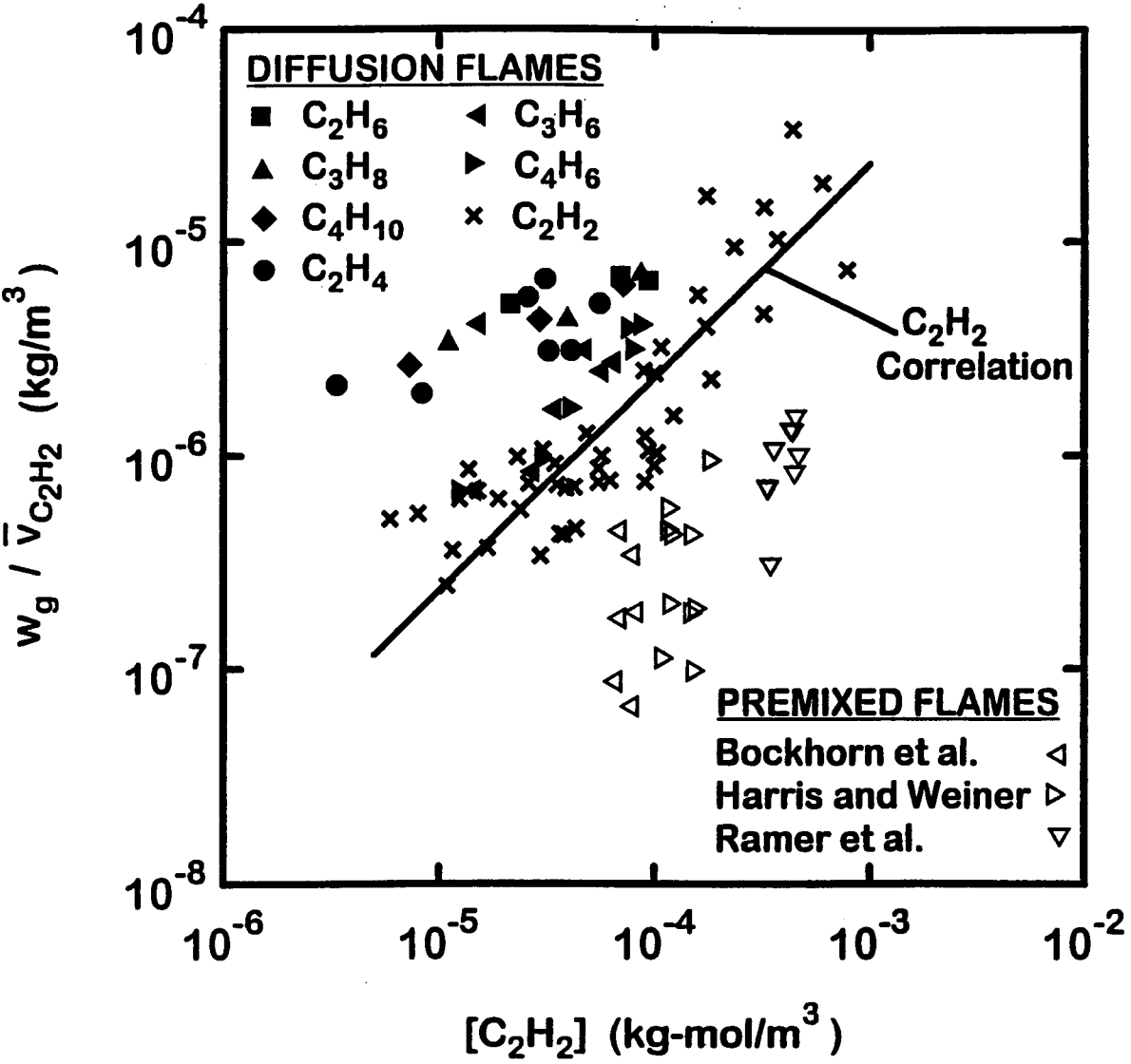

Figure 4.15 Net Soot Growth Rates of Hydrocarbon/Air Diffusion Flames

1983b, 1984; Ramer et al. 1986) where soot oxidation is less a factor and no oxidation correction has been made. When plotted in this manner, the measurements for hydrocarbon/air flames indicate behavior compatible with a first-order acetylene reaction within statistical significance, but with generally higher net soot growth rates than the results discussed in Chapter 3 for acetylene/air flames. The increased net growth rate can be quantified by an average collision efficiency from Eq. 4.5, attributing all net soot growth to a first-order reaction of acetylene. This yielded the relatively high acetylene collision efficiency of 1.56% with an uncertainty (95% confidence) of 0.53% for the present hydrocarbon/air flames, compared to 0.39% with an uncertainty (95% confidence) of 0.14% for the acetylene/air flames discussed in Chapter 3 and Lin et al. (1995). Finally, the oxidation corrections increase the differences between soot growth rates in the diffusion flames and premixed flames, however, these differences may still be explained by the uncertain optical estimates of soot surface areas for the premixed flame studies, as discussed in Chapter 3.

The enhancement of net soot growth rates seen in Fig. 4.15 for the present hydrocarbon/air flames, due to significant concentrations of light hydrocarbons other than acetylene in the soot growth region, will eventually be best treated by detailed models typified by the recent work of Mauss et al. (1994) and Kazakov et al. (1994), and references cited therein. In particular, such methods will eventually address effects of various species on active soot growth sites and parallel soot growth channels. Nevertheless, it would be premature to attempt this approach before the effect of uncertainties about existing premixed flame results on detailed soot growth models have been resolved. Thus, present results were interpreted, in terms of parallel channels, i.e., additive soot growth from various hydrocarbon species.

The first parallel soot growth mechanism that was considered assumed that soot growth due to acetylene was unchanged from the correlation of Lin et al. (1995),

implying an acetylene collision efficiency of 0.39%, and that the residual net soot growth rates were due to ethylene via a collision mechanism represented by Eq. 4.5. The resulting net growth rates, after accounting for oxidation and for growth due to acetylene, as a function of ethylene concentration, are shown in Fig. 4.16. The range of ethylene concentrations is too narrow for an accurate determination of the order of the growth rate with respect to ethylene. Instead, the best first-order correlation in terms of ethylene concentration is shown on the plot. The correlation provides a reasonable fit of the measurements, and yields an ethylene collision efficiency of 1.41% with an uncertainty (95% confidence) of 0.95%.

Several other mechanisms of soot growth for the hydrocarbon/air flames were considered, involving various parallel growth channels. Table 4.2 is a summary of the collision efficiencies found in this manner, including the following conditions: growth via acetylene for the acetylene/air flames discussed in Chapter 3; growth via acetylene alone for the present hydrocarbon/air flames as discussed above; parallel growth via acetylene and ethylene for the present hydrocarbon/air flames; parallel growth via acetylene and methane for the present hydrocarbon/air flames; and parallel growth via acetylene, ethylene and methane for the combined data set including the present acetylene/air flames, those of Lin et al. (1995) and the present hydrocarbon/air flames. The first two of these options represent mechanisms where growth occurs by acetylene with the other hydrocarbons mainly serving to modify the reactivity of the soot surface, while the remainder represent simple additive mechanisms. The 4:1 variations of the various collision efficiencies of acetylene are comparable to changes of surface reactivity attributed to soot growth processes in premixed flames (Harris and Weiner 1983a, 1983b, 1984; Ramer et al. 1986; Mauss et al. 1994; Kazakov et al. 1994) so the surface modification approach cannot be ruled out. Similarly, the parallel channel approach yields reasonable collision efficiencies, although the methane channel is not plausible in

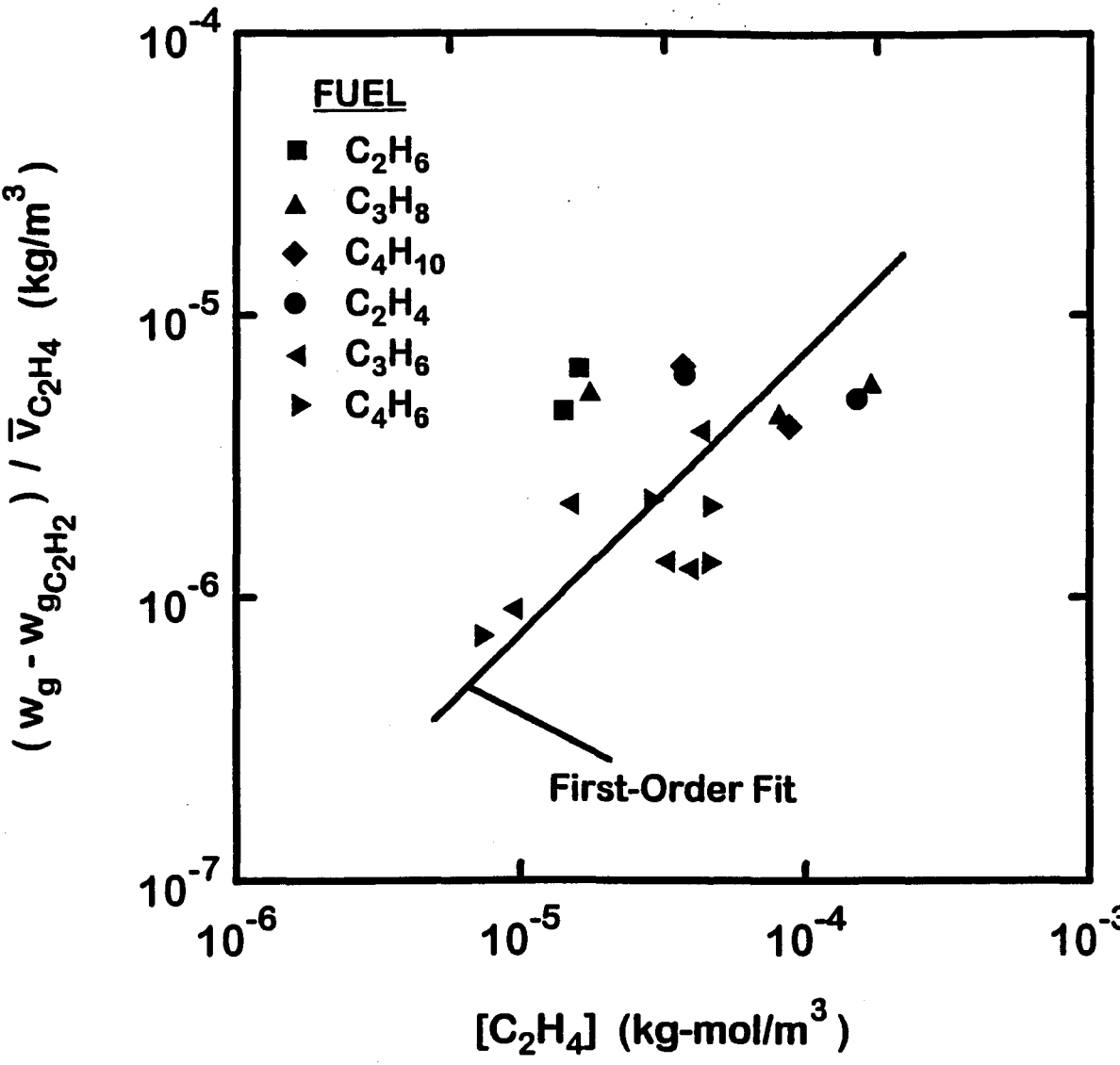

Figure 4.16 Net Soot Growth Rates, After Correction for Acetylene Reaction, of Hydrocarbon/Air Diffusion Flames

Table 4.2 Summary of Collision Efficiencies[a]

Mechanism	Flames	$\eta_{C_2H_2}$	$\eta_{C_2H_4}$	η_{CH_4}
C_2H_2	C_2H_2[b,c]	0.00386 (0.00139)	---	---
C_2H_2	present	0.0156 (0.0078)	---	---
C_2H_2	C_2H_2[b,c] & present	0.00663 (0.00234)	---	---
C_2H_2/C_2H_4	present	0.00386[c] (-)	0.0141 (0.0095)	---
C_2H_2/CH_4	present	0.00386[c] (-)	---	0.0260 (0.0153)
$C_2H_2/C_2H_4/CH_4$	C_2H_2[b,c] & present	0.00462 (0.00096)	0.000098 (0.0019)	0.0164 (0.0106)

[a]Numbers in parentheses are uncertainties (95% confidence).

[b]Chapter 3.

[c]Lin et al. (1995).

view of the low H:C ratios of soot, and only yields reasonable collision efficiencies because methane concentrations are comparable to those of acetylene and ethylene in the soot growth region. Clearly, consideration of a more detailed soot growth mechanism, and systematic measurements of soot growth for more flame environments, will be required to obtain a more complete treatment of soot growth in flames.

4.3.3 Soot Nucleation

Measurements along the axes of the six test flames were used to study soot nucleation, similar to the earlier work for acetylene/air flames discussed in Chapter 3. Based on the same assumptions used for soot growth rates in Eq. 4.2, the expression for soot nucleation rates for motion along a streamline becomes (see Chapter 3):

$$w_n = \rho d(n_p / \rho) / dt \tag{4.7}$$

The resulting measurements of w_n are illustrated in Figs. 4.8-4.13, along with the concentrations of major hydrocarbon species. These figures show that soot nucleation is associated with the presence of acetylene; and the rates correlate as a first-order acetylene reaction, similar to earlier findings for acetylene/air diffusion flames discussed in Chapter 3. This implies

$$w_n = k_n(T)[C_2H_2] \tag{4.8}$$

where $k_n(T)$ is an Arrhenius expression.

The present soot nucleation rates, expressed in terms of $k_n(T)$ according to Eq. 4.8, are plotted in Fig. 4.17. In addition, measured soot nucleation rates from acetylene/air flames from Chapter 3 and Lin et al. (1995), and a correlation by Leung et al. (1991) are shown on the plot. The new measurements in hydrocarbon/air diffusion flames are in agreement with the earlier measurements for acetylene/air diffusion flames discussed in Chapter 3, with the combined results yielding essentially the same first-order nucleation rate correlation, as follows:

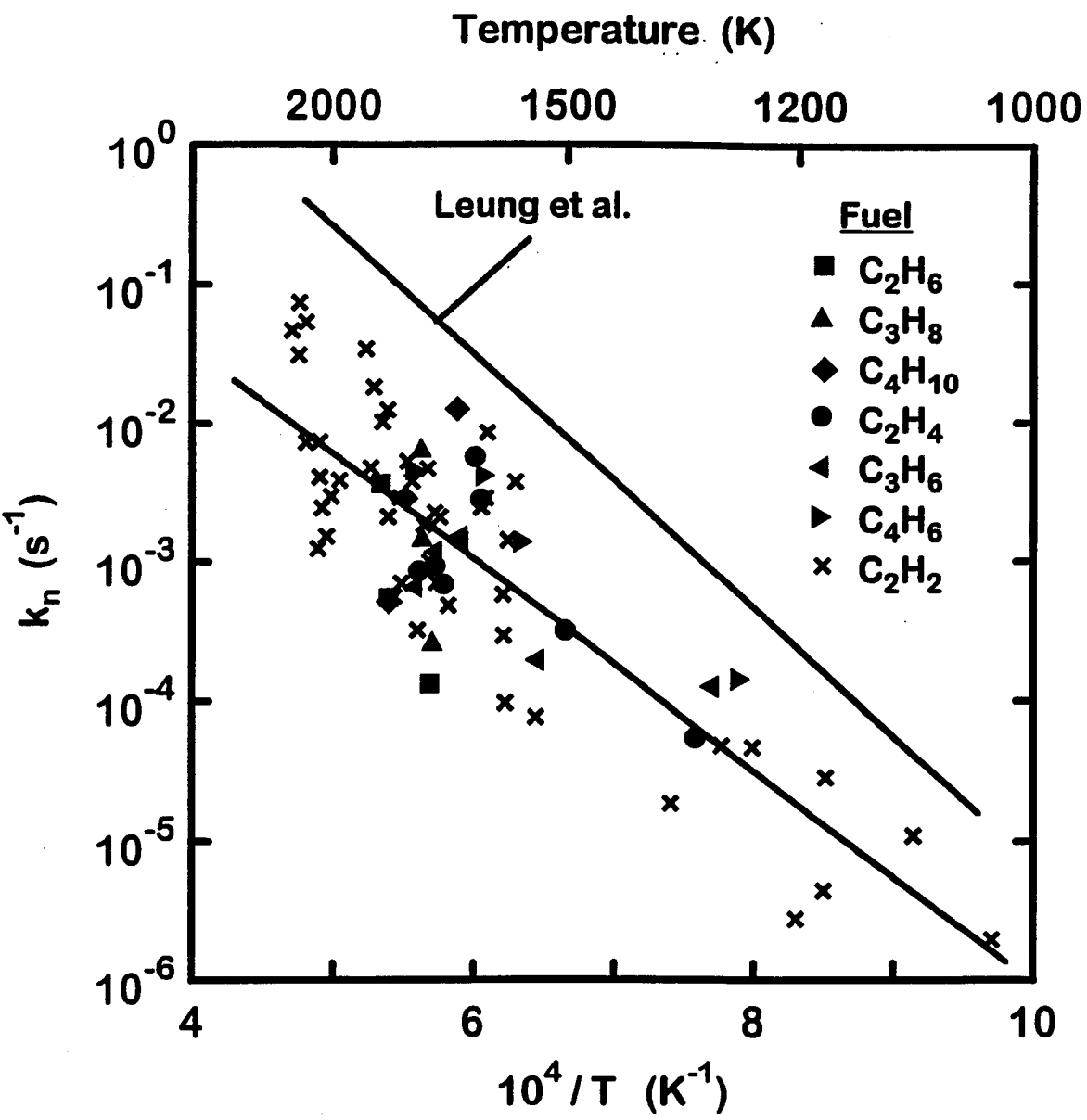

Figure 4.17 Soot Nucleation Rates of Hydrocarbon/Air Diffusion Flames

$$w_n = 37.9[C_2H_2]\exp(-17500 / T) \quad (4.9)$$

with the uncertainty (95% confidence) of the activation temperature of 2680 K, and a correlation coefficient of the fit of 0.84. This implies an activation energy of 35 kcal/gmol, which is reasonable for a recombination-like process like soot nucleation (Haynes and Wagner 1981; Tesner 1958, 1960; Leung et al. 1991). Furthermore, present results support earlier suggestions that soot nucleation can largely be associated with acetylene concentrations alone, i.e., nucleation does not involve parallel channels, in the same manner as soot growth.

As discussed in Chapter 3, and substantiated by present findings in Fig. 4.17, present values of w_n are significantly lower than the correlation by Leung et al. (1991) of data from various sources. This discrepancy is not surprising, as discussed in Chapter 3. In particular, the data used in Leung et al. (1991) involved optical determinations of primary particle size which are questionable (Köylü and Faeth 1994), and tend to overestimate soot surface area (Harris and Weiner 1983a, 1983b), which would cause overestimation of soot nucleation rates typical of the differences between Leung et al. (1991) and the present data correlation in Fig. 4.17.

Finally, attributing soot nucleation to acetylene alone is an oversimplification of a complex process involving polynuclear aromatic hydrocarbons (PAH) that eventually become visible primary soot particles (Howard 1990; Mauss et al. 1994; Kazakov et al. 1994). Nevertheless, acetylene offers a plausible surrogate for these complex molecules because PAH concentrations can be expressed in terms of acetylene concentrations through equilibrium constants (Mauss et al. 1994; Kazakov et al. 1994); furthermore, acetylene is a major contributor to the growth of PAH as they evolve toward soot (Howard 1990).

4.4 Conclusions

Flame structure and soot processes were studied in laminar hydrocarbon/air jet diffusion flames at pressures of 25-99 kPa emphasizing fuels other than acetylene, in order to supplement earlier findings in laminar acetylene/air jet diffusion flames already discussed in Chapter 3. Measurements were limited to processes along the axes of the flames where soot first nucleates in the cool core of the flow and experiences a monotonic decrease of mixture fraction along a soot path line. The major conclusions are as follows:

1. Similar to earlier findings for laminar acetylene/air diffusion flames discussed in Chapter 3, significant soot nucleation and growth began when temperatures reached 1250 K, and where acetylene was detectable, and ended when hydrocarbon concentrations became small (at fuel-equivalence ratios of roughly 1.4). Additionally, relative rates of soot nucleation and growth along the axis combined to yield maximum primary soot particles near the beginning of soot formation, although other paths through the flames can yield different behaviors (Lin et al. 1995).

2. Present net soot growth rates, corrected for soot oxidation, were higher than earlier observations in acetylene/air diffusion flames when correlated solely in terms of acetylene concentrations; this is attributed to parallel soot growth channels due to the presence of light hydrocarbons other than acetylene (mainly ethylene and methane) although modified soot surface reactivity due to the presence of these hydrocarbons cannot be ruled out. Assuming parallel soot growth channels involving only acetylene and ethylene, and an acetylene collision efficiency of 0.39% based on the earlier measurements in acetylene/air diffusion flames discussed in Chapter 3 and Lin et al. (1995), yielded an ethylene collision

efficiency of 1.41% which is reasonable, although a number of other soot growth mechanisms are discussed as well.

3. In contrast to soot growth rates, present soot nucleation rates agreed with earlier observations in laminar acetylene/air diffusion flames discussed in Chapter 3, and were correlated as a first-order reaction with respect to acetylene with an activation energy of 35 kcal/gmol. Although the present nucleation rate correlation is significantly lower than the expression suggested by Leung et al. (1991), this difference is attributable to problems with the approximations used by Leung et al. (1991) to estimate soot structure from optical measurements. Finally, it should be recognized that acetylene concentrations in the present soot nucleation rate expression serve only as surrogates for reaction processes involving heavier hydrocarbons, e.g., PAH, that eventually evolve to soot. Thus, a more complete treatment of soot nucleation must eventually involve more detailed mechanisms typified by the methods of Mauss et al. (1994) and Kazakov et al. (1994) and references cited therein.

CHAPTER V

SUMMARY AND CONCLUSIONS

5.1 Summary

The objectives of the present work were to study and quantify soot processes in laminar jet diffusion flames, at both normal- and reduced-gravity conditions. This work was motivated by the large impact of soot on practical combustion devices and on unwanted fires; it was warranted by the limited understanding of soot processes in flames. The three phases of the research were: laminar smoke points of nonbuoyant jet diffusion flames (Chapter 2), soot formation in acetylene/air diffusion flames (Chapter 3) and soot formation in hydrocarbon/air jet diffusion flames (Chapter 4).

The study of nonbuoyant soot processes (Chapter 2) sought to measure the laminar smoke point flame properties of nonbuoyant diffusion flames and to compare these properties to the corresponding properties of buoyant diffusion flames. This phase was carried out aboard the NASA KC-135 low-gravity aircraft. Fuels considered were propane and ethylene, burning in air at pressures of 0.5-2.0 atm. Flame luminosity lengths were controlled by test operators and recorded with a color video camera. Flame structure computations were undertaken to estimate flame residence time variations.

The study of soot formation (nucleation and growth) in acetylene/air laminar jet diffusion flames (Chapter 3) sought to complete detailed measurements of both soot and flame properties in weakly-buoyant flames, and to exploit these results to gain a better understanding of soot formation. This phase involved a burner contained within a

pressure vessel and four acetylene/air flames at pressures of 0.125-0.25 atm. Measurements included soot volume fractions using laser extinction, temperatures using both thermocouples and multiline emission, soot structure using thermophoretic sampling and analysis by transmission electron microscopy, concentrations of major gas species using sampling and analysis by gas chromatography, and velocities using laser velocimetry.

The study of soot formation in hydrocarbon/air laminar jet diffusion flames (Chapter 4) sought to supplement the results from the acetylene-fueled flames of Chapter 3 with results from six other hydrocarbon flames, and in particular to evaluate the effects of various hydrocarbons in the soot formation region. The flames were fueled with C_2H_6, C_3H_8, C_4H_{10}, C_2H_4, C_3H_6, and C_4H_6, burning in air at pressures of 0.25-1.0 atm. Measurements undertaken were the same as for the work of Chapter 3, outlined above.

5.2 Conclusions

The specific conclusions of the present work are given at the end of Chapters 2, 3 and 4 and are briefly summarized here.

The study of laminar smoke points of nonbuoyant jet diffusion flames (Chapter 2) concluded: (1) nonbuoyant laminar jet diffusion flames do exhibit laminar smoke point luminosity lengths; (2) laminar smoke point luminosity lengths of non-buoyant flames exhibit little variation with burner diameter and are roughly one fourth as long as the lengths of corresponding normal-gravity flames; and (3) the variation of laminar smoke point luminosity lengths with pressure and fuel type is similar for nonbuoyant and buoyant flames.

The study of soot formation in acetylene laminar jet diffusion flames (Chapter 3) concluded: (1) soot nucleation and growth began when temperatures reached roughly

1250 K, and ended when acetylene disappeared at a fuel-equivalence ratio of roughly 1.4; (2) maximum primary soot particle diameters along the flame axes were observed near the beginning of soot formation; (3) soot growth measurements, corrected for effects of soot oxidation, yielded first-order behavior with respect to acetylene with a collision efficiency of 0.41% and no effect of age; and (4) soot nucleation was first-order with respect to acetylene concentration with an activation energy of 32 kcal/gmol.

The study of soot formation in laminar jet diffusion flames burning hydrocarbon fuels other than acetylene (Chapter 4) concluded: (1) soot formation was bounded by the same temperature and fuel-equivalence ratio limits as in the acetylene flames; (2) soot growth rates in these flames were higher than in the acetylene-fueled flames at corresponding local acetylene concentrations; (3) soot growth in these flames was best explained by parallel acetylene and ethylene growth channels with collision efficiencies of 0.39% and 1.41%, respectively; and (4) no parallel soot nucleation channel was discernible, rather soot nucleation for all flames considered to date was first-order with respect to acetylene concentration, with an activation energy of 35 kcal/gmol.

5.3 Recommendations for Further Study

Laminar jet diffusion flames were selected for the present study because they simplified the present measurements. However, laminar jet diffusion flames do introduce two noteworthy complications into the determination of soot formation rates which may be simplified using other arrangements. In particular, laminar jet diffusion flames allow oxidizing species (O_2, CO_2, and H_2O) to diffuse into the entire soot formation region, and the complex two-dimensional structure of these flames presents difficulties for completing detailed models of soot reaction mechanisms. In order to avoid these difficulties it would be helpful to carry out similar studies in both premixed flames and in counterflow diffusion flames. Both of these flame configurations provide a one-dimensional flame system with only trace quantities of oxidizing species in the soot

formation region. Complications introduced by the oxidizing species in the present study were exacerbated by relatively large uncertainties of current correlations of soot oxidation rates, indicating that additional information about soot oxidation is needed.

The soot nucleation mechanism proposed during the present study assumes that soot nucleation is first-order in acetylene concentration, a considerable simplification of a process which instead involves complex polynuclear aromatic hydrocarbon (PAH) species. Improvement of this overly simplified approach will require gas-phase gas chromatography using a flame-ionization detector, mass spectrometry, etc., in order to quantify the PAH species, as well as a more extensive computational effort involving detailed soot kinetics modeling. Furthermore, the possible role in soot nucleation of the lightly-contrasting particles seen in the TEM grids at early flame residence times should be resolved.

Finally, several excellent low-gravity combustion facilities are currently available and should be used to enhance understanding of soot formation processes in nonbuoyant flames.

APPENDIX A

EXPERIMENTAL UNCERTAINTIES

A.1 Formulation

The following analysis of experimental uncertainties follows from Kline and McClintock (1953) and Moffat (1982). Consider a result R which is a function of n independent variables, υ_1, υ_2...υ_n:

$$R = R (\upsilon_1, \upsilon_2...\upsilon_n) \tag{A.1}$$

If the experimental uncertainties (chosen here to be the uncertainty at the 95% confidence level) of the υ_i are $\Delta\upsilon_i$, the resulting uncertainty in R is:

$$\Delta R = \left\{ [(\partial R/\partial \upsilon_1)\Delta\upsilon_1]^2 + [(\partial R/\partial \upsilon_2)\Delta\upsilon_2]^2 + ... + [(\partial R/\partial \upsilon_n)\Delta\upsilon_n]^2 \right\}^{0.5} \tag{A.2}$$

where the symbol ∂ signifies partial derivative.

In the following, Equation A.2 will be applied to estimate the uncertainties in soot growth rate and soot nucleation rate constant.

A.2 Soot Growth Rate Uncertainty

The definition of soot growth rate as discussed in Chapters 3 and 4 (see Equation 3.2) is:

$$w_g = (\rho/S) d(\rho_s f_s/\rho)/dt \tag{A.3}$$

To simplify the following analysis it is assumed here that $\Delta\rho$ does not impact Δw_g, because ρ appears once each in the denominator and numerator of Equation A.3 and furthermore the uncertainty in ρ is relatively small. Expanding the derivative, Equation A.3 may then be expressed as:

$$w_g = (\rho_s d_p/6) [\ln(f_{s2}) - \ln(f_{s1})] / (t_2 - t_1) \quad (A.4)$$

where the subscripts 1 and 2 represent adjacent measurement stations. Equation A.2 can then be applied, invoking the following uncertainties as presented in Chapters 3 and 4:

$$\Delta d_p/d_p=0.1; \Delta f_s/f_s=0.1; \Delta t/t=0.1 \quad (A.5)$$

and yielding the final result:

$$\Delta w_g/w_g = 0.41 \quad (A.6)$$

It is noted that the dominant contribution to this uncertainty arises from the uncertainty in soot volume fraction, f_s.

A.3 Soot Nucleation Rate Constant Uncertainty

The definition of soot nucleation rate constant, as determined in Chapters 3 and 4 and given in Equations 3.7 and 3.8 is:

$$k_n = \{ \rho \, d(n_p/\rho) / dt \} / [C_2H_2] \quad (A.7)$$

To simplify the following analysis it is assumed that $\Delta\rho$ does not impact Δk_n because ρ appears once each in the denominator and numerator of Equation A.7 and furthermore the uncertainty in ρ is relatively small. Upon substituting $n_p=6f_s/(\pi d_p)$ and $[C_2H_2]=R_uT/(X_{C_2H_2}p)$, where R_u is the universal gas constant, and expanding the derivative, Equation A.7 may then be expressed as:

$$k_n = [(R_uT / (X_{C_2H_2} p)] (f_{s2}/d_{p2}^3 - f_{s1}/d_{p1}^3) / (t_2 - t_1) \quad (A.8)$$

Equation A.2 can now be applied, invoking the following uncertainties as presented in Chapters 3 and 4:

$$\Delta T/T=0.028; \Delta X_{C_2H_2}/X_{C_2H_2}=0.15; \Delta f_s/f_s=0.10; \Delta d_p/d_p=0.10; \Delta t/t=0.10 \quad (A.9)$$

and yielding the final result:

$$\Delta k_n/k_n = 0.62 \quad (A.6)$$

It is noted that the dominant contribution to this uncertainty arises from the uncertainty in soot particle diameter, d_p, due to its appearance to the third power in Equation A.8.

APPENDIX B

TABULATION OF DATA FOR ACETYLENE/AIR DIFFUSION FLAMES

B.1 Structure Data

Table B.1 Structure Measurements for Acetylene/Air Diffusion Flames

FLAME 1						
z (mm)	u (m/s)	t (ms)	T (K)	d_p (nm)	f_s (ppm)	$\bar{N}$
1.5	3.25	0.434				
3.125	2.808	0.973	937.			
6.250	1.930	2.339	1176.	13.18	0.0	44
9.375	1.552	4.155	1607.	19.89	0.027	
12.500	1.427	6.257	1825.	23.33	0.580	58
15.625	1.372	8.491	1761.	16.65	0.845	
18.750	1.356	10.782	1720.	16.42	0.890	119
21.875	1.368	13.076	1653.	15.85	0.960	
25.000	1.410	15.327	1644.	15.00	1.020	224
28.125	1.441	17.519	1661.	15.50	1.040	
31.250	1.478	19.661	1643.	15.04	1.030	257
34.375	1.517	21.748	1630.	13.85	0.850	
37.500	1.556	23.782	1650.	12.93	0.739	373
40.625	1.602	25.762	1665.	12.53	0.659	
43.750	1.650	27.684	1596.	10.24	0.259	384
46.875	1.689	29.556	1491.		0.0	

FLAME 2					
z (mm)	u (m/s)	t (ms)	T (K)	d_p (nm)	f_s (ppm)
1.5	6.053	0.236			
3.125	5.373	0.522	877.		
6.250	3.901	1.213	1094.		0.0
9.375	2.716	2.189	1252.	15.10	0.0200
12.500	2.210	3.471	1611.	20.78	0.1401
15.625	1.940	4.984	1856.	17.51	0.5700
18.750	1.802	6.656	1827.	13.12	0.6258
21.875	1.722	8.431	1800.	12.39	0.7700
25.000	1.672	10.272	1763.	11.41	0.8500
28.125	1.651	12.153	1725.	12.69	0.8763
31.250	1.655	14.044	1703.	12.38	0.9200
34.375	1.674	15.921	1722.	11.93	0.9300
37.500	1.707	17.770	1734.	10.86	0.9217
40.625	1.747	19.580	1780.	10.96	0.8000
43.750	1.790	21.347	1804.	9.76	0.5800
46.875	1.830	23.074	1627.	9.26	0.3600
50.000	1.842	24.776	1441.		0.0

FLAME 3

z (mm)	u (m/s)	t (ms)	T (K)	d_p (nm)	f_s (ppm)
1.5	11.12	0.131			
3.125	10.416	0.282			
6.250	8.382	0.619	1000.		
9.375	6.132	1.060	1174.		0.0
12.500	4.476	1.664	1287.	14.66	0.017
15.625	3.639	2.442	1745.	18.92	0.040
18.750	3.070	3.381	2020.	15.09	0.205
21.875	2.748	4.458	2032.	14.69	0.283
25.000	2.542	5.641	2039.	12.60	0.315
28.125	2.387	6.911	2007.	11.19	0.330
31.250	2.261	8.256	1982.	11.13	0.332
34.375	2.182	9.663	1934.	10.46	0.326
37.500	2.153	11.105	1905.	9.76	0.310
40.625	2.155	12.556	1939.	9.89	0.293
43.750	2.168	14.002	1955.	9.30	0.208
46.875	2.171	15.442	1813.		0.0

FLAME 4

z (mm)	u (m/s)	t (ms)	T (K)	d_p (nm)	f_s (ppm)
1.5	4.476	0.327			
3.125	4.202	0.702	813.		
6.250	3.535	1.5162	1031.		0.
9.375	2.753	2.5258	1204.	18.38	0.0080
12.500	2.510	3.7875	1553.	24.43	0.0180
15.625	2.004	5.2613	1787.	17.13	0.0960
18.750	1.855	6.8833	1773.	19.14	0.3590
21.875	1.762	8.6124	1810.	13.56	0.5190
25.000	1.718	10.409	1764.	12.37	0.6614
28.125	1.669	12.254	1764.	12.51	0.6790
31.250	1.664	14.130	1700.	12.53	0.7080
34.375	1.676	16.001	1746.	11.70	0.6700
37.500	1.701	17.852	1736.	10.45	0.6030
40.625	1.734	19.671	1767.	10.88	0.5090
43.750	1.767	21.457	1744.	10.78	0.2420
46.875	1.795	23.211	1622.	9.64	0.

B.2 Chemical Composition Data

Table B.2 Chemical Composition Measurements for Acetylene/Air Diffusion Flames

FLAME 1 Mole Fractions

z (mm)	H_2	O_2	CO_2	C_2H_2	N_2	CO	H_20	M (g/mol)	f	ϕ
3.125	.02375	.00000	.01485	.75550	.17280	.03294	.00000	26.141	.77620	45.43
6.250	.03730	.00530	.03270	.41920	.40390	.08150	.01980	26.561	.46670	11.46
9.375	.04460	.00770	.04300	.23060	.52280	.11610	.03500	26.766	.30150	5.65
12.500	.04503	.00680	.05330	.10920	.58700	.14470	.05400	26.966	.20100	3.30
15.625	.05620	.01220	.06370	.05910	.63730	.13040	.04080	27.094	.14995	2.31
18.750	.04300	.01220	.06760	.03080	.67590	.11980	.05070	27.457	.11790	1.75
21.875	.02160	.00990	.07420	.01300	.69010	.11710	.07410	27.911	.10120	1.47
25.000	.01450	.00940	.08870	.00430	.71290	.09345	.07655	28.318	.08760	1.26
28.125	.00670	.01200	.10580	.00000	.73480	.06295	.07760	28.803	.07620	1.08
31.250	.00270	.01243	.11660	.00000	.75310	.03975	.07550	29.103	.06990	0.98
34.375	.00000	.01600	.13020	.00000	.75060	.02540	.07780	29.382	.06890	0.97
37.500	.00000	.02120	.13040	.00000	.75270	.02025	.07530	29.431	.06670	0.94
40.625	.00000	.02700	.12780	.00000	.75540	.01730	.07250	29.440	.06400	0.90
43.750	.00000	.02940	.11405	.00000	.77970	.01320	.06360	29.319	.05640	0.78
46.875	.00000	.03920	.11750	.00000	.76810	.01090	.06420	29.407	.05680	0.79
50.000	.00000	.04430	.11340	.00000	.77640	.00620	.05980	29.406	.05290	0.73

FLAME 2 Mole Fractions

z (mm)	H_2	O_2	CO_2	C_2H_2	N_2	CO	H_20	M (g/mol)	f	ϕ
3.125	.02130	.00210	.00860	.87840	.10710	.01920	.00000	25.946	.86420	83.35
6.250	.03750	.00520	.02070	.57230	.29140	.06660	.00620	26.197	.61200	20.66
9.375	.04640	.00830	.03410	.33010	.44350	.11140	.02630	26.470	.39600	8.59
12.500	.05360	.00980	.04020	.16490	.53600	.15260	.04280	26.548	.25610	4.51
15.625	.04650	.00970	.04070	.09980	.61010	.14630	.04700	26.827	.18750	3.02
18.750	.06020	.01200	.05410	.07210	.60060	.15620	.04490	26.770	.17220	2.72
21.875	.04870	.01220	.07310	.04870	.60980	.14630	.06100	27.258	.15120	2.33
25.000	.03000	.01490	.06990	.03000	.64830	.13470	.07240	27.627	.12460	1.86
28.125	.02050	.01350	.08620	.01430	.65760	.11510	.08010	28.084	.11980	1.78
31.250	.01090	.01090	.08740	.00440	.67680	.11790	.09170	28.245	.09860	1.43
34.375	.00410	.01300	.12120	.00000	.69180	.07560	.09430	28.954	.08840	1.27
37.500	.00000	.01370	.14030	.00000	.69450	.05420	.09730	29.339	.08620	1.24
40.625	.00000	.01470	.14160	.00000	.70760	.04360	.09260	29.411	.08190	1.17
43.750	.00000	.01550	.14800	.00000	.71750	.03140	.08970	29.542	.07880	1.12
46.875	.00000	.01600	.12370	.00000	.75690	.02770	.07570	29.299	.06720	0.94
50.000	.00000	.02160	.12290	.00000	.76220	.02120	.07200	29.345	.06390	0.89

FLAME 3 Mole Fractions

z (mm)	H_2	O_2	CO_2	C_2H_2	N_2	CO	H_20	M (g/mol)	f	ϕ
3.125	.01870	.00080	.00620	.90270	.06220	.00930	.00000	25.846	.91800	146.36
6.250	.03430	.00390	.01560	.71820	.18740	.04060	.00000	25.968	.74850	38.98
9.375	.04830	.00650	.02420	.50000	.33870	.07900	.00330	26.150	.54900	15.94
12.500	.05930	.00780	.03120	.31230	.45280	.12020	.01640	26.220	.38500	8.20
15.625	.06690	.00880	.03500	.19930	.51000	.15290	.02700	26.205	.29120	5.38
18.750	.06210	.01010	.03570	.11790	.57410	.16290	.03720	26.405	.21400	3.57
21.875	.09620	.01050	.04570	.07560	.54970	.19700	.02520	25.883	.19790	3.23
25.000	.07300	.01110	.03660	.05770	.57800	.19870	.04470	26.183	.17420	2.76
28.125	.04300	.01170	.04300	.03910	.58590	.19920	.07810	26.771	.15560	2.41
31.250	.04030	.01070	.04260	.01420	.61610	.19670	.07930	26.868	.12950	1.95
34.375	.04360	.01130	.05500	.00000	.64450	.17440	.07110	27.093	.11010	1.62
37.500	.02820	.01140	.06690	.00000	.66900	.14610	.07830	27.612	.10030	1.46
40.625	.02250	.01220	.08260	.00000	.67540	.12570	.08160	27.982	.09680	1.40
43.750	.02290	.01140	.09850	.00000	.68550	.10370	.07820	28.257	.09300	1.34
46.875	.02070	.01230	.09800	.00000	.70840	.08810	.07240	28.368	.08540	1.22
50.000	.00530	.01150	.11080	.00000	.73900	.05540	.07770	28.917	.07480	1.06

FLAME 4 Mole Fractions

z (mm)	H_2	O_2	CO_2	C_2H_4	C_2H_2	N_2	CH_4	CO	H_20	M (g/mol)	f	ϕ
3.125	.01290	.00150	.00530	.00000	.65200	.31840	.00000	.00990	.00000	26.481		
6.250	.02960	.00470	.01950	.00039	.46710	.43590	.00000	.04210	.00081	26.644	.48660	47.13
9.375	.04160	.00610	.03080	.00077	.30820	.52390	.00000	.07700	.01150	26.725	.35330	12.44
12.500	.05240	.00900	.04260	.00082	.16370	.58120	.00290	.12240	.02500	26.760	.24160	5.55
15.625	.04880	.01090	.04420	.00038	.09290	.62750	.00193	.13550	.03780	26.910	.17790	3.41
18.750	.04010	.01170	.05310	.00000	.05820	.66170	.00000	.14740	.05950	27.183	.14690	2.56
21.875	.04080	.01180	.06060	.00000	.02870	.69050	.00000	.11890	.05980	27.322	.11230	1.82
25.000	.03240	.01280	.07100	.00000	.01340	.69710	.00000	.11360	.06370	27.695	.09910	1.57
28.125	.01760	.01000	.07810	.00000	.00880	.70520	.00000	.10580	.07440	28.083	.09330	1.47
31.250	.01240	.01130	.09310	.00000	.00000	.73310	.00000	.07740	.07290	28.496	.07780	1.18
34.375	.00230	.01380	.10880	.00000	.00000	.74010	.00000	.05610	.08010	28.947	.07400	1.11
37.500	.00170	.01250	.11180	.00000	.00000	.76780	.00000	.03460	.07150	29.092	.06550	0.97
40.625	.00000	.01580	.11860	.00000	.00000	.74340	.00000	.04190	.08030	29.170	.07160	1.07
43.750	.00000	.01830	.12450	.00000	.00000	.77040	.00000	.01640	.07040	29.374	.06240	0.92

46.875	.00000	.02060	.11580	.00000	.00000	.78910	.00000	.01110	.06340	29.314	.05620	0.82
50.000	.00000	.03330	.11700	.00000	.00000	.77790	.00000	.00880	.06290	29.389	.05570	0.81

B.3 Growth and Nucleation Rate Data

Table B.3 Growth and Nucleation Rates for Acetylene/Air Diffusion Flames

FLAME 1

z	$[C_2H_2]$	gross w_g	net w_g	$w_{ox}/w_{g,net}$	10000/T	n_p	w_n	kn
mm	kgmol/m^3	kg/m^2-s	kg/m^2-s	-	K^{-1}	μm^{-3}	kgmol/m^3-s	s^{-1}
3.125	.24568E-02	.00000E+00	.00000E+00	.00000E+00	10.6724	.00000	.00000E+00	.00000E+00
6.250	.10861E-02	.00000E+00	.00000E+00	.00000E+00	8.5034	.00000	.48223E-08	.44399E-05
9.375	.43723E-03	.38680E-01	.39029E-01	.90212E-02	6.2228	.00655	.42473E-07	.97141E-04
12.500	.18232E-03	.22433E-02	.27908E-02	.24407E+00	5.4795	.08723	.12700E-06	.69657E-03
15.625	.10226E-03	.33947E-03	.12358E-02	.26404E+01	5.6786	.34964	.10205E-06	.99799E-03
18.750	.54562E-04	.38179E-04	.88040E-03	.22060E+02	5.8140	.38395	.26264E-07	.48136E-03
21.875	.23963E-04	.65459E-04	.64633E-03	.88739E+01	6.0496	.46045	.58275E-07	.24319E-02
25.000	.79696E-05	.55032E-04	.61590E-03	.10192E+02	6.0827	.57720	.22729E-07	.28520E-02
28.125	.00000E+00	-.19259E-04	.73833E-03	-.39337E+02	6.0205	.53338	-.58321E-08	.00000E+00
31.250	.00000E+00	-.24101E-03	.49171E-03	-.30402E+01	6.0864	.57822	.21841E-07	.00000E+00
34.375	.00000E+00	-.36793E-03	.46666E-03	-.22683E+01	6.1350	.61104	.28700E-07	.00000E+00
37.500	.00000E+00	-.23718E-03	.87572E-03	-.46922E+01	6.0606	.65291	.16945E-07	.00000E+00
40.625	.00000E+00	-.72358E-03	.66971E-03	-.19256E+01	6.0060	.63978	-.86330E-07	.00000E+00
43.750	.00000E+00	-.22022E-02	-.12233E-02	-.44451E+00	6.2657	.46068	.00000E+00	.00000E+00
46.875	.00000E+00	-.22022E-02	-.12233E-02	-.44451E+00	6.7069	.00000	.00000E+00	.00000E+00

FLAME 2

z	$[C_2H_2]$	gross w_g	net w_g	$w_{ox}/w_{g,net}$	10000/T	n_p	w_n	kn
mm	kgmol/m^3	kg/m^2-s	kg/m^2-s	-	K^{-1}	μm^{-3}	kgmol/m^3-s	s^{-1}
3.125	.22889E-02	.00000E+00	.00000E+00	.00000E+00	11.4025	.00000	.00000E+00	.00000E+00
6.250	.11955E-02	.00000E+00	.00000E+00	.00000E+00	9.1408	.00000	.13102E-07	.10960E-04
9.375	.60252E-03	.19063E-01	.19083E-01	.10065E-02	7.9872	.01109	.28488E-07	.47281E-04
12.500	.23391E-03	.10527E-01	.10853E-01	.30930E-01	6.2073	.02982	.13483E-06	.57641E-03
15.625	.12288E-03	.14496E-02	.18943E-02	.30676E+00	5.3879	.20278	.25956E-06	.21123E-02
18.750	.90183E-04	.31433E-03	.91792E-03	.19202E+01	5.4735	.52922	.26060E-06	.28897E-02
21.875	.61828E-04	.23898E-03	.92084E-03	.28532E+01	5.5556	.77318	.23396E-06	.37841E-02
25.000	.38886E-04	.52172E-04	.83789E-03	.15060E+02	5.6721	1.09286	-.60147E-08	-.15467E-03
28.125	.18944E-04	.23623E-04	.73957E-03	.30307E+02	5.7971	.81897	-.99495E-07	-.52520E-02
31.250	.59043E-05	.27178E-04	.59503E-03	.20893E+02	5.8720	.92603	.87058E-07	.14745E-01
34.375	.00000E+00	-.17597E-04	.74807E-03	-.43512E+02	5.8072	1.04608	.19005E-06	.00000E+00
37.500	.00000E+00	-.11559E-03	.75305E-03	-.75148E+01	5.7670	1.37436	.62373E-07	.00000E+00
40.625	.00000E+00	-.37118E-03	.65191E-03	-.27563E+01	5.6180	1.16054	-.65315E-07	.00000E+00
43.750	.00000E+00	-.69102E-03	.44886E-03	-.16496E+01	5.5432	1.19146	-.17159E-06	.00000E+00
46.875	.00000E+00	-.14748E-02	-.84954E-03	-.42398E+00	6.1463	.86591	.00000E+00	.00000E+00
50.000	.00000E+00	-.14748E-02	-.84954E-03	-.42398E+00	6.9396	.00000	.00000E+00	.00000E+00

FLAME 3

z	$[C_2H_2]$	gross w_g	net w_g	$w_{ox}/w_{g,net}$	10000/T	n_p	w_n	kn
mm	kgmol/m^3	kg/m^2-s	kg/m^2-s	-	K^{-1}	μm^{-3}	kgmol/m^3-s	s^{-1}
6.250	.10942E-02	.00000E+00	.00000E+00	.00000E+00	10.0000	.00000	.00000E+00	.00000E+00
9.375	.64884E-03	.00000E+00	.00000E+00	.00000E+00	8.5179	.00000	.18680E-07	.28790E-04
12.500	.36968E-03	.10551E-01	.10568E-01	.16828E-02	7.7700	.01031	.18025E-07	.48758E-04
15.625	.17400E-03	.19329E-01	.19550E-01	.11420E-01	5.7307	.01128	.12238E-06	.70333E-03
18.750	.88920E-04	.28511E-02	.32280E-02	.13219E+00	4.9505	.11394	.13498E-06	.15180E-02
21.875	.56681E-04	.79151E-03	.12854E-02	.62400E+00	4.9213	.17050	.13827E-06	.24395E-02
25.000	.43112E-04	.16105E-03	.58451E-03	.26294E+01	4.9044	.30075	.17668E-06	.40982E-02
28.125	.29680E-04	-.25946E-05	.43412E-03	-.16832E+03	4.9826	.44981	.88074E-07	.29674E-02
31.250	.10915E-04	-.75060E-04	.31073E-03	-.51397E+01	5.0454	.45989	.42131E-07	.38599E-02
34.375	.00000E+00	-.15092E-03	.25952E-03	-.27196E+01	5.1706	.54403	.81758E-07	.00000E+00
37.500	.00000E+00	-.14435E-03	.29295E-03	-.30295E+01	5.2493	.63682	.10306E-07	.00000E+00
40.625	.00000E+00	-.36272E-03	.22824E-03	-.16292E+01	5.1573	.57847	-.80807E-07	.00000E+00
43.750	.00000E+00	-.14017E-02	-.68470E-03	-.51151E+00	5.1151	.49387	.00000E+00	.00000E+00
46.875	.00000E+00	-.14017E-02	-.68470E-03	-.51151E+00	5.5157	.00000	.00000E+00	.00000E+00

FLAME 4

z	$[C_2H_2]$	gross w_g	net w_g	$w_{ox}/w_{g,net}$	10000/T	n_p	w_n	kn
mm	kgmol/m^3	kg/m^2-s	kg/m^2-s	-	K^{-1}	μm^{-3}	kgmol/m^3-s	s^{-1}
3.125	.24436E-02	.00000E+00	.00000E+00	.00000E+00	12.3001	.00000	.00000E+00	.00000E+00
6.250	.13804E-02	.00000E+00	.00000E+00	.00000E+00	9.6993	.00000	.26916E-08	.19498E-05
9.375	.77996E-03	.72835E-02	.72951E-02	.15868E-02	8.3056	.00246	.21599E-08	.27693E-05
12.500	.32118E-03	.16139E-01	.16434E-01	.18295E-01	6.4391	.00236	.24734E-07	.77010E-04
15.625	.15840E-03	.60331E-02	.67769E-02	.12329E+00	5.5960	.03648	.50586E-07	.31936E-03
18.750	.10002E-03	.21008E-02	.29321E-02	.39574E+00	5.6402	.09778	.18288E-06	.18285E-02
21.875	.48314E-04	.64418E-03	.15403E-02	.13911E+01	5.5249	.39755	.25653E-06	.53098E-02
25.000	.23146E-04	.20485E-03	.11739E-02	.47304E+01	5.6689	.66735	.10879E-06	.47002E-02
28.125	.15200E-04	.26607E-05	.81160E-03	.30403E+03	5.6689	.66237	-.10638E-07	-.69984E-03
31.250	.00000E+00	-.54838E-04	.75710E-03	-.14806E+02	5.8824	.68736	.48816E-07	.00000E+00

34.375	.00000E+00	-.14971E-03	.98630E-03	-.75880E+01	5.7274	.79895	.14213E-06	.00000E+00
37.500	.00000E+00	-.23356E-03	.80199E-03	-.44338E+01	5.7604	1.00918	-.18082E-07	.00000E+00
40.625	.00000E+00	-.65131E-03	.71410E-03	-.20964E+01	5.6593	.75480	-.29110E-06	.00000E+00
43.750	.00000E+00	-.20151E-02	-.55560E-03	-.72428E+00	5.7339	.36894	.00000E+00	.00000E+00
46.875	.00000E+00	-.20151E-02	-.55560E-03	-.72428E+00	6.1652	.00000	.00000E+00	.00000E+00

APPENDIX C

TABULATION OF DATA FOR HYDROCARBON/AIR DIFFUSION FLAMES

C.1 Structure Data

Table C.1 Structure Measurements for Hydrocarbon/Air Diffusion Flames

C_2H_6 FLAME

z (mm)	u (m/s)	t (ms)	T (K)	d_p (nm)	f_s (ppm)
6.	0.1653	50.405			
10.	0.4026	67.472			
13.	0.5719	73.821			
16.	0.7266	78.508			
22.	0.9872	85.676			
28.	1.2064	91.201			
34.	1.4081	95.819	1298.		
37.	1.5016	97.883	1340.		0.
40.	1.5937	99.823	1683.	28.15	0.052
43.	1.6798	101.657	1760.	28.07	0.115
46.	1.7637	103.401	1855.	25.92	0.272
49.	1.8342	105.069	1875.	23.80	0.619
52.	1.9021	106.675	1895.	19.69	0.745
55.	1.9661	108.227	1935.	19.18	0.732
58.	2.0247	109.731	1900.	19.44	0.618
61.	2.0771	111.194	1970.	19.44	0.433
64.	2.1318	112.619	1857.	18.25	0.22
67.	2.1745	114.013	1729.		0.

C_3H_8 FLAME

z (mm)	u (m/s)	t (ms)	T (K)	d_p (nm)	f_s (ppm)
6.	0.1476	57.872			
10.	0.3880	76.577			
14.	0.6421	84.846			
18.	0.8248	90.386			
22.	0.9983	94.814	1186.		
26.	1.1606	98.541	1253.		0.
30.	1.3050	101.797	1309.	24.03	0.033
34.	1.4373	104.721	1557.	27.15	0.128
38.	1.5287	107.421	1754.	29.42	0.330
42.	1.6319	109.954	1777.	30.28	1.170
46.	1.7317	112.335	1780.	24.57	1.510
50.	1.8248	114.586	1753.	22.70	1.725
54.	1.9088	116.730	1820.	21.96	1.547
58.	1.9876	118.784	1849.	23.13	1.390
62.	2.0617	120.760	1902.	22.76	0.935
66.	2.1233	122.672	1787.	17.49	0.346
70.	2.1741	124.534	1557.		0.

C_4H_{10} FLAME

z (mm)	u (m/s)	t (ms)	T (K)	d_p (nm)	f_s (ppm)
6.	0.1317	65.35			
10.	0.3774	85.84			
14.	0.6128	94.40			
18.	0.8151	100.12			
22.	0.9947	104.59	1191.		
26.	1.1610	108.32	1263.		0.
30.	1.3084	111.57	1508.	31.37	0.062
34.	1.4108	114.52	1644.	27.35	0.140
38.	1.5128	117.26	1855.	28.08	0.550
42.	1.6273	119.81	1815.	26.51	1.305
46.	1.7215	122.20	1701.	21.36	1.650
50.	1.8156	124.46	1753.	20.99	1.905
54.	1.8991	126.62	1735.	20.05	1.800
58.	1.9765	128.68	1780.	19.15	1.605
62.	2.0461	130.67	1800.	19.49	1.250
66.	2.1054	132.60	1721.	19.30	0.477
70.	2.1556	134.48	1546.		0.

C_2H_4 FLAME

z (mm)	u (m/s)	t (ms)	T (K)	d_p (nm)	f_s (ppm)
6.	0.2259	37.619			
10.	0.4809	50.631			
14.	0.7131	57.595	1122.		
18.	0.9309	62.548	1278.		0.
22.	1.0847	66.540	1319.	26.16	0.035
26.	1.2366	70.001	1504.	28.72	0.087
30.	1.3805	73.068	1730.	27.27	0.340
34.	1.5045	75.846	1785.	31.49	1.330
38.	1.6026	78.423	1748.	26.83	1.920
42.	1.6749	80.865	1653.	26.63	2.100
46.	1.7598	83.196	1665.	25.35	2.310
50.	1.8414	85.418	1704.	25.86	2.351
54.	1.9189	87.547	1695.	23.84	2.228
58.	1.9965	89.591	1770.	22.80	2.030
62.	2.0594	91.564	1765.	22.29	1.170
66.	2.1273	93.475	1632.	20.08	0.496
70.	2.1798	95.333	1510.		0.

C_3H_6 FLAME

z (mm)	u (m/s)	t (ms)	T (K)	d_p (nm)	f_s (ppm)
1.5	1.931	0.744			
3.125	1.741	1.632			
6.250	1.332	3.702	889.		
9.375	1.149	6.235	1034.		0.
12.500	1.119	8.992	1134.	18.73	0.02
15.625	1.159	11.736	1302.	19.15	0.061
18.750	1.227	14.358	1555.	22.18	0.128
21.875	1.307	16.827	1799.	22.79	0.276
25.000	1.369	19.163	1753.	23.17	0.727
28.125	1.411	21.412	1700.	21.95	0.891
31.250	1.458	23.591	1697.	19.95	0.935
34.375	1.502	25.703	1687.	20.33	0.950
37.500	1.554	27.749	1719.	20.35	0.851
40.625	1.606	29.727	1762.	19.04	0.735
43.750	1.660	31.641	1804.	18.5	0.591
46.875	1.715	33.494	1627.		0.
50.000	1.744	35.301			

C_4H_6 FLAME

z (mm)	u (m/s)	t (ms)	T (K)	d_p (nm)	f_s (ppm)
1.5	1.448				
3.125	1.337	2.171	717.		
6.250	1.097	4.764	892.		0.
9.375	1.019	7.721	1048.	21.29	0.031
12.500	1.059	10.730	1266.	24.13	0.062
15.625	1.130	13.588	1575.	20.51	0.175
18.750	1.192	16.282	1794.	15.21	0.594
21.875	1.225	18.868	1645.	14.08	1.040
25.000	1.263	21.381	1628.	14.16	1.143
28.125	1.298	23.822	1605.	14.60	1.184

31.250	1.348	26.185	1630.	14.60	1.091
34.375	1.396	28.463	1637.	14.10	0.968
37.500	1.441	30.667	1634.	13.73	0.774
40.625	1.486	32.802	1576.	13.08	0.692
43.750	1.527	34.877	1476.	12.59	0.312
46.875	1.563	36.900	1240.	12.59	0.276
50.000	1.589	38.883	1191.		0.

C.2 Chemical Composition Data

Table C.2 Chemical Composition Measurements for Hydrocarbon/Air Diffusion Flames

C_2H_6 FLAME MOLE FRACTIONS

z	H_2	O_2	CO_2	C_2H_4	C_2H_2	C_2H_6	N_2	CH_4	CO	H_2O	M (g/mol)	f	ϕ
4.	.03685	.00103	.00665	.01038	.00000	.80776	.07686	.00218	.03035	.02793	28.522	0.88337	120.27
10.	.01798	.00498	.04706	.02239	.00000	.35772	.37258	.00430	.04006	.13294	27.674	0.46267	13.67
16.	.02327	.00641	.05440	.02849	.00000	.18262	.47533	.00624	.05581	.16743	26.932	0.30075	6.83
22.	.02996	.00671	.06313	.03559	.00000	.09094	.51642	.00787	.06120	.18818	26.483	0.21870	4.45
28.	.04020	.00736	.06220	.03883	.00000	.02347	.51982	.00911	.08465	.21436	25.790	0.16360	3.11
34.	.04067	.00700	.06474	.01540	.00000	.00096	.52162	.00759	.10959	.23244	25.607	0.12603	2.29
37.	.02432	.00712	.06620	.01326	.00000	.00030	.54286	.00720	.10164	.23710	26.012	0.11685	2.10
40.	.02450	.00792	.07587	.00225	.00000	.00000	.57680	.00359	.08773	.22135	26.365	0.09793	1.72
43.	.00634	.00826	.07393	.00209	.01387	.00000	.61094	.00362	.05935	.22160	26.777	0.09480	1.66
46.	.00231	.00817	.07807	.00032	.01083	.00000	.61806	.00141	.05791	.22292	26.967	0.08900	1.55
49.	.00207	.00854	.08306	.00010	.00341	.00000	.62384	.00103	.05961	.21834	27.120	0.08353	1.45
52.	.00302	.00842	.09736	.00000	.00000	.00000	.64006	.00050	.04314	.20749	27.445	0.07725	1.33
55.	.00171	.00881	.11078	.00000	.00000	.00000	.64633	.00000	.02716	.20520	27.724	0.07480	1.28
58.	.00128	.00876	.11839	.00000	.00000	.00000	.63879	.00000	.02259	.21019	27.807	0.07623	1.31
61.	.00054	.00895	.12147	.00000	.00000	.00000	.65363	.00000	.01349	.20191	27.959	0.07260	1.24
64.	.00038	.00884	.12179	.00000	.00000	.00000	.65876	.00000	.01117	.19906	27.996	0.07140	1.22
70.	.00004	.00890	.12819	.00000	.00000	.00000	.66973	.00000	.00036	.19278	28.171	0.06860	1.17

C_3H_8 FLAME MOLE FRACTIONS

z	H_2	O_2	CO_2	C_2H_4	C_2H_2	C_2H_6	N_2	CH_4	CO	C_3H_8	H_2O	M (g/mol)	f	ϕ
2.	.030351	.000759	.004685	.047519	.000000	.003239	.067454	.048523	.018885	.778533	.000052	39.251	.939700	241.07
10.	.107102	.005342	.031760	.009934	.000000	.002442	.393038	.016984	.139317	.178593	.115488	27.278	.403400	10.46
18.	.079701	.006161	.050585	.019697	.000000	.002710	.481457	.022153	.122059	.067527	.147950	26.123	.248800	5.12
26.	.092468	.006626	.054832	.018117	.000000	.002047	.521659	.022312	.128945	.003904	.149090	24.822	.152850	2.79
30.	.042287	.007165	.067621	.018665	.000000	.000460	.565328	.015065	.099704	.000645	.183060	26.025	.125700	2.22
34.	.035793	.007365	.069358	.010580	.000000	.000121	.584014	.010967	.096497	.000258	.185049	26.245	.111450	1.94
38.	.005283	.008130	.074805	.002567	.012742	.000020	.638742	.005089	.059401	.000014	.193206	27.087	.092250	1.57
42.	.002616	.008337	.080513	.000201	.005900	.000000	.667399	.001593	.051343	.000000	.182096	27.415	.078100	1.31
46.	.001011	.008370	.090171	.000049	.001651	.000000	.681194	.000570	.040869	.000000	.176114	27.692	.071650	1.19
50.	.001041	.008800	.103428	.000000	.000000	.000000	.682072	.000175	.029029	.000000	.175453	27.919	.069850	1.16
54.	.000409	.009086	.110388	.000000	.000000	.000000	.690292	.000046	.018444	.000000	.171335	28.091	.067450	1.12
58.	.000163	.009000	.116993	.000000	.000000	.000000	.692219	.000000	.011056	.000000	.170568	28.211	.066700	1.11
62.	.000270	.009099	.121999	.000000	.000000	.000000	.691059	.000000	.006505	.000000	.171068	28.284	.066800	1.11
66.	.000041	.008717	.127548	.000000	.000000	.000000	.692075	.000000	.000684	.000000	.170934	28.378	.066450	1.10
70.	.000041	.008586	.127418	.000000	.000000	.000000	.693624	.000000	.000207	.000000	.170125	28.384	.066100	1.09

C_4H_{10} FLAME MOLE FRACTIONS

z	H_2	O_2	CO_2	C_2H_4	C_2H_2	C_2H_6	N_2	CH_4	CO	C_3H_8	C_4H_{10}	H_2O	M (g/mol)	f	ϕ
2.	.015948	.001291	.008273	.033961	.000000	.012536	.099003	.040957	.030897	.040930	.708472	.007732	49.187	.924800	187.63
10.	.074977	.006214	.048905	.025551	.000000	.004122	.447470	.019575	.106347	.009972	.144235	.112630	30.023	.407050	10.47
18.	.040249	.007219	.063365	.042780	.000000	.003341	.516725	.023222	.088460	.012014	.053795	.148830	28.065	.268400	5.60
26.	.068740	.007188	.061851	.020738	.000000	.001045	.534479	.014821	.125580	.001238	.000351	.163970	25.460	.143200	2.55
30.	.050228	.007318	.057148	.011137	.000000	.000364	.530507	.011373	.139303	.000293	.000209	.192118	25.606	.131950	2.32
34.	.026348	.008008	.072331	.005106	.000000	.000000	.573904	.006779	.109279	.000000	.000115	.198132	26.458	.109300	1.87
38.	.004435	.008902	.080282	.001649	.011133	.000000	.635316	.003803	.063914	.000000	.000083	.190482	27.248	.092700	1.56
42.	.001541	.009150	.084437	.000052	.004488	.000000	.671571	.001077	.052322	.000000	.000000	.175359	27.585	.077400	1.28
46.	.000693	.009876	.094274	.000000	.001043	.000000	.684425	.000331	.040396	.000000	.000000	.168961	27.847	.071550	1.18
50.	.000542	.009669	.104281	.000000	.000025	.000000	.690081	.000066	.029128	.000000	.000000	.166207	28.043	.069200	1.13
54.	.000394	.010498	.106673	.000000	.000000	.000000	.691635	.000033	.025709	.000000	.000000	.165058	28.100	.068450	1.12
58.	.000175	.009874	.117325	.000000	.000000	.000000	.692572	.000000	.014922	.000000	.000000	.165132	28.274	.067950	1.11
62.	.000044	.009338	.127344	.000000	.000000	.000000	.686522	.000000	.007830	.000000	.000000	.168923	28.397	.069150	1.13
66.	.000043	.009117	.134427	.000000	.000000	.000000	.685146	.000000	.001457	.000000	.000000	.169811	28.501	.069300	1.14
70.	.000043	.009746	.133722	.000000	.000000	.000000	.688923	.000000	.000202	.000000	.000000	.167363	28.517	.068250	1.12

C_2H_4 FLAME MOLE FRACTIONS

z	H_2	O_2	CO_2	C_2H_4	C_2H_2	C_2H_6	N_2	CH_4	CO	H_2O	M (g/mol)	f	ϕ
4.	.002453	.000365	.002496	.945285	.000000	.002573	.036125	.000928	.006617	.003158	27.992	.954950	309.25
10.	.051791	.005312	.052130	.299927	.000000	.001870	.394235	.001873	.098133	.094730	26.568	.399000	9.69
18.	.054448	.006932	.069413	.108645	.000000	.000585	.536957	.002907	.104320	.115793	26.548	.208750	3.85
22.	.050141	.007129	.071404	.083784	.003593	.000399	.536381	.003420	.111355	.132393	26.512	.191350	3.45
26.	.044336	.007492	.069677	.019061	.003289	.000139	.543048	.002718	.142235	.168007	26.287	.138550	2.35
30.	.028660	.008035	.077987	.005431	.004524	.000000	.580873	.002404	.120319	.171768	26.792	.115500	1.91
34.	.003491	.011021	.089424	.000403	.008348	.000000	.638984	.001181	.077025	.170124	27.665	.093850	1.51
38.	.002025	.008829	.095136	.000153	.006035	.000000	.642416	.001068	.073130	.171208	27.781	.091750	1.47
42.	.000973	.009030	.110329	.000024	.001158	.000000	.661183	.000288	.053396	.163622	28.147	.082950	1.32
46.	.000755	.009074	.118468	.000024	.000469	.000000	.670632	.000143	.041198	.159239	28.330	.079600	1.26
50.	.000422	.008961	.128224	.000000	.000000	.000000	.680945	.000036	.026824	.154590	28.543	.076200	1.20
54.	.000187	.009187	.137024	.000000	.000000	.000000	.689305	.000000	.013730	.150567	28.731	.073600	1.16
58.	.000193	.009367	.148436	.000000	.000000	.000000	.679848	.000000	.006956	.155199	28.868	.075500	1.19
62.	.000188	.009070	.145554	.000000	.000000	.000000	.689430	.000000	.005196	.150562	28.868	.073250	1.15
66.	.000187	.009038	.149063	.000000	.000000	.000000	.686971	.000000	.002933	.151809	28.911	.073750	1.16
70.	.000118	.008949	.150065	.000000	.000000	.000000	.687287	.000000	.001817	.151764	28.929	.073600	1.16

C_3H_6 FLAME MOLE FRACTIONS

z	H_2	O_2	CO_2	C_2H_4	C_2H_2	N_2	CH_4	CO	C_3H_6	H_2O	M (g/mol)	f	ϕ
3.125	.02240	.00190	.00900	.00150	.00000	.11220	.00260	.01270	.83770	.00000	39.343	0.9060	140.58
6.250	.06290	.00510	.02640	.00710	.00000	.30300	.00710	.04450	.54310	.00100	34.370	0.7022	34.39
9.375	.08850	.00710	.04110	.00820	.00300	.45700	.01270	.06690	.31120	.00980	30.509	0.4919	14.12
12.500	.10430	.00880	.05030	.01580	.00550	.53300	.01790	.08200	.17840	.01560	28.269	0.3276	7.11
15.625	.08840	.00910	.05440	.01660	.02340	.58160	.02190	.08840	.06040	.05590	26.605	0.2242	4.22
18.750	.07280	.00890	.05720	.01640	.03190	.59430	.02000	.09360	.01480	.09000	26.077	0.1676	2.94
21.875	.05690	.00900	.05830	.00870	.02710	.62480	.01040	.08810	.01040	.10620	26.409	0.1370	2.32
25.000	.04160	.01010	.06170	.00540	.01920	.64710	.00460	.08320	.00930	.11790	26.818	0.1183	1.96
28.125	.03690	.01010	.07550	.00000	.01470	.64510	.00220	.07750	.00900	.12870	27.089	0.1097	1.80
31.250	.02900	.01030	.09450	.00000	.00790	.64540	.00000	.06970	.00000	.14310	27.365	0.0921	1.48
34.375	.01630	.01070	.09800	.00000	.00000	.64860	.00000	.07230	.00000	.15390	27.664	0.0862	1.38
37.500	.00620	.01080	.11100	.00000	.00000	.69340	.00000	.03700	.00000	.14180	28.253	0.0734	1.16
40.625	.00200	.00990	.10910	.00000	.00000	.72420	.00000	.02380	.00000	.13100	28.436	0.0654	1.02
43.750	.00000	.01340	.10950	.00000	.00000	.73770	.00000	.01490	.00000	.12440	28.574	0.0610	0.95

46.875	.00000	.01820	.10850	.00000	.00000	.74290	.00000	.01090	.00000	.11940	28.628	0.0584	0.90
50.000	.00000	.02860	.10630	.00000	.00000	.74840	.00000	.00510	.00000	.11150	28.713	0.0544	0.84

C_4H_6 FLAME MOLE FRACTIONS

z	H_2	O_2	CO_2	C_2H_4	C_2H_2	N_2	CH_4	CO	C_4H_6	H_2O	M (g/mol)	f	ϕ
3.125	.01520	.00360	.01800	.00470	.00580	.40720	.00160	.01960	.51280	.01150	41.148	0.6936	
6.250	.02710	.00710	.03990	.01050	.01880	.51910	.00370	.04890	.28590	.03897	34.960	0.5005	32.50
9.375	.03520	.00840	.05580	.01610	.02790	.58810	.00500	.06420	.14510	.05450	31.148	0.3441	10.39
12.500	.03890	.00920	.06020	.01950	.03680	.63930	.00660	.07720	.04780	.06450	28.452	0.2126	4.43
15.625	.03920	.01010	.06920	.01510	.03990	.66200	.00600	.08280	.00600	.06990	27.449	0.1430	2.57
18.750	.02640	.00990	.07630	.00440	.02450	.68210	.00330	.07770	.00027	.09510	27.555	0.1059	1.76
21.875	.02240	.01360	.08480	.00000	.01670	.69440	.00000	.06860	.00000	.10100	27.799	0.0906	1.47
25.000	.00950	.01420	.09660	.00000	.00680	.70520	.00000	.05800	.00000	.10980	28.257	0.0801	1.27
28.125	.00320	.01290	.11050	.00000	.00000	.72080	.00000	.04170	.00000	.11100	28.639	0.0718	1.12
31.250	.00000	.01790	.11440	.00000	.00000	.73510	.00000	.02680	.00000	.10590	28.856	0.0661	1.02
34.375	.00000	.02490	.11210	.00000	.00000	.74760	.00000	.01790	.00000	.09750	28.931	0.0607	0.93
37.500	.00000	.03480	.12180	.00000	.00000	.72790	.00000	.01510	.00000	.10260	29.072	0.0634	0.98
40.625	.00000	.04010	.10170	.00000	.00000	.76500	.00000	.00960	.00000	.08350	28.965	0.0519	0.78
43.750	.00000	.04580	.10410	.00000	.00000	.76050	.00000	.00660	.00000	.08300	29.031	0.0515	0.78
46.875	.00000	.05510	.09520	.00000	.00000	.77190	.00000	.00370	.00000	.07420	29.014	0.0460	0.69
50.000	.00000	.06630	.08810	.00000	.00000	.77560	.00000	.00220	.00000	.06780	29.009	0.0420	0.62

C.3 Growth and Nucleation Rate Data

Table C.3 Growth and Nucleation Rates for Hydrocarbon/Air Diffusion Flames

C_2H_6 FLAME

z	$[C_2H_2]$	$[C_2H_4]$	$w_{g,gross}$	$w_{g,net}/vc_2h_2$	$w_{ox}/w_{g,gross}$	$w_{g,par}/vc_2h_4$	n_p	k_n
mm	kgmol/m^3	kgmol/m^3	kg/m^2-s	kg/m^3	-	kg/m^3	μm^{-3}	s^{-1}
34.000	.00000E+00	.14087E-03	.00000E+00	.00000E+00	.00000E+00	.00000E+00	.00000	.00000E+00
37.000	.00000E+00	.11749E-03	.00000E+00	.00000E+00	.00000E+00	.00000E+00	.00000	.00000E+00
40.000	.00000E+00	.15874E-04	.52288E-02	.62017E-05	.38727E+00	.64373E-05	.00445	.00000E+00
43.000	.93571E-04	.14100E-04	.49045E-02	.65476E-05	.59682E+00	.45443E-05	.00993	.13266E-03
46.000	.69320E-04	.20482E-05	.43978E-02	.68788E-05	.92072E+00	.54718E-05	.02983	.54993E-03
49.000	.21594E-04	.63325E-06	.17189E-02	.50598E-05	.26341E+01	.47324E-05	.08769	.36677E-02
52.000	.00000E+00	.00000E+00	.31217E-03	.44824E-05	.16821E+02	.46527E-05	.18639	.00000E+00
55.000	.00000E+00	.00000E+00	-.34747E-03	.50185E-05	-.19114E+02	.52092E-05	.19814	.00000E+00
58.000	.00000E+00	.00000E+00	-.98517E-03	.41838E-05	-.62777E+01	.43427E-05	.16066	.00000E+00
61.000	.00000E+00	.00000E+00	-.18777E-02	.49193E-05	-.43153E+01	.51062E-05	.11256	.00000E+00
64.000	.00000E+00	.00000E+00	-.41703E-02	.10589E-05	-.13120E+01	.10991E-05	.06913	.00000E+00
67.000	.00000E+00	.00000E+00	-.41703E-02	.10974E-05	-.13120E+01	.11390E-05	.00000	.00000E+00

C_3H_8 FLAME

z	$[C_2H_2]$	$[C_2H_4]$	$w_{g,gross}$	$w_{g,net}/vc_2h_2$	$w_{ox}/w_{g,gross}$	$w_{g,par}/vc_2h_4$	n_p	k_n
mm	kgmol/m^3	kgmol/m^3	kg/m^2-s	kg/m^3	-	kg/m^3	μm^{-3}	s^{-1}
22.000	.00000E+00	.18138E-03	.00000E+00	.00000E+00	.00000E+00	.00000E+00	.00000	.00000E+00
26.000	.00000E+00	.17168E-03	.00000E+00	.00000E+00	.00000E+00	.00000E+00	.00000	.00000E+00
30.000	.00000E+00	.16930E-03	.54246E-02	.53670E-05	.20582E-01	.55709E-05	.00454	.00000E+00
34.000	.00000E+00	.80681E-04	.38409E-02	.41959E-05	.22899E+00	.43553E-05	.01222	.00000E+00
38.000	.86255E-04	.17377E-04	.54971E-02	.69874E-05	.51779E+00	.51770E-05	.02475	.25336E-03
42.000	.39422E-04	.13430E-05	.19043E-02	.42864E-05	.17052E+01	.35005E-05	.08049	.14351E-02
46.000	.11013E-04	.32685E-06	.54845E-03	.33290E-05	.63013E+01	.31904E-05	.19443	.63192E-02
50.000	.00000E+00	.00000E+00	.48884E-04	.28598E-05	.68835E+02	.29684E-05	.28165	.00000E+00
54.000	.00000E+00	.00000E+00	-.27669E-03	.35543E-05	-.16625E+02	.36893E-05	.27899	.00000E+00
58.000	.00000E+00	.00000E+00	-.72355E-03	.36796E-05	-.72346E+01	.38194E-05	.21453	.00000E+00
62.000	.00000E+00	.00000E+00	-.19882E-02	.35877E-05	-.32438E+01	.37240E-05	.15146	.00000E+00
66.000	.00000E+00	.00000E+00	-.41290E-02	.13577E-06	-.10396E+01	.14093E-06	.12351	.00000E+00
70.000	.00000E+00	.00000E+00	-.41290E-02	.14545E-06	-.10396E+01	.15098E-06	.00000	.00000E+00

C_4H_{10} FLAME

z	$[C_2H_2]$	$[C_2H_4]$	$w_{g,gross}$	$w_{g,net}/vc_2h_2$	$w_{ox}/w_{g,gross}$	$w_{g,par}/vc_2h_4$	n_p	k_n
mm	kgmol/m^3	kgmol/m^3	kg/m^2-s	kg/m^3	-	kg/m^3	μm^{-3}	s^{-1}
22.000	.00000E+00	.20674E-03	.00000E+00	.00000E+00	.00000E+00	.00000E+00	.00000	.00000E+00
26.000	.00000E+00	.19496E-03	.00000E+00	.00000E+00	.00000E+00	.00000E+00	.00000	.00000E+00
30.000	.00000E+00	.87689E-04	.37050E-02	.38820E-05	.16005E+00	.40294E-05	.00384	.00000E+00
34.000	.00000E+00	.36877E-04	.57086E-02	.63349E-05	.28284E+00	.65755E-05	.01307	.00000E+00
38.000	.71260E-04	.10555E-04	.33614E-02	.62403E-05	.12797E+01	.47624E-05	.04744	.51429E-03
42.000	.29360E-04	.34018E-06	.12270E-02	.42818E-05	.32387E+01	.37379E-05	.13378	.28629E-02
46.000	.72804E-05	.00000E+00	.46598E-03	.26570E-05	.57048E+01	.25827E-05	.32336	.12712E-01
50.000	.16933E-06	.00000E+00	.12997E-03	.30628E-05	.27130E+02	.31751E-05	.39342	.23459E+00
54.000	.00000E+00	.00000E+00	-.23772E-03	.26583E-05	-.14280E+02	.27593E-05	.42651	.00000E+00
58.000	.00000E+00	.00000E+00	-.45844E-03	.31265E-05	-.92034E+01	.32453E-05	.43649	.00000E+00
62.000	.00000E+00	.00000E+00	-.13955E-02	.26975E-05	-.33381E+01	.27999E-05	.32246	.00000E+00
66.000	.00000E+00	.00000E+00	-.43102E-02	-.85826E-06	-.76448E+00	-.89087E-06	.12672	.00000E+00
70.000	.00000E+00	.00000E+00	-.43102E-02	-.90553E-06	-.76448E+00	-.93994E-06	.00000	.00000E+00

C_2H_4 FLAME

z	$[C_2H_2]$	$[C_2H_4]$	$w_{g,gross}$	$w_{g,net}/vc_2h_2$	$w_{ox}/w_{g,gross}$	$w_{g,par}/vc_2h_4$	n_p	k_n
mm	kgmol/m^3	kgmol/m^3	kg/m^2-s	kg/m^3	-	kg/m^3	μm^{-3}	s^{-1}
14.000	.00000E+00	.11497E-02	.00000E+00	.00000E+00	.00000E+00	.00000E+00	.00000	.00000E+00
18.000	.00000E+00	.10094E-02	.00000E+00	.00000E+00	.00000E+00	.00000E+00	.00000	.00000E+00
22.000	.32344E-04	.75421E-03	.30664E-02	.30808E-05	.40346E-01	.24195E-05	.00373	.55363E-04
26.000	.25965E-04	.15048E-03	.54271E-02	.54573E-05	.11186E+00	.50397E-05	.00701	.31682E-03
30.000	.31049E-04	.37274E-04	.52430E-02	.66076E-05	.49453E+00	.61114E-05	.03202	.68281E-03
34.000	.55529E-04	.26807E-05	.20953E-02	.50830E-05	.19221E+01	.39396E-05	.08135	.85069E-03
38.000	.40993E-04	.10393E-05	.51558E-03	.31011E-05	.61698E+01	.22324E-05	.18986	.93318E-03
42.000	.83179E-05	.17239E-06	.20754E-03	.19601E-05	.99479E+01	.18344E-05	.21238	.28113E-02
46.000	.33445E-05	.17115E-06	.21602E-03	.21479E-05	.10567E+02	.21490E-05	.27082	.56724E-02
50.000	.00000E+00	.00000E+00	-.55136E-04	.24398E-05	-.53079E+02	.25325E-05	.25964	.00000E+00
54.000	.00000E+00	.00000E+00	-.21304E-03	.22866E-05	-.13599E+02	.23735E-05	.31405	.00000E+00
58.000	.00000E+00	.00000E+00	-.83894E-03	.30093E-05	-.53026E+01	.31236E-05	.32711	.00000E+00
62.000	.00000E+00	.00000E+00	-.23865E-02	.15538E-05	-.17798E+01	.16128E-05	.20177	.00000E+00
66.000	.00000E+00	.00000E+00	-.41989E-02	-.18727E-05	-.48630E+00	-.19439E-05	.11700	.00000E+00
70.000	.00000E+00	.00000E+00	-.41989E-02	-.19469E-05	-.48630E+00	-.20209E-05	.00000	.00000E+00

C_3H_6 FLAME

z	$[C_2H_2]$	$[C_2H_4]$	$w_{g,gross}$	$w_{g,net}/vc_2h_2$	$w_{ox}/w_{g,gross}$	$w_{g,par}/vc_2h_4$	n_p	k_n
mm	kgmol/m^3	kgmol/m^3	kg/m^2-s	kg/m^3	-	kg/m^3	μm^{-3}	s^{-1}
6.250	.00000E+00	.24335E-04	.00000E+00	.00000E+00	.00000E+00	.00000E+00	.00000	.00000E+00
9.375	.88403E-05	.24164E-04	.00000E+00	.00000E+00	.00000E+00	.00000E+00	.00000	.24761E-03
12.500	.14778E-04	.42453E-04	.39052E-02	.40748E-05	.17962E-02	.38740E-05	.00581	.41323E-03
15.625	.54761E-04	.38848E-04	.25102E-02	.24825E-05	.17397E-01	.12588E-05	.01659	.12734E-03
18.750	.62507E-04	.32135E-04	.27712E-02	.27386E-05	.11105E+00	.13382E-05	.02240	.19330E-03
21.875	.45899E-04	.14735E-04	.30893E-02	.31242E-05	.22296E+00	.21382E-05	.04453	.65592E-03
25.000	.33372E-04	.93860E-05	.12210E-02	.16428E-05	.60613E+00	.90205E-06	.11162	.11741E-02
28.125	.26347E-04	.00000E+00	.28683E-03	.83937E-06	.24400E+01	.23716E-06	.16091	.15066E-02
31.250	.14184E-04	.00000E+00	.50137E-04	.68272E-06	.14993E+02	.36728E-06	.22490	.13608E-02
34.375	.00000E+00	.00000E+00	-.16063E-03	.50840E-06	-.47065E+01	.52772E-06	.21593	.00000E+00
37.500	.00000E+00	.00000E+00	-.37305E-03	.43014E-06	-.23630E+01	.44648E-06	.19286	.00000E+00
40.625	.00000E+00	.00000E+00	-.47868E-03	.36898E-06	-.19225E+01	.38300E-06	.20337	.00000E+00
43.750	.00000E+00	.00000E+00	-.18418E-02	-.48413E-06	-.68169E+00	-.50253E-06	.17827	.00000E+00
46.875	.00000E+00	.00000E+00	-.18418E-02	-.50979E-06	-.68169E+00	-.52915E-06	.00000	.00000E+00

C_4H_6 FLAME

z	$[C_2H_2]$	$[C_2H_4]$	$w_{g,gross}$	$w_{g,net}/vc_2h_2$	$w_{ox}/w_{g,gross}$	$w_{g,par}/vc_2h_4$	n_p	k_n
mm	kgmol/m^3	kgmol/m^3	kg/m^2-s	kg/m^3	-	kg/m^3	μm^{-3}	s^{-1}
3.125	.24648E-04	.19973E-04	.00000E+00	.00000E+00	.00000E+00	.00000E+00	.00000	.00000E+00
6.250	.64219E-04	.35867E-04	.00000E+00	.00000E+00	.00000E+00	.00000E+00	.00000	.38454E-04
9.375	.81117E-04	.46809E-04	.29120E-02	.31573E-05	.74649E-03	.13250E-05	.00614	.38224E-04
12.500	.88569E-04	.46932E-04	.41136E-02	.40859E-05	.76192E-02	.21096E-05	.00843	.14373E-03
15.625	.77190E-04	.29212E-04	.40489E-02	.39255E-05	.96999E-01	.22169E-05	.03874	.13803E-02
18.750	.41611E-04	.74731E-05	.11836E-02	.16692E-05	.70307E+00	.73112E-06	.32240	.46270E-02
21.875	.30933E-04	.00000E+00	.37722E-03	.96140E-06	.19472E+01	.25346E-06	.71158	.41619E-02
25.000	.12727E-04	.00000E+00	.64648E-04	.67736E-06	.11053E+02	.39679E-06	.76888	-.62138E-03
28.125	.00000E+00	.00000E+00	-.59264E-04	.47973E-06	-.10246E+02	.49796E-06	.72660	.00000E+00
31.250	.00000E+00	.00000E+00	-.18207E-03	.60148E-06	-.48028E+01	.62433E-06	.66953	.00000E+00
34.375	.00000E+00	.00000E+00	-.32054E-03	.69289E-06	-.34935E+01	.71921E-06	.65951	.00000E+00
37.500	.00000E+00	.00000E+00	-.38457E-03	.84588E-06	-.35349E+01	.87802E-06	.57112	.00000E+00
40.625	.00000E+00	.00000E+00	-.70124E-03	.27376E-06	-.14419E+01	.28416E-06	.59059	.00000E+00
43.750	.00000E+00	.00000E+00	-.15485E-02	-.92247E-06	-.34747E+00	-.95752E-06	.29859	.00000E+00
46.875	.00000E+00	.00000E+00	-.13010E-02	-.12269E-05	-.53216E-01	-.12735E-05	.26414	.00000E+00
50.000	.00000E+00	.00000E+00	-.13010E-02	-.12519E-05	-.53216E-01	-.12994E-05	.00000	.00000E+00

APPENDIX D

LISTING OF RATE ANALYSIS FORTRAN COMPUTER PROGRAM

```
c---> program rate to determine growth and nucleation rates for soot.
c     peter sunderland, 7-1994

      character *8 alpha

      dimension x(100),t(100),temp(100),dp(100),fs(100),
     +          xo2(100),xco2(100),xc2h4(100),xc2h2(100),xc2h6(100),
     +          xch4(100),xc3(100),xc4(100),xh2o(100),weight(100),
     +          fstw(100),pn(100),pntw(100)

      open (unit=11,file='~dat',status='old')
      open (unit=12,file='~chm',status='old')
      open (unit=21,file='~out',status='new')

c---> soot density: kg/m3; gas const: kJ/kmol-K; avocado's number: 1/kmol;
c     boltzman k: Nm/K
      pi = 3.1415927
      rhos = 1.85E3
      runiv = 8.314
      avo = 6.023e26
      boltz = 1.38e-23

c---> read p, atm, and headers:
      read(11,*) p
      read(11,10) alpha
      read(12,10) alpha
   10 format(a8)
      write(21,59)

c---> read input data files *.dat and *.chm:
c     t:s, temp:K, dp:m, fs:-, x's:-, d is dummy.
      do 20 i=1,100
       read(11,*,end=30) x(i),t(i),temp(i),dp(i),fs(i)
       read(12,*) z,d,xo2(i),xco2(i),xc2h4(i),xc2h2(i),xc2h6(i),d,
     +            xch4(i),d,xc3(i),xc4(i),xh2o(i),weight(i),d
       if (z.ne.x(i)) then
        write(*,*) 'positions do not match'
        goto 99
       endif

c--->  compute quantities needed for derivatives (pn:kmole/m3):
       fstw(i)=0.
       pn(i)=0.
       pntw(i)=0.
       if (weight(i).ne.0.) fstw(i)=fs(i)*temp(i)/weight(i)
       if (dp(i).ne.0.)     pn(i) = 6.*fs(i) / (pi*avo*dp(i)**3)
       if (weight(i).ne.0.) pntw(i) = pn(i) * temp(i)/weight(i)
   20 continue
   30 continue
      iend = i-1

c---> loop through stations and determine rates:
      do 90 i=1,iend

       dfstdt=0.
       dnptdt=0.
       if (fstw(i).ne.0.)   call linfit(t,fstw,i-1,i+1,a,dfstdt,rsquar)
       if (pntw(i+1).ne.0.) call linfit(t,pntw,i-1,i+1,a,dnptdt,rsquar)
```

```
c--->  O2 oxidation:
       wo2=0.
       po2 = p*xo2(i)
       call naglesc (temp(i),po2,wo2)
c      blake w=8.71e4*po2*exp(-18000./temp(i))
c      blake conco2=xo2(i)*p*101.33/(runiv*temp(i))
c      leung wo2=12.e4 * temp(i)**0.5 * exp(-19680./temp(i)) * conco2

c--->  co2 oxidation from szekely (libby and blake):
       wco2=0.
       wco2 = 2470.*exp(-21098/temp(i)) * p*xco2(i)
c      bradley wco2 = 9.e3 * exp(-34280./temp(i)) * (p*xco2(i))**0.5

c--->  h2o oxidation from szekely (johnstone):
       wh2o=0.
       wh2o = 1.515e-2 * exp(-16457./temp(i)) * p*xh2o(i)
c      bradley wh2o = 4.8e5 * exp(-34640./temp(i)) * (p*xh2o(i))**0.5

c----> concentration factor and mean gas velocities:
       cfac = p*101.33 / ( runiv*temp(i) )
       vc2h2 = ( 8.*boltz*temp(i)*avo/(pi*26.038) )**0.5
       vc2h4 = ( 8.*boltz*temp(i)*avo/(pi*28.054) )**0.5
       vch4  = ( 8.*boltz*temp(i)*avo/(pi*16.043) )**0.5

c--->  determine growth rate; toggle oxidation correction statement:
       s = avo * pi * dp(i)**2 * pn(i)
       wg = 0.
       if (s.ne.0.) then
        wgun = rhos*weight(i)*dfstdt / (temp(i)*s)
        frcox=(wo2+wco2+wh2o)/wgun
        wgcor=wgun+wo2+wco2+wh2o
c       for parallel channels, subtract c2h2 growth:
        wgc2h2 = 0.0231862 * cfac*xc2h2(i) * vc2h2
        wgpar  = wgcor - wgc2h2
       endif

c--->  compute nucleation rate:
       wn = weight(i)/temp(i)*dnptdt
       xkn = 0.
       if (xc2h2(i).ne.0.) xkn = wn / (cfac*xc2h2(i))

       c2h2f = 6.*vc2h2/(temp(i)**0.5)*cfac*xc2h2(i)
       ch4f  = 3.*vch4/(temp(i)**0.5)*cfac*xch4(i)
       c2h4f = 6.*vc2h4/(temp(i)**0.5)*cfac*xc2h4(i)

       write(21,60) x(i),cfac*xc2h2(i),wgun,wgcor,frcox,1.e4/temp(i),
     +              pn(i)*avo/1.e18,wn,xkn
   59  format('  x       [c2h2]  wgun   wgcor   frcox   1.e4/t      ',
     +        '   pn     wn    kn  ')
   60  format (f6.3,e11.5,3e12.5,f8.4,f8.5,2e12.5)

   90 continue

      write(21,*)
   99 continue
      stop
      end

c*************************************************************
      subroutine linfit(xar,yar,istart,iend,a,b,rsqare)
c     peter sunderland, 11-93
c---> fit least-square line through (x,y) points; y=a+bx
c     use points xar(istart) to xar(iend)
c     line cannot be vertical.

      dimension xar(100),yar(100)

      sumx=0.
      sumy=0.
      sumxy=0.
      sumx2=0.
      sumy2=0.

      do 10 i=istart,iend
       x=xar(i)
       y=yar(i)
       sumx = sumx+x
       sumy = sumy+y
       sumxy = sumxy + x*y
       sumx2 = sumx2 + x**2
```

```
        sumy2 = sumy2 + y**2
   10 continue

      xn = float(iend-istart+1)
      b = (xn*sumxy - sumx*sumy) / (xn*sumx2 - sumx**2)
      a = (sumy - b*sumx) / xn
      rsqare = (xn*sumxy - sumx*sumy)**2 /
     +         (xn*sumx2 - sumx**2) / (xn*sumy2 - sumy**2)

      return
      end

c*************************************************************
      subroutine naglesc (temp,po2,wnsc)
c     compute nagle/strickland-constable oxidation rates
c     ref Proc. 5th Carbon Conf, vol 1, 1962,
c     and Park and Appleton, C&F 20, 1973.
c     units are:  temp-K; po2-atm; wnsc-kg/m2-s
      if (po2.le.0.) then
       wnsc=0.
      else
       zk = 21.3 * exp(2060./temp)
       tk = 1.51e5 * exp(-48800./temp)
       bk = 4.46e-3 * exp(-7640./temp)
       ak = 20. * exp(-15100./temp)

c      note nsc paper mistake in chi formula!
       chi = 1. / (1. + tk/bk/po2)
       wnsc = 120. * ( ak*po2/(1.+zk*po2)*chi + bk*po2*(1.-chi) )
      endif

      return
      end
```

BIBLIOGRAPHY

Axelbaum, R. L., Flower, W. L., and Law, C. K. (1988a), "Dilution and Temperature Effects of Inert Addition on Soot Formation in Counterflow Diffusion Flames," Combust. Sci. Tech. 61, pp. 51-73.

Axelbaum, R. L., Law, C. K. and Flower, W. L. (1988b), "Preferential Diffusion and Concentration Modification in Sooting Counterflow Diffusion Flames, "Twenty-Second Symposium (International) on Combustion, The Combustion Institute, Pittsburgh, pp. 379-386.

Bockhorn, H., Fetting, F., Heddrich, A., and Wannemacher, G. (1984), "Investigation of the Surface Growth of Soot in Flat Low Pressure Hydrocarbon Oxygen Flames," Twentieth Symposium (International) on Combustion, The Combustion Institute, Pittsburgh, pp. 979-988.

Bockhorn, H., Fetting, F., Wannemacher, G., and Wenz, H. W. (1982), "Optical Studies of Soot Particle Growth in Hydrocarbon Oxygen Flames," Nineteenth Symposium (International) on Combustion, The Combustion Institute, Pittsburgh, pp. 1413-1420.

Boedeker, L. R., and Dobbs, G. M. (1986), "CARS Temperature Measurements in Sooting, Laminar Diffusion Flames," Combust. Sci. Tech. 46, pp. 301-323.

Bradley, D., Dixon-Lewis, G., El-Din Habik, S., and Muchi, E. M. J. (1984), "The Oxidation of Graphite Powder in Flame Reaction Zones," Twentieth Symposium (International) on Combustion, The Combustion Institute, Pittsburgh, pp. 931-940.

Bradley, D., and Entwistle, A. G. (1961), "Determination of the Emissivity, for Total Radiation, of Small Diameter Platinum-10% Rhodium Wires in the Temperature Range 600-1450° C," Brit. J. Appl. Phys. 12, pp. 708-711.

Brunauer, S., Emmett, P. H., and Teller, E. (1938), "Adsorption of Gases in Multimolecular Layers," J. Am. Chem. Soc. 60, pp. 309-314.

Cashdollar, K. L. (1979), "Three-Wavelength Pyrometry for Measuring Flame Temperature," Appl. Optics 18, pp. 2595-2597.

Clarke, A. E., Hunter, T. C., and Garner, F. H. (1946), "The Tendency to Smoke of Organic Substances on Burning, Part I," J. Inst. Petrol. 32, pp. 627-642.

Colket, M. B., III, Seery, D. J., and Palmer, H. B. (1989), "The Pyrolysis of Acetylene Initiated by Acetone," Combust. Flame 75, pp. 343-366.

Colket, M. B., III, Seery, D. J., and Palmer, H. B. (1991), "On Impurity Effects in Acetylene Pyrolysis," Combust. Flame 84, pp. 434-437.

Dalzell, W. H., and Sarofim, A. F. (1969), "Optical Constants of Soot and their Application to Heat Flux Calculations," J. Heat Trans. 91, pp. 100-104.

Dobbins, R. A., Fletcher, R. A., and Lee, W. (1994), "Laser Microprobe Analysis of Soot Precursor Particles and Carbonaceous Soot," Combust. Flame, in press.

Edelman, R. B., and Bahadori, M. Y. (1986), "Effect of Buoyancy on Gas-Jet Diffusion Flames: Experiment and Theory," Acta Astronautica 13, pp. 681-688.

Faeth, G. M. (1991), "Homogeneous Premixed and Non-premixed Flames in Microgravity: A Review," Proceedings of the AIAA/IKI Microgravity Science Symposium—Moscow, AIAA, Washington, p. 281.

Faeth, G. M., Gore, J. P., Chuech, S. G. and Jeng, S. -M. (1989), "Radiation from Turbulent Diffusion Flames," Annual Review of Numerical Fluid Mechanics and Heat Transfer 2, Hemisphere Publishing Corp., Washington, pp. 1-38.

Flower, W. L., and Bowman, C. T. (1984), "Measurements of the Effect of Elevated Pressure on Soot Formation in Laminar Diffusion Flames," Combust. Sci. Tech. 37, pp. 93-97.

Flower, W. L., and Bowman, C. T. (1986), "Soot Production in Axisymmetric Laminar Diffusion Flames at Pressures from One to Ten Atmospheres," Twenty-First Symposium (International) on Combustion, The Combustion Institute, Pittsburgh, pp. 1115-1129.

Flower, W. L., and Bowman, C. T. (1987), "Observations on the Soot Formation Mechanism in Laminar Ethylene-Air Diffusion Flames at One and Two Atmospheres," Combust. Sci. Tech. 53, pp. 217-224.

Garo, A., Lahaye, J., and Prado, G. (1986), "Mechanisms of Formation and Destruction of Soot Particles in a Laminar Methane-Air Diffusion Flame," Twenty-First Symposium (International) on Combustion, The Combustion Institute, Pittsburgh, pp. 1023-1031.

Garo, A., Prado, G., and Lahaye, J. (1990), "Chemical Aspects of Soot Particles Oxidation in a Laminar Methane-Air Diffusion Flame," Combust. Flame 79, pp. 226-233.

Glassman, I. (1988), "Soot Formation in Combustion Processes," Twenty-Second Symposium (International) on Combustion, The Combustion Institute, Pittsburgh, pp. 295-311.

Glassman, I., and Yaccarino, P. (1980a), "The Temperature Effect in Sooting Diffusion Flames," Eighteenth Symposium (International) on Combustion, The Combustion Institute, pp. 1175-1183.

Glassman, I., and Yaccarino, P. (1980b), "The Effect of Oxygen Concentration on Sooting Diffusion Flames," Combust. Sci. Tech. 24, pp. 107-114.

Gomez, A., Sidebotham, G., and Glassman, I. (1984), "Sooting Behavior in Temperature-Controlled Laminar Diffusion Flames," Combust. Flame 58, pp. 45-57.

Gore, J. P., and Faeth, G. M. (1986), "Structure and Spectral Radiation Properties of Turbulent Ethylene/Air Diffusion Flames," Twenty-First Symposium (International) on Combustion, The Combustion Institute, Pittsburgh, pp. 1521-1531.

Gore, J. P., and Faeth, G. M. (1988), "Structure and Radiation Properties of Luminous Turbulent Acetylene/Air Diffusion Flames," J. Heat Trans. 110, pp. 173-181.

Haggard, J. B. Jr., and Cochran, T. H. (1972), "Stable Hydrocarbon Diffusion Flames in a Weightless Environment," Combust. Sci. Tech. 5, pp. 291-298.

Hamins, A., Gordon, A. S., Saito, K., and Seshadri, K. (1986), "Acetone Impurity in Acetylene from Tanks," Combust. Sci. Tech. 45, pp. 309-410.

Harris, S. J., and Weiner, A. M. (1983a), "Surface Growth of Soot Particles in Premixed Ethylene/Air Flames," Combust. Sci. Tech. 31, pp. 155-167.

Harris, S. J., and Weiner, A. M. (1983b), "Determination of the Rate Constant for Soot Surface Growth," Combust. Sci. Tech. 32, pp. 267-275.

Harris, S. J., and Weiner, A. M. (1984), "Soot Particle Growth in Premixed Toluene/Ethylene Flames," Combust. Sci. Tech. 38, pp. 75-87.

Haynes, B. S., and Wagner, H. Gg. (1981), "Soot Formation," Prog. Energy Combust. Sci. 7, pp. 229-273.

Honnery, D. R., and Kent, J. H. (1990), "Soot Formation in Long Ethylene Diffusion Flames," Combust. Flame 82, pp. 426-434.

Honnery, D. R., Tappe, M., and Kent, J. H. (1992), "Two Parametric Models of Soot Growth Rates in Laminar Ethylene Diffusion Flames," Combust. Sci. Tech. 83, pp. 305-321.

Howard, J. B. (1990), "Carbon Addition and Oxidation Reactions in Heterogeneous Combustion and Soot Formation," Twenty-Third Symposium (International) on Combustion, The Combustion Institute, Pittsburgh, pp. 1107-1127.

Hura, H. S., and Glassman, I. (1987), "Fuel Oxygen Effects on Soot Formation in Counterflow Diffusion Flames," Combust. Sci. Tech. 53, pp. 1-21.

Hura, H. S., and Glassman, I. (1988), "Soot Formation in Diffusion Flames of Fuel/Oxygen Mixtures," Twenty-Second Symposium (International) on Combustion, The Combustion Institute, Pittsburgh, pp. 371-378.

Johnstone, J. F., Chen, C. Y., and Scott, D. S. (1952), "Kinetics of the Steam-Carbon Reaction in Porous Graphite Tubes," Ind. Engr. Chem. 44, pp. 1564-1569.

Kazakov, A., Wang, H., and Frenklach, M. (1994), "Detailed Modeling of Soot Formation in Laminar Premixed Ethylene Flames, Combust. Flame, in press.

Kent, J. H., and Honnery, D. R. (1990), "A Soot Formation Rate Map for a Laminar Ethylene Diffusion Flame," Combust. Flame 79, pp. 287-298.

Kent, J. H., and Honnery, D. R. (1991), "Soot Formation Rates in Diffusion Flames – A Unifying Trend," Combust. Sci. Tech. 75, pp. 167-177.

Kent, J. H., Jander, H., and Wagner, H. Gg. (1980), "Soot Formation in a Laminar Diffusion Flame," Eighteenth Symposium (International) on Combustion, The Combustion Institute, Pittsburgh, pp. 1117-1126.

Kent, J. H., and Wagner, H. Gg. (1982), "Soot Measurements in Laminar Ethylene Diffusion Flames," Combust. Flame 47, pp. 53-65.

Kent, J. H., and Wagner, H. Gg. (1984), "Why Do Diffusion Flames Emit Smoke?" Combust. Sci. Tech. 41, pp. 245-269.

Kline, S. J., and McClintock, F. A. (1953), "Describing Uncertainties in Single-Sample Experiments," Mech. Eng., January, pp. 3-8.

Klingenberg, G. (1985), "Invasive Spectroscopic Technique for Measuring Temperature in Highly Pressurized Combustion Chambers," Optical Engrg. 24, pp. 692-696.

Köylü, Ü. Ö., and Faeth, G. M. (1991), "Carbon Monoxide and Soot Emissions from Liquid-Fueled Buoyant Turbulent Diffusion Flames," Combust. Flame 87, pp. 61-76.

Köylü, Ü. Ö., and Faeth, G. M. (1994), "Optical Properties of Overfire Soot in Buoyant Turbulent Diffusion Flames at Long Residence Times," J. Heat Trans. 116, pp. 152-159.

Köylü, Ü. Ö., Sivathanu, Y. R., and Faeth, G. M. (1991), "Carbon Monoxide Emissions from Buoyant Turbulent Diffusion Flames," Third International Symposium on Fire Safety Science, Elsevier, London, pp. 625-634.

Law, C. K., and Faeth, G. M. (1994), "Opportunities and Challenges of Combustion in Microgravity," Prog. Energy Combust. Sci. 20, pp. 65-113.

Leung, K. M., Lindstedt, R. P., and Jones, W. P. (1991), "A Simplified Reaction Mechanism for Soot Formation in Nonpremixed Flames," Combust. Flame 87, pp. 289-305.

Libby, P. A., and Blake, T. R. (1979), "Theoretical Study of Burning Carbon Particles," Combust. Flame 36, pp. 139-169.

Libby, P. A., and Blake, T. R. (1981), "Burning Carbon Particles in the Presence of Water Vapor," Combust. Flame 41, pp. 123-147.

Lin, K. -C., Sunderland, P. B., and Faeth, G. M. (1995), "Soot Nucleation and Growth in Acetylene/Air Laminar Coflowing Jet Diffusion Flames," Combust. Flame, in press.

Markstein, G. H. (1988), "Correlations for Smoke Points and Radiant Emission of Laminar Hydrocarbon Diffusion Flames," Twenty-Second Symposium (International) on Combustion, The Combustion Institute, Pittsburgh, pp. 363-370.

Mauss, F., Schäfer, T., and Bockhorn, H. (1994), "Inception and Growth of Soot Particles in Dependence of the Surrounding Gas Phase," Combust. Flame 99, pp. 697-705.

Megaridis, C. M., and Dobbins, R. A. (1988), "Soot Aerosol Dynamics in a Laminar Ethylene Diffusion Flame," Twenty-Second Symposium (International) on Combustion, The Combustion Institute, Pittsburgh, pp. 353-362.

Megaridis, C. M., and Dobbins, R. A. (1989), "Comparison of Soot Growth and Oxidation in Smoking and Non-Smoking Ethylene Diffusion Flames," Combust. Sci. Tech. 66, pp. 1-16.

Miller, J. H., Honnery, D. R., and Kent, J. H. (1992), "Modeling the Growth of Polynuclear Aromatic Hydrocarbons in Diffusion Flames," Twenty-Fourth Symposium (International) on Combustion, The Combustion Institute, Pittsburgh, pp. 1031-1039.

Moffat, R. J. (1982), "Contributions to the Theory of Single-Sample Uncertainty Analysis," J. Fluids Engr. 104, pp. 250-258.

Mortazavi, S., Sunderland, P. B., Jurng, J., Köylü, Ü. Ö., and Faeth, G. M. (1993), "Structure of Soot-Containing Laminar Jet Diffusion Flames," AIAA Paper No. 93-0708.

Nagle, J., and Strickland-Constable, R. F. (1962) "Oxidation of Carbon Between 1000-2000° C," Proceedings of Fifth Carbon Conference 1, pp. 154-164.

Neoh, K. G., Howard, J. B., and Sarofim, A. F. (1980), Particulate Carbon (D. C. Siegla and B. W. Smith, eds.), Plenum Press, New York, pp. 261-277.

Park, C., and Appleton, J. P. (1973), "Shock-Tube Measurements of Soot Oxidation Rates," Combust. Flame 20, pp. 369-379.

Puri, R., Richardson, T. F., Santoro, R. J., and Dobbins, R. A. (1993), "Aerosol Dynamic Processes of Soot Aggregates in a Laminar Ethene Diffusion Flame," Combust. Flame 92, pp. 320-333.

Puri, R., Santoro, R. J., and Smyth, K. C. (1994), "The Oxidation of Soot and Carbon Monoxide in Hydrocarbon Diffusion Flames," Combust. Flame 97, pp. 125-144.

Ramer, E. R., Merklin, J. F., Sorensen, C. M., and Taylor, T. W. (1986), "Chemical and Optical Probing of Premixed Methane/Oxygen Flames," Combust. Sci. Tech. 48, pp. 241-255.

Rosner, D. E., Mackowski, D. W., and Garcia-Ybarra, P. (1991), "Size- and Structure-Insensitivity of the Thermophoretic Transport of Aggregated 'Soot' Particles in Gases," Combust. Sci. Tech. 80, pp. 87-101.

Saito, K., Gordon, A. S., Williams, F. A., and Stickle, W. F. (1991), "A Study of the Early History of Soot Formation in Various Hydrocarbon Diffusion Flames," Combust. Sci. Tech. 80, pp. 103-119.

Santoro, R. J., and Semerjian, H. G. (1984), "Soot Formation in Diffusion Flames: Flow Rate, Fuel Species and Temperature Effects," Twentieth Symposium (International) on Combustion, The Combustion Institute, Pittsburgh, pp. 997-1006.

Santoro, R. J., Semerjian, H. B., and Dobbins, R. A. (1983), "Soot Particle Measurements in Diffusion Flames," Combust. Flame 51, pp. 203-218.

Santoro, R. J., Yeh, T. T., Horvath, J. J., and Semerjian, H. G. (1987), "The Transport and Growth of Soot Particles in Laminar Diffusion Flames," Combust. Sci. Tech. 53, pp. 89-115.

Schalla, R. L., Clark, T. P., and McDonald, G. E. (1954), "Formation and Combustion of Smoke in Laminar Flames," NACA Report 1186.

Schalla, R. L., and Hubbard, R. R. (1959), "Formation and Combustion of Smoke in Flames," NACA Report 1300.

Schalla, R. L., and McDonald, G. E. (1954), "Mechanism of Smoke Formation in Diffusion Flames," Fifth Symposium (International) on Combustion, The Combustion Institute, Pittsburgh, pp. 316-324.

Schug, K. P., Manheimer-Timnat, Y., Yaccarino, P., and Glassman, I. (1980), "Sooting Behavior of Gaseous Hydrocarbon Diffusion Flames and the Influence of Additives," Combust. Sci. Tech. 22, pp. 235-250.

Sivathanu, Y. R., and Faeth, G. M. (1990a), "Soot Volume Fractions in the Overfire Region of Turbulent Diffusion Flames," Combust. Flame 81, pp. 133-149.

Sivathanu, Y. R., and Faeth, G. M. (1990b), "Temperature/Soot Volume Fraction Correlations in the Fuel-Rich Region of Buoyant Turbulent Diffusion Flames," Combust. Flame 81, pp. 150-165.

Sivathanu, Y. R., and Faeth, G. M. (1990c), "Generalized State Relationships for Scalar Properties in Nonpremixed Hydrocarbon/Air Flames," Combust. Flame 82, pp. 211-230.

Smyth, K. C., Miller, J. H., Dorfman, R. C., Mallard, W. G., and Santoro, R. J. (1985), "Soot Inception in a Methane/Air Diffusion Flame as Characterized by Detailed Species Profiles," Combust. Flame 62, pp. 157-181.

Spalding, D. B. (1979), Combustion and Mass Transfer, Pergamon Press, New York, Chapter 10.

Spengler, G., and Kern, J. (1969), "Untersuchungen an Diffusionsflammen Konzentrationsverteilung in einer Hexan-Diffusionsflamme," Brennstoff Chemie 50, pp. 321-324.

Tesner, P. A. (1958), "Formation of Dispersed Carbon by Thermal Decomposition of Hydrocarbons," Seventh Symposium (International) on Combustion, The Combustion Institute, Pittsburgh, pp. 546-553.

Tesner, P. A. (1960), "Dispersed Carbon Formation in Acetylene Self-Combustion," Eighth Symposium (International) on Combustion, The Combustion Institute, Pittsburgh, pp. 627-633.

Tesner, P. A. (1991), "Growth Rate of Soot Particles," Combust. Flame 85, pp. 279-281.

Tesner, P. A., and Schurupov, S. V. (1993), "Soot Formation from Acetylene-Benzene Mixture," Combust. Sci. Tech. 92, pp. 61-67.

Tesner, P. A., and Schurupov, S. V. (1994), "Kinetics of Soot Formation During Pyrolysis of Methane and Methane-Acetylene and Methane-Benzene Mixtures," Combust. Flame, in press.

Tien, C. L., and Lee, S. C. (1982), "Flame Radiation," Prog. Energy Combust. Sci. 8, pp. 41-59.

Vandsburger, U., Kennedy, I. M., and Glassman, I. (1984a), "Sooting Counterflow Diffusion Flames with Varying Oxygen Index," Combust. Sci. Tech. 39, pp. 263-285.

Vandsburger, U., Kennedy, I. M., and Glassman, I. (1984b), "Sooting Counterflow Diffusion Flames with Varying Velocity Gradients," Twentieth Symposium (International) on Combustion, The Combustion Institute, Pittsburgh, pp. 1105-1112.

Viskanta, R. and Mengüc, M. P. (1987), "Radiation Heat Transfer in Combustion Systems," Prog. Energy Combust Sci. 13, pp. 97-160.